An investigation into different phosphate glass processing routes and the role of phosphate glass in dental collagen-based scaffolds

Vincenzo Farano

THESE de DOCTORAT DE L'UNIVERSITE DE LYON
opérée au sein de
l'Université Claude Bernard Lyon 1

Ecole Doctorale N° accréditation
(ECOLE DOCTORALE INTERDISCIPLINAIRE SCIENCES SANTE)

Spécialité de doctorat : **Biomatériaux**
Discipline : (Eventuellement)

Soutenue publiquement/à huis clos le 04/10/2018,
par : **(Vincenzo Farano)**

An investigation into different phosphate glass processing routes and the role of phosphate glass in dental collagen-based scaffolds

Devant le jury composé de :

GUIGAND Martine	PU-PH	Université de Reims	Rapporteure
MIGONNEY Véronique	PU	Université Paris 13	Rapporteure
HUCK Olivier	PU-PH	Université de Strasbourg	Rapporteur
JACKSON Phil		Directeur division santé Lucideon LTD	Examinateur
GROSGOGEAT Brigitte	PU-PH	Université Lyon 1	Examinatrice
ATTIK Nina	IR	CNRS	Examinatrice
MAURIN Jean-Christophe	PU-PH	Université Lyon 1	Directeur de thèse
GRITSCH Kerstin	MCU-PH	Université Lyon 1	Co-directrice de thèse

INDEX

LIST OF FIGURES

LIST OF TABLES

ABBREVIATIONS

AcOH: acetic acid

Al: silver

Ba: barium

BET: Brunauer-Emerett-Teller test

BJH: Barrett-Joyner-Halenda analysis

BOs: bridging oxygens

Bt/P: butyl-phosphate

Ca: calcium

CaAc: calcium acetate

CaOEt: calcium ethoxide

CME: calcium methoxyethoxide

Co: cobalt

Col: collagen

ctr: control

Cu: cupper

DIW: deionised water

DMEN: Dulbecco Modified Eagle Medium

DMFA: dimethyl formamide

EDC: n-(3-(dimethylamino)propyl)-n'-ethylcarbodiimide hydrochloride

EDTA: ethylenediaminetetraacetic acid

EG: ethylene glycol

EtOH: ethanol

Et/P: ethyl-phosphate

FBS: fetal bovine serum

Fe: iron

FED: factorial experimental design

FTIR: Fourier-transform infrared spectroscopy

Ga: gallium

HA: hydroxyapatite

hGFs: human gingival fibroblasts

ICP: inductively coupled plasma

K: potassium

KPP: potassium pyrophosphate

Li: lithium

M: molar concentration

MAP: Monoammonium phosphate

Mg: magnesium

Mn: manganese

mol: mole(s)

MQ: melt-quench

MtOH: methanol

Mx: any metal

Na: sodium

NaAc: sodium acetate

NaG: sodium glycolate

NaOEt: sodium ethoxide

NaOMe: sodium methoxide

NaPP: Graham's salt

NBOs: non-bridging oxygens

NHS: n-hydroxysuccimide

O: oxygen

OH: hydroxyl

P: phosphate

Pb: lead

PBGs: phosphate-based glasses

PBS: phosphate buffer solution

PCL: polycaprolactone

Pen-Strep: penicillin-streptomycin

PLA: polylactic aid

ppm: parts-per-million

p.s.: pore size

p.v.: pore volume

QZ-crucible: quartz crucible

SBF: simulated body fluid

SCFs: scaffolds

SEM/EDX: scanning electron microscopy/energy-dispersive X-ray spectroscopy

SG: sol-gel

Sr: strontium

SrAc: strontium acetate

Ti: titanium

TGA/DSC: thermal gravimetric analysis/differential scanning calorimetry

TSPP: tetrasodium pyrophosphate

UPW: ultra-pure water

vol: volume

wt: weight

XRD: X-ray diffraction

XRF: X-ray fluorescence

Zn: zinc

ABSTRACT

This thesis concerns the development of a new series of Sr-doped phosphate-based glasses for biomedical applications. Such glasses in powder form are envisaged to have applications in novel composite restorations where the following is achievable: dentin cell-mediated bioremineralization, dental pulp regeneration and as carrier for therapeutics or antibacterial ions.

The initial aim was to produce soluble porous phosphate glasses using the sol-gel method (phosphate-alkoxide based sol-gel process). Knowing the effect that the variation of Ca content has on the dissolution properties of the glass, a series of glasses where Ca was progressively increased at the expense of Na was produced. The structure of the prepared samples was probed by XRD, XRF and FTIR to confirm the successful synthesis of the target phosphate-based glass compositions. After that a promising methodology was established, attempts were made to replace Ca with Sr. Different Sr sources were used without success due to the difficulty to fully dissolve those precursors in the sol-gel mixture.

Subsequently, the issue of the toxicity of some precursors and solvents used in the sol-gel procedure was recognised. To overcome this obstacle, efforts were made to replace the toxic precursor chemicals with safer ones. Nevertheless, due to the low solubility of some new precursors and the low reactivity of others, the sol-gel process did not proceed in a predictable and reproducible fashion.

At this stage, the sol-gel route was put aside, and two alternative soft and water-based chemical approaches were experimented: the precipitation method and the coacervation process. The first one was found to be unsuitable for our needs for two main reasons: 1) the presence of Na in the composition generated a crystalline material (instead of a glassy amorphous one); 2) the Ca/P ratio of our composition fell in the range of crystalline phase by using this method. In addition, the yield was really low. The second method (coacervation process) was a complete success. The glassy nature of the materials obtained was proved by XRD and XRF and the surface features were tested by BET and SEM. The process was retained for a while as the preferred synthesis route and both the scale-up effect and the possibility to add Sr were analysed. The production scale of the material was increased by 5 times and different Sr sources were tested to find the best one. XRD and XRF analysis proved both the success of the scale-up and the incorporation of the Sr in glass composition.

However, despite the promising results, due to both issues on the reliability of reaching the composition and lack of porosity / surface area meaning, in the end, the melt-quench technique was chosen as a definitive and reliable method to produce the above mentioned compositional series. Quaternary phosphate-based melt-quenched derived glasses in the P_2O_5–CaO–Na_2O–SrO system were synthesised in a way that by increasing Sr, Ca decreases. The glasses obtained have the general formula of $(P_2O_5)53$–$(CaO)(32-x)$–$(Na_2O)15$–$(SrO)x$, where x = 0, 5, 10 or 15 (mol%). Substituting Sr in place of Ca improves the stability and prolongs the degradation of these glasses.

To try to mimic the real architecture of deep dentine tissue and provide for a 3D support for cells, these glasses were mixed as powders with collagen fibres to make scaffolds. The presence of the collagen as an organic polymer guarantees the three-dimensionality of the structure and provides for an excellent and natural binding sites for cells to easily adhere and proliferate. The glass particles, on the other hand, ensure improved mechanical properties and release over time of important ions such as Ca, P and Sr to trigger and sustain cell differentiation.

In the end, to test the cytocompatibility of such prepared materials, hGFs were seeded in direct contact with the scaffolds and the viability checked at day 2, 4 and 7. As control, cells were seeded in an empty well. Although the control cells showed a high metabolic activity indicating the good health of the cells used, those in contact with the tested scaffolds displayed a significant low viability due to the acidification of the cell medium following glass particles dissolution.

1 INTRODUCTION

The human tooth is an organ composed of three mineralized tissues (enamel, dentin and cement) and one connective tissue (the pulp). The enamel is the outer layer of the crown. It is the hardest and the most highly mineralized tissue in the human body. Indeed, 96% of enamel consists of hydroxyapatite (HA) (a calcium phosphate rich mineral). Water and organic materials (mainly proteins such as amelogenin) make up the remaining part. The layer underlying the enamel is the dentine. The structure of dentine consists of microscopic channels called dentinal tubules which radiate outward through the dentine. It is made up of 70% inorganic materials, 20% organic materials (90% of which is collagen 1) and 10% water. This structure gives to the dentine high permeability leading to more vulnerability towards demineralization. At the crown level, the dental pulp is confined into the pulp chamber. This tissue, located in the centre of crown and root, forms with the dentin a complex called dentin-pulp complex. The dental pulp is a highly innervated, vascularized and non-mineralized connective tissue. At the interface between dentin and pulp highly specialized cells called odontoblast are responsible for the synthesis of the dentin. Those cells are large columnar cells forming the so-called odontoblast cell layer: the cell bodies are in the pulp, whereas the cell processes are thrown into the dentinal tubules.

During its life, the tooth undergoes lot of physiopathological processes. Among them the stress caused by microorganisms assumes an important role concerning dental health. In the human mouth more than 500 species of bacteria have been identified and some of them live attached to the tooth surface. Those bacteria are organized in communities called biofilms, better known as dental plaque. Under some circumstances (such as high sugar diet or poor hygiene), the metabolic activity of those bacteria can be detrimental for the tooth. While metabolising sugars, they produce acids that are secreted in the oral environment. Due to the accumulation of those acids, the pH of the saliva reduces below the HA critical value (5.5) leading to the dissolution of enamel and dentine. Those pathological conditions form the carious process contributing to the development of tooth decay. If the process is not stopped, the exposure of the pulp to the oral environment can be observed due to the loss of the dental mineralized tissues.

The main route to treat caries is the surgical removal of the infected tissues. The tooth is then restored by applying materials to replace damaged tissues. In this regard, different

materials are available: metals, alloys, glass ionomer cements (GICs) and resins. Two of the most used metals were titanium and gold. Among the alloys it is possible to include the gold alloys, cobalt-chrome and nickel-chrome alloys and the amalgam. However, despite their long lifespan and good mechanical properties, the lack of aesthetics and the risk of intoxication (the amalgam contains mercury) have limited their use over time being replaced by safer and highly aesthetic materials. Cements are widely used to fill the cavity: GICs are one of the most representative of this category. They are white, biocompatible and offer the possibility to release fluorite by being recharged after each brush. Composite resins are made by a resin (methacrylate-based polymers) and a filler (glass-like powder dispersed in the resin). Different fillers have been developed and the silica-based glass (also called bioglass or bioactive glass) fillers are the most used. Bioglasses have the interesting property of making grow on the surface a HA layer if soaked in a high concentrated ionic solution (such as the saliva) miming the natural organisation of the tooth mineralised tissues.

The two main routes to synthesize bioglasses are melt-quench technique and sol-gel process. In the first case oxides are melted together and rapidly quenched to create the amorphous network; the second is a chemical approach where the precursors polymerize at room temperature to form the glass network. As the MQ has the drawbacks of high temperature processing, the sol-gel route has been extensively researched as an alternative over the last few years. Two of the advantages of the sol-gel compared with melt-quench is the high porosity achievable and the possibility to incorporate bioactive molecules. Due to their high resistance in water, those materials are mainly used as permanent implants and the effects of a long-term exposure to such resistant materials are still debated.

A new generation of (bio)resorbable materials is under studying to create temporal implants. Resorbable means the ability of those materials to completely dissolve in water environment to be replaced by new growing tissues. One of the greatest exponents of this new kind of materials are the phosphate-based glasses. Those glasses have the properties to dissolve in water, alongside, they offer the possibility to tailor the dissolution rate in agreement with the targeted tissue's turnover. Due to this, they can be combined with resorbable organic biopolymers, such as collagen, to mimic the natural 3D architecture of a

tissue. In addition, likewise Si-glasses, they can be synthesized both by sol-gel and melt-quench.

The aim of this thesis is to develop a new biomaterial by combining collagen scaffolds and PBGs to be placed at the DPJ and recreate, by recruiting cells from the pulp, a new odontoblast-like layer for a cell-mediated dental restauration.

2 LITERATURE REVIEW

2.1   Biomaterials: an introduction

Biomaterials have attracted a great interest in the past few decades as reliable replacements for hard and soft tissue. The most accepted definition of biomaterials is currently the one employed by the American National Institute of Health that describes biomaterial as "any substance or combination of substances, other than drugs, synthetic or natural in origin, which can be used for any period of time, which augments or replaces partially or totally any tissue, organ or function of the body, in order to maintain or improve the quality of life of the individual".

From this definition it seems that biocompatibility is a key property that any biomaterial must possess. The Williams Dictionary of Biomaterials (Williams 1999) defined biocompatibility as ''the ability of a material to perform with an appropriate host response in a specific situation''[1]. However, this definition appeared incomplete since a list of "non-properties" has been developed such as nontoxic, non-immunogenic, non-thermogenic, non-carcinogenic, and so on. Thus, the Williams Dictionary of Biomaterials (Williams 2008) updated the definition of biocompatibility: ''the ability of a biomaterial to perform its desired function with respect to a medical therapy, without eliciting any undesirable local or systemic effects in the recipient or beneficiary of that therapy, but generating the most appropriate beneficial cellular or tissue response to that specific situation, and optimizing the clinically relevant performance of that therapy''[2].

Globally, biomaterials can be realized from natural or synthetic sources, thus, biomaterials are classified into two categories: biological (natural origin) and biomedical (artificial origin). Naturally derived biomaterials have some limitations such as risk of infection and batch to batch variability[3]. On the other hand, biomedical biomaterials can be easily sterilized reducing the risk of infection. In addition, they are more stable over time making them the favoured choice. Among the artificial bioactive materials, of particular interest as well as the subject of this thesis are the bioglasses.

2.1.1 Bioglasses

Generally, the term glass identifies any solid that possesses an amorphous phase and exhibits a (glass) transition temperature when heated towards the liquid state. Therefore, a bioactive glass (or bioglass) is a glass able to elicit a biological response when in contact with the organic matter showing a specific surface reaction.

A great advancement on the formulation and study of bioglasses was achieved when Prof. L. Hench published papers on his famous BioGlass (also known as 45S5), a melt-quenched derived silica-based glass with composition 45% SiO_2, 24.5% CaO, 24.5% Na_2O and 6.0% P_2O_5 in wt%[4]. The bioactivity of this material is attributed to its capacity to form a hydroxyapatite-like (HA) layer at its surface when soaked in simulated body fluid (SBF).

Hench and Thompson classified biomaterials in three categories or generations[5]:

- First generation or bio-inert materials: the aim was to achieve a suitable combination of mechanical/physical properties to match those of the replaced tissues or organs with no toxic effects (examples are metals and alloys);

- Second generation or bioactive materials: they are able to interact with the surrounding tissue to elicit an active response (among these materials, we can count bioceramics, bioglasses, glassceramics and biopolymers). It is commonly accepted that the bioactivity of the material is a function of its ability to grow an HA layer on the surface when interacting with a physiologic fluid;

- Third generation or bioresorbable and biodegradable materials: these are materials that linger temporarily in the host, being replaced by a natural growing tissue and are metabolized by the body into non-toxic by-products. An example are the phosphate-based glasses, the subject of this PhD thesis.

2.2 Phosphate-based glasses

Phosphorus is element 15 of the periodic table, placed in the group 15 (pnictogen) and period 3; Its electron configuration is [Ne] 3s2 3p3. To comply with the octet rule, phosphorus can bond to four atoms of oxygen forming the phosphate ion where one out of the four

oxygens is linked by a double bond. This determines that the phosphate ion has five resonance structure due to the delocalization of the electrons. All those physical-chemical properties of the phosphate are at the base of the atomic structure and particular properties of the phosphate-based glasses.

2.2.1 The structure

Phosphate glasses are inorganic polymers based upon the tetrahedral phosphate anions formed by the sp3 hybridisation of the phosphorus outer-shell electrons (3s2 3p3) with oxygen atoms. The remaining fifth electron is promoted to the 3d orbital where it creates strong π-bonding molecular orbitals with oxygen 2p electrons[6,7]. Based on the covalent oxygen bonds, phosphate tetrahedra are present in glass structures in different anionic forms classified in agreement with the Qi terminology, where "i" represents the number of bridging oxygens (POP bonds)[8]: in particular, Q0 is the orthophosphate, Q1 the pyrophosphate, Q2 the metaphosphate and Q3 the ultraphosphate configuration. By considering the glass network, Q1 represents the end unit, Q2 the middle unit and Q3 the branching unit; Q0 can be considered an isolated/free unit dispersed in the network. The prevalence of one unit with respect to the other depends on the oxygen-to-phosphorus ration (O/P) that means, on the relative concentration of other cations in the glass composition[8,9]. When the ratio is 2.5, a Q3 structure was found to predominate the network: in this context the glass is made by branched chains and rings in a 3-dimention structured network. For O/P equal to 3, Q2 prevails and the ultrastructure of the glass appears to be largely made of endless linear chains where cations act as cross-linking agents. When the concentration of cations is so great that the O/P is 3.5, the glass is dominated by pyrophosphate in Q1 configuration. When the O/P fraction reaches the value of 4, free Q0 orthophosphates units are the majority constituents of the structure.

More recently, computational molecular dynamic models have elucidated the position and configuration of modifiers in the phosphate glass network helping to understand the role they play in determining the properties of such glasses[10,11,12]. It was argued that the distribution of the cations into the glass bulk is quite homogenous and that they coordinate

oxygens in a peculiar manner depending on the type (and so radius) of cation and concentration. Considering the most common glass modifiers Ca and Na in the glass bulk, on average, a Ca^{2+} is bonded to 3.9–4.0 chains, while a Na^+ is only bonded to 3.2–3.3 chains. These values fall at the surfaces of phosphate glass particles to 2.8–3.0 chains bonded to Ca^{2+} and 2.5–2.7 chains bonded to Na^+.

Other modifiers can be added to the basic phosphate glass composition with different effects on the structure. In recent times, strontium has attracted a lot of attention as a glass doping agent for its interesting bone therapeutic properties[13,14]. In the network Sr bonds to a similar number of phosphate chains as calcium. However, due to its bigger radius, it changes the structure of the glass. Introducing Sr into the glass causes an increase in density that correlates well with the Sr concentration; furthermore, the amount of Q2 phosphorus decreases slightly, resulting in a slight increase in the number of Q1 and Q3 environments[15].

Li (as Na) acts as a strong network modifier. Due to its really small size, when it is added it disrupts the PO double bond at the surface of the glass creating the PO^-Li^+ ionic bond. This results in a changing in the structure from a 3D network of trigonally interconnected tetrahedra to a 1D network of long chains[16]. Similar effects are found when K is in the glass: it progressively breaks the structure of metaphosphate chains into short pyrophosphate groups $(P_2O_7)^{2-}$ [17].

Mn, in contrast, breaks the structure of metaphosphate chains $(P_2O_6)^{2-}$ into pyrophosphate predominant groups $(P_2O_7)^{4-}$ and the POP bonds are depolymerized by the incorporation of distorted Mn units that create POMn bonds[17].

The Mg coordination number is around 5-6 and the metaphosphate structure dominates the glass network. Increasing its concentration entails a transition from the open structure (of the metaphosphate glass) to a more compact one which presumably is reflected in the increase of mass density[18].

Fe or Al-doped phosphate glasses have a metaphosphate to pyrophosphate intermediate structure depending on their relative concentration compared to P. By increasing Al concentration, Q2 groups are disproportionated into Q1 and Q3 groups. The Fe-doped melted glasses Q4 are transformed into Q3 and even Q2 depending on the ionic status of the Fe that determines how rich in oxygens the network is; this in turn depends on the concentration of

the Fe[19]. This determines that an increase of FeOP or AlOP units crosslink the phosphate chains. Cs acts by shifting Q2 into Q1 and Q0[20,21].

When Ti is added, Q2 and Q3 species decrease and Q1 units become the dominant phase[22].

In Zn-doped phosphate glasses the network is dominated by Q2 chains[23,24]. Zn has a coordination number ranging from 4 to 6 and it is present in tetrahedral or octahedral configuration[25].

When Pb is added, phosphate glasses undergo gradual structural changes from metaphosphate, to pyrophosphate and to orthophosphate depending on the P/Pb ratio[26]. This suggests a gradual decrease in the number of bridging oxygens and increase in the resonance behaviour of non-bridging oxygens as the mole percentage of metal oxide (PbO) increases in the glass[27].

The presence of copper lead to an increase in the amount of Q3 species, resulting in the formation of non-bridging oxygen as CuO breaks P=O bonds with the formation of P-O-Cu covalent bonds[28].

The addition of Ba provides ionic cross-linking between non-bridging oxygens (NBOs), and that results in the decrease of isolated Q0 units. In other words, the decrease of the Q0 content leads to an increase in Q2 units[23],[29].

Due to the hygroscopic property of the phosphate network, water will react to create P-OH groups that will be part of the structure acting as chain terminator. Due to this, the concentration of Q2 tetrahedra increases and the number of Q3 types decreases[30].

2.2.2   Composition

Chemical composition and structure are very interdependent and contribute to determine the properties of that particular material (phosphate glass in this case). In the previous chapter (1.2.1) the structure of Ca-Na-P ternary glass was discussed and the effect of adding different ions (dopants) on the organization of the phosphate glass network was also examined. In this section, their effect on the dissolution rate is investigated.

Another property that has attracted the interest of researchers on phosphate glasses for medical applications is the possibility to tailor the dissolution rate of the glass in agreement with the host tissue by tuning the composition. The ternary system Ca-Na-P is very sensitive to the composition. The reciprocal effect of Ca and Na on the stability of the phosphate glass network has been extensively studied[31]. It is well known that increasing the concentration of calcium at the expense of Na makes the glass network more resistant to the hydrolytic action of the water. It has been proved that increasing the Ca content, and decreasing Na, reduces the solubility of the glass. Meanwhile, increasing Na creates a faster solubility of the network. This phenomenon is understandable and explainable by looking at the structure of such a glass discussed in the previous chapter (1.2.1). The higher coordination number of Ca compared to Na provides for a higher crosslink between the phosphate chains. In turn, this generates a more compact network then if a high amount of Na was present. A denser structure is more resistant to the penetration of the water resulting in greater stability in aqueous environments. This effect is even more evident considering that Na prefers the surface of the glass rather than the bulk as Ca does[32]. This along with the drop in the coordination number gives an understanding of why by increasing Ca and reducing Na the glass is more stable.

Li and K belong to group 1 of the periodic table like Na however, the ionic size differs. Li is smaller than Na whereas K has the biggest radius. This affects the field strength of the respective ions and so the depolymerisation (disruption ability) effect that each of them has on the network. Considering all this, it is possible to conclude than the durability of the glasses decreases in the order of Li>Na>K[33,34].

Mg[35], Sr[36] and Fe[37] (as ferrous) have the same effect as Ca: their presence in the glass composition reduces the glass dissolution rate. In general, it is possible to conclude that replacing alkali with alkaline earth elements enhances the durability of the glass.

Trivalent cations such as Ti[38], Al and Fe[37] (as ferric) have been found to show a significant effect on the dissolution rate of the glass network due to a resultant strengthening of the phosphate network. Their occurrence in the glass composition, strongly increases the durability of the glass. Overall, high valence ions decrease the dissolution of the glass by

increasing the network connectivity through the ability of each ion to link with 3 or more P-OH (or P-O-) groups.

Putting these considerations all together it is possible to conclude then the hydration energy (defined as the amount of energy released when one mole of ions is combined with water) for the phosphate glasses decreases in the order Q2>Q1>Q0.

It possible also to add small amounts of other network formers beside phosphate (that remains the main component in any case). The most frequently added network formers are Si and B. They drastically improve the glass durability by increasing the connectivity number of the glass network. In other words, they exert their effect by increasing the average number of bridging anions (bridging oxygen) per network unit[39].

Fluoride has a singular effect on the dissolution properties of the phosphate glass. Addition of (F-) reduces chemical dissolution via increasing network connectivity due to its ability to induce re-polymerization via stripping the modifiers (cations) from phosphate glass network[40].

Since the main component of phosphate glasses is the phosphate that act as a network former, changing its concentration has a deep impact on the dissolution rate of the network. Specifically, it was found that by reducing the P_2O_5 content the durability of the glass increases[41]. This is due to changes in the structure of the glass network from long phosphate chains more prone to hydrolysis, to shorter chains more resistant to hydrolytic attack.

2.2.3   Synthesis methods

The main route to synthesize phosphate-based glasses is melt-quenching. To overcome the limitations of this technique (see 1.2.3.1), during the last ten years, sol-gel methodologies have been increasingly researched. However, this method also has some issues that require attention. For example, the toxicity of some precursors, solvents used and the volatility of the phosphate precursors. To this end, other techniques have been developed such as precipitation and coacervate processes.

Here, a brief description of those techniques with advantages and disadvantages of each is provided.

2.2.3.1 Melt-quenching

In melt-quenching a mixture of oxides (or carbonates) is melted together in a kiln at temperatures often higher than 1000 °C. Subsequently, the homogeneous molten mixture is rapidly quenched (cooling) to obtain a solid material. The quenching rate is very crucial: this part has to be performed as fast as possible to avoid the formation of nucleation centres where crystals can develop. If the cooling is made very fast, the melt's disordered state is maintained in the final solid state and a glassy material with 100% amorphous phase is obtained.

A further step can be added to increase the stability of the network of the glass. This process is called annealing. Annealing a glass consists of slowly cooling hot glasses after they have been formed below their glass transition temperature for a given time. This additional thermal treatment removes all the residual internal stresses introduced during the manufacture and increases stability and crack toughness of the material. Such a process is critical for the production of 3-D shaped glass products but not critical for powder glass applications such as those explored in this thesis.

The melt-quench technique has some drawbacks mainly coming from the high temperature and precursors used. The elevated temperature processing removes opportunities for adding any bioactive molecule to the glass pending the decomposition of the substance. The nature of the technique gives a highly compact material with no porosity. The raw materials used can compromise the purity of the glass (unless highly expensive high purity materials are sought) and in general its homogeneity. On the other hand, the technique presents many advantages. For example, scalability to tonnage level and higher, absolute reliability (in terms of composition and phase), atoxicity, easier to control (fewer process variables to deal with) and it guarantees for high yield in a short time.

2.2.3.2 Sol-gel

To overcome all those limits, the sol-gel method represents a valid alternative to conventional melt-quenching[42]. The advantages of the method are: room temperature chemistry (low energy required and compatibility in terms of co-mixing with organic actives

during processing), high purity and homogeneity, the possibility to explore new compositions otherwise precluded and porosity. Beyond all these attractive properties, the most important advantage is the possibility to fine tune the structure and surface features of the sol-gel glass[43]. This opens up control of pore size, pore volume, degree of porosity, type of pores and degree of surface roughness (all things are not achievable with melt-quenching). However, this introduces a lot of variables that potentially need to be controlled. Choosing the right precursors, aging time and temperature, pH, type of precursors and order of addition, to name a few, are critical for consistently producing the desired sol-gel material.

When it comes to phosphate glass sol-gel formation, the processing becomes even more challenging: despite the basic unit in the glass network being tetrahedral, as for silica $(SiO_4)^{4-}$, the monophosphate is not as good a gel former as silica due to different chemical behaviour in solution[44]; in addition, much less work has been done on the sol-gel synthesis of phosphates as compared with silicates. Phosphoric acid cannot be used because of its high reactivity in water leading to salt precipitation instead of gellation. Phosphate esters have a slow hydrolysis and lead to loss of phosphorus from the composition during calcination due to volatility. Phosphoryl chloride has the same drawback of high phosphorus loss. Improvements have been seen through the use of alkyl phosphates[45,46]: they are more reactive and generate less phosphate loss. An alkoxide is the conjugate base of an alcohol, therefore it consists of an organic group bonded to a negativelly charged oxygen atom of the phosphate. These compounds are quite easy to obtain by mixing phosphoric acid with the parental alcohol. In the literature, the two most commonly used phosphate alkoxides are buty-phosphate (as mixture of 1:1 of mono and di-butyl) and ethyl-phosphate (mono- and di-ester mixture)[47]. The latter with a lower boiling temperature and lower polarity effect, ensures shorter drying time and better solubility of the modifier precursors.

To ensure homogeneity into the developing sol-gel system, when adding modifiers, corresponding metal alkoxides are often used. The main modifiers are Ca and Na, usually in the form of calcium methoxyethoxide, 20% in methoxyethanol and sodium methoxide solution 25 (or 30) wt. % in methanol. These are added to the phosphate precursor. $NaOCH_3$ is a strong Lewis base and it is believed to activate P-alkoxides and start the polymerization.

Due to their high reactivity in water, anhydrous conditions are preferred during the preparation of the sol-gel. The extreme toxicity of those precursors and solvents represent the real barrier for scale-up and commercialisation of this technique. In order to get over the problem, researchers have developed safer methods to produce phosphate glasses by soft and wet chemistry (refer to 1.2.3.3, 1.2.3.4 and 1.2.3.5).

The sol-gel process occurs when elements are used to form a sol from which a homogeneous amorphous gel is obtained by transition from a liquid sol to a gel. This process can be divided in different steps.

2.2.3.2.1   Preparation of the sol

The first step is the preparation of the sol. It is achieved by mixing components (precursors) in solution to generate a series of successive reactions leading to the formation of the sol. The sol is a colloidal suspension of solid particles that do not adhere to one another, the particles are completely dispersed in the solvent(s).

2.2.3.2.2   Colloid formation

When particles start to grow through further aggregation a colloid is formed. Colloids are bigger solid particles dispersed in a liquid with an amorphous or crystalline structure.

2.2.3.2.3   Gel formation

During the formation of the gel, particles cluster together to produce a continuous polymeric three-dimensional network containing the fluids.

An important parameter of a gel is the adhesion number (or coordination number) defined as the number of adhesive points of each particle and it depends on the mechanism of gelation. It determines the structure of the gel and its strength: if the adhesion is strong enough the gel does not crack when the water is removed (high adhesion number) otherwise it can crack and form particles / fragments.

2.2.3.2.4 Ageing

Ageing, if controlled can be used to strengthen and protect the gel network from cracking during the drying step. Throughout this process more bond formation occurs, and polymers and particles continue to aggregate and attach themselves. Through this process the gel shrinks, and the liquid is pushed out of the pores. This contributes to determining the final structure of the gel.

2.2.3.2.5 Drying

In this step the liquid is removed by evaporation. At the very beginning, the more external liquid vaporises determining the volume reduction of the gel; subsequently, due to an increase in capillary pressure, liquid trapped deeper in the gel structure and pores starts to come out and evaporate creating further shrinkage of the network. It is at this stage that cracks are likely to occur.

2.2.3.2.6 Thermal treatment

If necessary, the dry gel can undergo thermal treatment with the aim to (i) further densify and stabilize the network and (ii) remove any remaining organics. Failure to perform (ii) properly can lead to carbon entrapment. It is important to note that if an amorphous glassy material is required, the heat treatment should be performed below the glass crystallization temperature. Besides this, temperature ramping, holding time and cooling rate are parameters that have to be optimised accordingly.

Sometimes, a washing step before the thermal treatment might be required to render the dry gel free from organic solvents and by-products of the reaction.

2.2.3.3 *Glass by precipitation*

This method[48] is based on the possibility to obtain an amorphous solid (pyro)phosphate glass from two liquid solutions. A solution of calcium chloride is added to a

pyrophosphate precursor salts solution (tetrapotassium pyrophosphate). A suspension starts to form and ultimately sediments at the bottom of the reaction vessel.

This method has the advantages of being easy to perform and safe, as the only solvent involved is water. In addition, it is a room temperature reaction and fast (no heat treatment required). However, there are several limitations with such a technique that are deemed to be not favourable for further development of useful dental materials. First of all, the phase of the material is strongly dependent on both Ca/P ratio and pyrophosphate salt used. In the first case by increasing the Ca/P ratio the material becomes more and more prone to unwanted crystallization. In the second case, replacing the tetrapotassium pyrophosphate salt with tetrasodium pyrophosphate seems to inhibit the formation of any amorphous solid material. This is due to the different size and ionic strength of the cations Na and K. Thus, there are significant limitations to the range of possible compositions. Furthermore, the yield is very low and Ca-dependent: to increase the yield it is necessary to increase Ca concentration. However, by doing this the Ca/P will increase so the phase of the material will change from amorphous to crystal.

2.2.3.4   *Coacervation process*

The coacervation process[49] generates an aggregation of colloidal droplets held together by electrostatic attractive forces. In general, the coacervation process involves the liquid–liquid phase separation of a homogeneous solution of charged macromolecules resulting in a dense, polymer-rich 'coacervate' phase which coexists with its supernatant. In relation to PBG, the process entails the addition of a high concentrated solution of polyvalent cations ($CaCl_2$, $MgCl_2$ etc.) to an almost saturated solution of sodium polyphosphate (Graham's salt[50]). When in solution, electrostatic interactions between the long polyphosphate chains and polyvalent cations lead to the formation of the dense coacervate phase. The coacervate phase can be extracted and dried to form a solid glassy material.

The advantages of this route are numerous: It is a safe process as only water is required; a totally amorphous glass material is obtained (the phase is also not dependent on any cation/anion ratio); the reaction is easy and fast to perform (no thermal treatment) and

involves a room temperature reaction; there exists the possibility to add additional cations (this widens greatly the range of compositions it is possible to explore). Finally, there is the possibility to control reaction and chain length by adjusting the pH at which the reaction occurs. The only limit is that it is physically impossible to incorporate any anion in the composition due to the repulsive force that is generated between the phosphate and the anion (both are negatively charged).

In addition, it seems that the material obtained with this technique lacks porosity; however, one study[51] reported a type II hysteresis for a coacervate phosphate glass after thermal treatment. Due to this, and some doubts about the reliability of the actual composition matching the expected one, the melt-quench technique was ultimately chosen as the preferred route to produce the glasses argument of this thesis.

2.2.3.5   *Other methods*

Recently an amorphous calcium phosphate porous material has been synthesized through a microwave-hydrothermal method using fructose 1,6-bisphosphate trisodium salt as an organic phosphorus source and $CaCl_2$[52].

2.2.4   Dissolution behaviour

One of the most important properties of phosphate glasses is their ability to dissolve in aqueous environments: the POP bond of the glass network is broken down by the hydrolytic action of the water and eventually ions (modifiers) spread into the aqueous medium to become available as Mx+ aqueous ions.

According to literature, the network breakage happens in two steps: hydration and hydrolysis[53]. In the first one, hydration, an exchange reaction takes place at the glass-water interface between the high mobility ions (mainly Na) and the protons (H_3O^+) from the water. Protons replace Na ions in the glass network and the ions are dissolved in the water. As a consequence of this process, a hydrated layer forms on the surface at the glass-water interface level. During the second step, hydrolysis, the actual breaking of the network takes

place due to the cleavage of the POP bonds by the water at the level of the hydrated layer. As a result, the phosphate glass network is broken down and phosphate chains of different length are released into the water. This step generates decrease of pH and so acidification of the medium.

It is known that three main factors affect the dissolution of the glass network and they are pH, ionic strength of the medium and formulation (directly correlated to the structure).

2.2.4.1 *pH*

The dissolution process is strongly dependent on the pH of the media. In particular, hydrolysis is sensitive to the pH. The phosphate glass network is stable around neutral pH[33], but by reducing the pH the dissolution rate increases dramatically[54]. This happens because in acidic solutions, protons enhance the POM bond disruption resulting in a higher rate of hydration. The rate of dissolution is also enhanced in basic solutions, but the effect is less pronounced[33].

2.2.4.2 *Ionic strength of the medium*

The dissolution rate of the phosphate glass network decreases with increased ionic strength of the medium the glass is soaked in[55,56]. It is thought that this is due to saturation or limitation of reactant transport away from the dissolving glass. Also, ion exchange can be a cause of the decrease in dissolution rate. It means that, at the level of the hydrated layer, a saturated micro-domain might be created limiting the exchange reaction. Otherwise, a competition between the ions from the glass to the medium and/or from the medium to the glass might explain the increased resistance of the glass to dissolution.

2.2.4.3 *Glass formulation*

The dissolution of the phosphate glass network is a formulation-dependent process. A pure PBG (without modifiers) is made by PO_4 groups forming chains and rings and many NBOs. Due to the presence of the double bonded oxygen, only 75% of the oxygen is bridging

giving 25% of NBOs making the POP links easy to hydrate. The addition of modifiers (M) results in the replacement of the POP bonds with POM links which consequently increases the durability of the glass. In particular, monovalent and divalent cations occupy "network modifying" positions; whereas, multivalent cations occupy "network forming" positions. The first, by coordinating inter or intra-chains oxygens, densify and stabilize the network. The latter, by substituting the P in the POP bond and creating a cross-link between the NBOs of two phosphate chains, increase the network connectivity giving a great and positive effect to the stability and durability of the network[57,58]. (For further details on the effect of the composition see chapter 1.2.2).

2.2.4.4   *Species released*

When a phosphate glass system is soaked in water, several anions and cations are released whose type and kinetics depend on time and concentration[59,60].

2.2.4.5   *Cation release*

The types of cation released are strictly dependent on the type of modifier oxides included in the composition. The two most common cations used and studied are Na and Ca. When such a glass is soaked in water, they are released as a consequence of glass network degradation. In particular, Na is the first to be released due to the exchange reaction mentioned previously. Ca is then released as the glass network is broken down more and more.

Other cations like Sr, Li etc. can be leached out if present in the composition. The associated kinetics depend on their concentration, glass soaking time and type of ions. Valency, field strength charge and coordination number of additional ions influence the overall dissolution rate of the glass network and so the relative leaching speed by determining changes on the structure as discussed previously.

Since phosphate is the network former in these glasses, a range of anions can be released during dissolution. Those species have been identified as PO_4^{3-}, $P_2O_7^{4-}$, $P_3O_9^{3-}$ and $P_3O_{10}^{5-}$. $P_2O_7^{4-}$ and $P_3O_{10}^{5-}$ are considered branched anions, whereas $P_3O_9^{3-}$ is unbranched. In addition, $P_2O_7^{4-}$ and $P_3O_{10}^{5-}$ were found to be released at earlier time points; PO_4^{3-} and $P_3O_9^{3-}$ required more time to be detected in water, however P_3O_9 exhibits the highest rate of release.

By comparing the release kinetics of $Ca2^+$ with PO_4^{3-}, $P_2O_7^{4-}$ and $P_3O_{10}^{5-}$ and considering that the last two polyphosphates are branched, it was supposed that those anions exerted a chelating action on the Ca ions. On the other hand, due to the unbranched nature of PO_4^{3-} and considering the release rate of Na^+, it was thought the kinetics might be linked to Na taking up the residual charge. In addition, $P_3O_9^{3-}$ anionic species exhibit the highest rates of release. Putting all these factors together, it seems that $P_3O_9^{3-}$ dominates the degradation rates of the glass.

Considering the chelating effect of the phosphate anions towards Ca, and their branched/unbranched nature, a further explanation for the observation that increasing Ca results in a reduced glass dissolution rate supports the previous considerations.

2.2.5 Bioglasses: medical applications

Due to their osteoconductive and osteoinductive abilities, bioglasses (BGs) have attracted attention in tissue engineering, especially for mineralized tissue. When their surface is soaked in a fluid, it undergoes complex ion exchange reactions with the medium leading to the formation of a HA layer. This mechanism can explain the strong ability of BGs to bind bones. Moreover, this layer plays an important role in favouring cells migration and adhesion.

Bioglasses can be produced by melt-quenching and sol-gel routes. By SG, lot of important therapeutic ions can be incorporated into the glass network: for instance, Cu and Co have to promote angiogenesis; Li and Sr to trigger bone development through the *wnt* pathway. Moreover, biogactive glasses have been shown to regulate gene expression and promote cells differentiation. Due to their high resistance in water, the effects of a long-term exposure to

such resistant materials are still debated. Thus, PBGs, a new generation of (bio)resorbable materials, are under studying for medical usage.

2.2.6 Phosphate-based glasses for biomedical applications

Phosphate-based glasses have attracted huge interest in the field of biomaterials and tissue engineering due to their properties: chemical similarity with the natural components of bone and teeth (no inflammatory response), water solubility (bioresorbable material) and a controllable degradation profile.

The simplest and easiest phosphate glass is the binary Na-P glass. Despite evidence showing that it does not trigger any inflammatory response[61], the biocompatibility is absolutely time dependent. Upon long term culture, cells struggle to adhere to the glass due to the advanced state of dissolution[62,63]. The network solubility seems to be the factor that influences the most the ability of those materials to support cell adhesion and proliferation: if the glass dissolves too quickly, cells will lose their support and die[64]. In addition, the dissolution rate, in terms of ion release, has a deep effect on the environment: the glass dissolution rate and by-products have been associated with decrease in the pH (due to increased release of HPO_4 and PO_4^{3-} species eventually leading to bioincompatibility) and osmotic pressure and this may well influence how cells behave[65].

As mentioned before, Ca has a strong effect on the dissolution rate of the glass network and by varying its concentration it is possible to tailor the degradation rate of the glass. Glasses with low calcium content have higher solubility with a deleterious effect on cells. On the other hand, glasses with high Ca content have lower solubility and better biocompatibility[65,64]. This could be linked to a more stable and life-compatible pH and/or osmotic pressure associated with a more controllable ion release rate. In addition, Ca was proved to enhance the expression of some important bone marker genes in osteoblast-like cells[66]. Therefore, the most relevant formulation of PBGs for medical applications is the P_2O_5-CaO-Na_2O ternary system typically ranging from 35–55 mol% P_2O_5 (encompassing ultraphosphate, metaphosphate and polyphosphate glasses) and at least 40 mol% of CaO.

From what has been said so far, it is clear that the behaviour of the phosphate glass strictly depends on its composition and the presence of further elements. It is possible to classify the dopants under three categories: elements with a deep impact on the dissolution behaviour of the glass; elements able to promote differentiation (therapeutic ions); and dopants with antibacterial effect. Using one rather than another or a combination depends on the application.

Other therapeutic ions that can be added to the glass are for example Sr and Zn. Strontium is able to promote osteoblast activity, bone regeneration and inhibit bone resorption by inhibiting osteoclasts[13],[67]. Additionally, Sr enhances HA formability by increasing Ca absorption at the earlier stages and, because of its high similarity with Ca, it can be incorporated into the HA increasing bone density. For all those reasons, Sr is the good candidate for the purpose of this thesis. Zinc, on the other hand, drastically promotes cell adhesion at the surface by increasing hydrophilicity[68].

Ti[69], Fe[70] and Mg[71] have a strong effect on the dissolution rate: by varying their concentration in the glass it is possible to increase glass network durability accordingly to the host tissue. The presence of any one of those ions increases the biocompatibility of the glass by providing a more durable support for cells to adhere and proliferate.

As mentioned before, combinations of these ions can be employed to further improve cell response to phosphate glass. Ti and Ca[69,72] or Ti and Zn[73] have been proved to strongly enhance a cell response to the glass. It was believed that this was due to the beneficial effect of the ions and a more reactive surface.

Fluoride releasing glasses have been proved to be able to release fluoride in the oral cavity to aid remineralization of carious lesions[74].

Since phosphate is the main component in phosphate glasses, varying its concentration can have an effect on the dissolution rate of the network and in turn on cell response. By increasing phosphate content in the glass, the cytotoxicity decreases. This is related to a more stable glass network leading to a more stable environment for cells especially in term of pH change[65].

Phosphate glasses are hygroscopic materials and wettability or hydrophilicity has been associated with enhanced protein adsorption and, consequently, cell adhesion on biomaterials[75].

Due to their tuneable dissolution rate, another clinical application for phosphate glasses is as a carrier of antibacterial agents. Placed close to an injury, these glasses can release antibacterial ions to help wound-healing. Alternatively, as a coating layer for implants, catheters or tubes where nonsterile biological liquids flow, they can be used to prevent the growth of microorganisms introduced unwittingly as infection during surgical practices[76].

Examples of antibacterial ions incorporated into phosphate glasses are Al, Cu and Ga. Al was proved to be effective against *S. sanguinis*, *S. aureus*, *E. coli* and *C. albicans*[77]. Cu was shown to kill *S. sanguinis* biofilm[78] and prevent snail hosts of schistosomiasis. Ga has been shown to be effective in inhibiting the growth of both Gram positive (*S. aureus* and *C. difficile*) and Gram negative (*E. coli* and *P. aeruginosa*) bacteria[79]. The most effective element for killing the bacteria has proven to be the Al followed by Ga and Cu. The advantage of using such a method instead of the more conventional antibiotics is to avoid the occurrence of resistant strains.

The recent developments in phosphate-based glasses sol-gel chemistry allows the incorporation of biologically active molecules that are not stable to high temperature (such as proteins, antibiotic and other drugs). The resultant materials have potential to be used in devices to target the delivery of such molecules in the human body and provide controlled, sustained release in situ therapy. Finally, there exists the potential to coat biomedical devices with a sol-gel derived antimicrobial coating via the inclusion of biocidal metal ions such as Ag[80] and Ga[81].

2.2.7 Phosphate glass-based scaffolds and composites

There is much interest in the development of composites for biomedical applications and in particular for hard tissue surgery. The driving force for this interest is due to the possibility of producing materials with a high resistance to fracture (fracture toughness) and also to develop implants with a stiffness close to that found in bone.

The possibility of producing degradable composites has elicited much research and melt-quench phosphate-based glasses may be used as an initial reinforcing phase that leads ultimately to completely degradable composites[82]. The advantage of using these glasses for the production of composites compared to conventional additives such as hydroxyapatite is that more variation in the composition of the glass filler phase is available thus allowing tailoring of the end properties, including mechanical properties and control of the overall dissolution rate of the composite[9].

Moreover, PBGs could be used in combination with either natural (e.g. collagen) or synthetic polymers (e.g. PCL and PLA) to help the in-growth of vascularisation and the diffusion of nutrient and waste through 3D scaffolds for soft and hard tissue engineering: e.g., the engineering of muscle, ligament, tendon, or bone[83].

For the past decade, collagen has been the most widely used biomaterials for biomedical applications, due to its excellent biological features and physicochemical properties. Three-dimensional collagen scaffold materials have been designed to mimic one or more of the bone-forming components, to facilitate the growth of vasculature into the material, and to provide an ideal environment for bone formation. The mechanical properties of these porous scaffolds were generally poor, therefore porous collagen scaffolds have been combined with ceramic or glass particles for bone tissue engineering purposes. Based on the advantageous properties of degradable materials, PBGs have been incorporated within the collagen scaffold matrix for medical application. Collagen-based porous scaffolds containing PBGs have been used for skeletal muscle regeneration[84], guided nervous tissue regeneration[85], and for bone regeneration[86].

Whilst sol-gel phosphate glasses might not exhibit significant porosity (possibly as a result of the necessary heat treatment to removes organic solvents), but their use with bioactive polymers may well produce materials with improved mechanical properties for use in tissue engineering reconstruction. Such composites can also be used to produce flexible porous foams, which have potential applications as tissue engineering scaffolds.

In this thesis, a new application for collagen-based scaffolds containing PBGs is proposed: the possibility to use those materials for dental pulp regeneration and cell-mediated remineralization is suggested.

2.3   Summary

In using these materials, it is important to consider how the structure gives rise to physiochemical and biomedical properties and how these properties can be controlled by manipulating the composition. Perhaps the most important property of phosphate glasses is the solubility which determines how fast ions are released from the material, how well cells attach and proliferate and how chemically durable the glass is. It has been shown that varying the concentration of metal ions in the composition can be used to control the solubility. For example, the dissolution rate of Ca-Na-P glass exhibits an inverse trend with respect to the Ca concentration. Measurements show that the Ca ions induce structural changes in the phosphate network where the connectivity varies, giving rise to different solubility. PBGs can be incorporated into collagen scaffolds to create a complete biodegradable material for medical applications.

3 Materials and methods

3.1   Materials

A complete list of all the reagents and solvents used for the experiments described in this thesis, together with their manufacturers and abbreviations is provided below:

- n-Butyl phosphate, mixture of mono-n-butyl and di-n butyl ($[CH_3(CH_2)_3O]_2P(O)OH/[CH_3(CH_2)_3O]P(O)(OH)_2$, Alfa Aesar)
- Calcium methoxyethoxide, 20% in methoxyethanol ($C_6H_{14}CaO_4$, Gelest)
- Sodium methoxide solution 25 wt. % in methanol (CH_3ONa, Sigma-Aldrich)
- Ethyl phosphate mono- and di- ester mixture ($C_6H_{18}O_8P_2$, TCI)
- Calcium ethoxide, ($C_4H_{10}CaO_2$, Gelest)
- Sodium ethoxide solution 21 wt. % in ethanol (CH_3CH_2ONa, Sigma)
- Calcium acetate (($CH_3COO)_2Ca$, Sigma)
- Sodium acetate (CH_3COONa, Sigma)
- Acetic acid, glacial (CH_3CO_2H, Sigma)
- Ethanol, absolute (C_2H_5OH, Fisher Scientific)
- Ethylene glycol ($HOCH_2CH_2OH$, Sigma)
- Ultra-pure water
- Tetrasodium pyrophosphate ($Na_4P_2O_7$, Sigma)
- Potassium pyrophosphate ($K_4P_2O_7$, Sigma)
- Calcium chloride dihydrate ($CaCl_2 \cdot 2H_2O$, Sigma) (used as solvent)
- Graham's salt (($NaPO_3)_n$, Sigma)
- Calcium chloride dihydrate ($CaCl_2 \cdot 2H_2O$, Sigma)
- Strontium nitrate ($Sr(NO_3)_2$, Sigma)
- Strontium chloride hexahydrate ($SrCl_2 \cdot 6H_2O$, Sigma)
- Calcium carbonate ($CaCO_3$)
- Strontium carbonate ($SrCO_3$)
- Sodium carbonate (Na_2CO_2)
- Monoammonium phosphate ($NH_4H_2PO_4$)
- Quartz crucible (QZ-crucible)

- Collagen from bovine achilles tendon bibbers (Sigma)

- N-(3-(dimethylamino)propyl)-N'-ethylcarbodiimide hydrochloride ($C_8H_{17}N_3$ · HCl, Sigma)

- N-hydroxysuccinimide ($C_4H_5NO_3$, Sigma)

- DMEN (Gibco / ThermoFisher)

- Heat inactivated FBS (Gibco / ThermoFisher)

- Pen-Strep (10.000 Units/mL of pen, 10.000 µg/mL of strep - Gibco / ThermoFisher)

- Trypsin 2.5% (10x) without EDTA (Gibco / ThermoFisher)

- PBS 1x (Gibco / ThermoFisher)

3.2 Methods

3.2.1 Glass synthesis

3.2.1.1 Sol-gel

The sol-gel glasses were synthesized as follows. Briefly, under constant stirring, n-butyl phosphate (Bt/P) was added dropwise to sodium methoxide (NaOMe) in a vertical three-neck round-bottom flask and left mixing for 1h. Afterwards, the Ca precursor (Ca-methoxyethoxide, CME) was added dropwise. The resulting ternary mixture was left stirring for 24hrs at room temperature.

The following day, the temperature was raised up to 60 °C and the sols were left aging under a reflux condenser and constant stirring for one week. After this period, the wet gels were poured into glass beakers and put in the oven at 120°C for about 10-15 days. To help with the removal of the solvents and unreacted precursors, the dried gels were washed two-three times with absolute ethanol and filtered. The obtained powders were put in glass Petri dishes and placed in the oven at 120°C for 1h to ensure full ethanol evaporation. The dried gels were milled down using a pestle and mortar and calcined in an electric kiln at the following settings: ramp 1°C/min up to 250°C and holding for 15min. A schematic representation is shown in fig. 1 (adapted from[87])

To test the effect of the phosphate precursors, samples were prepared in which ethyl-phosphate (Et/P) was used instead of Bt/P without altering further the protocol.

To verify the actual applicability of less toxic sources both for Ca and Na, calcium ethoxide (CaOEt) and sodium ethoxide (NaOEt) were used by replacing both Ca-methoxyethoxide and NaOMt without varying the procedure.
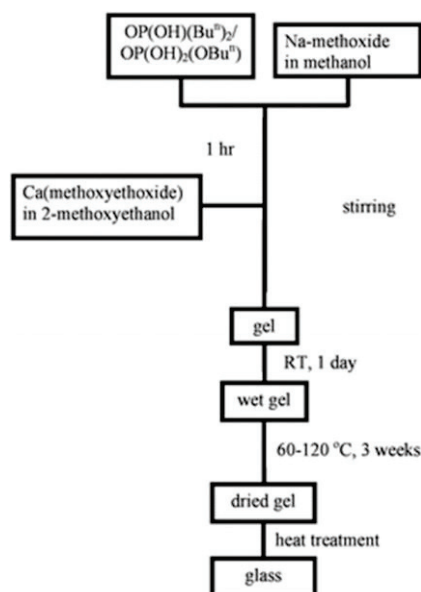
Figure 1 Flow chart of the sol-gel route to produce phosphate glasses

3.2.1.2 *Glass by precipitation*

Calcium and pyrophosphate reagent solutions were prepared separately by dissolving $CaCl_2 \cdot 2H_2O$ and $Na_4P_2O_7$ or $K_4P_2O_7$ in ultra-pure water (UPW). The calcium chloride solution was then added to the pyrophosphate solutions using a peristaltic pump at a constant volumetric flowrate (7.5 mL min^{-1}) for all samples. After the complete addition of the calcium reagent, the solutions were stirred for five minutes, and the final colloidal solutions centrifuged at 5000 rpm for 10 min. The resulting gel was washed two times with UPW. The resulting gels were poured into a Petri dish and heated at 70 °C for 7 days.

Aliquots of the solutions were collected during each step in order to measure the pH.

3.2.1.3 *Coacervate-based phosphate glasses*

The samples were prepared, as shown in fig. 2 (adapted from[88]), by slowly adding a 2 M solution of the calcium chloride to an equal volume of a 4 M solution of sodium polyphosphate (Graham's salt) at a rate of 5 mL/min. The sodium polyphosphate solution was stirred during this addition and the resultant mixture stirred for a further hour after the

addition was complete to ensure homogeneity. The stirring was then stopped, and the mixture allowed to stand for 1 hr. During this time two layers formed: an aqueous layer and a coacervate layer. The coacervate layer was twice washed with UPW before leaving to stand overnight. After removal of the water layer, a clear, viscous coacervate remained. The coacervate layer was dried at room temperature in a vacuum desiccator containing silica gel for several days to produce a friable powder.

To prove the possibility of incorporating Sr into the glass by using this procedure, at first, $CaCl_2$ was totally replaced by $SrCl_2 \cdot 6H_2O$ (2M). Subsequently, in order to partially replace Ca with Sr in the composition, the Sr salt was solubilised along with the Ca: Specifically, 1M of $SrCl_2$ was mixed with 1M of $CaCl_2$ prior addition the Graham's salt.
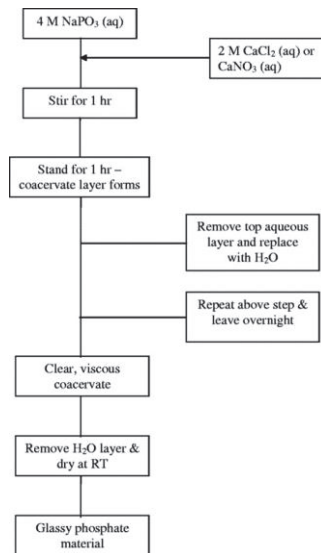
Figure 2 Schematic representation of the coacervate process to produce phosphate glasses

3.2.1.4 Melt-quenched glasses

The melt-quenched glasses were prepared as follows (fig. 3). A batch calculation was performed to determine the wt% of the raw materials needed to deliver the final target oxide formulation $(P_2O_5)53–(CaO)(32-x)–(Na_2O)15–(SrO)x$, where x = 0, 5, 10 or 15. The raw materials were weighed out and manually mixed to generate a homogeneous blend. Quartz (QZ) crucibles were pre-heated at 1150°C and the mixed powders were poured in little by little. When all the powders were in the crucible, the temperature was raised up to 1300°C

for about four hours to allow a proper melt homogenisation. After four hours, the molten mixtures were quickly quenched by pouring onto a steel plate. After quenching, the obtained glasses were milled to a particle size ranging between 20 and 200 µm using a TEMA Mill (model T 750 k).
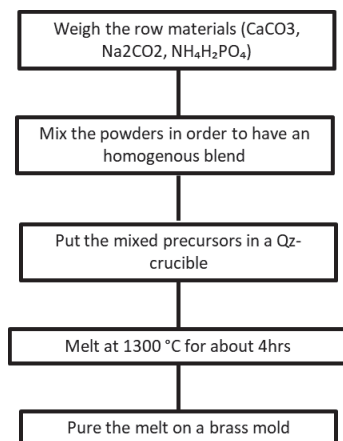
Figure 3 Route to produce melt-quenched phosphate-based glasses

3.2.2 Glass characterization

The protocols described below were applied to all glasses independently of the synthesis technique.

3.2.2.1 *Semi-quantitative X-ray fluorescence (XRF)*

This analysis was performed using a Panalytical Axios XRF Spectrometer. A small amount of material was smeared onto a filter paper and presented to the XRF spectrometer. The analysis was run using the preinstalled semi-quantitative XRF package.

3.2.2.2 *X-ray diffraction (XRD)*

This analysis was performed using a Bruker D8 Advance run in Bragg-Brentano para-focussing mode. Copper K alpha radiation was used throughout. A fixed divergence slit of 0.3 degrees was used, with a fixed 3 degree receiving slit employed prior to the detector. A Lynxeye 1-d detector was used covering a 3-degree two theta window. 192 channels

simultaneously collected the data. A 0.02-degree step size was used from 5 to 65 degrees (two theta data) with a dwell time per step of 0.5 seconds. A 20-micron thick nickel foil was used to monochromate the copper K alphaAlpha X-ray beam. The samples were continuously rotated with respect to omega at a rate of 15 times per minute throughout the data collecting procedure. Bruker Diffrac Eva was used to examine the collected diffraction trace.

3.2.2.3 *Fourier Transform Infrared Spectroscopy (FTIR)*

The infrared transmittance spectra were recorded using an SAFAS Monaco IR700. The analytical software used was SAFAS SP2000. The glass powders were placed in the centre of the sample holder (on the prism) and a pressure of 12kg was applied prior to measurement. The infrared spectra were recorded in the range from 4000 to 600 cm^{-1} in transmission mode.

3.2.2.4 *pH measurement*

The milled glass powders were weighed to create a suspension concentration of 1mg/mL: specifically, 25mg of powder was soaked in 25mL of UPW. The system (powder+water) was sealed in a Falcon tube and left shaking in an incubator-shaker at 37 °C, 120 rpm for 2, 6, 24, 48, 168, and 504 hours. For each time point, to remove the glass particles, the solutions were filtered twice using a 0.2μm filter; the filtrates were collected in clean tubes and the pH measured using a Hanna pH-meter.

3.2.2.5 *Inductively coupled plasma (ICP) coupled with mass spectroscopy*

After recording the pH, the solutions created as defined in section 2.2.2.4 were sent for ICP analysis. Before performing the analysis on the samples, a calibration curve was made using the following ICP standards: phosphorus standard for ICP (Sigma), sodium standard for ICP (Sigma), strontium standard for ICP and calcium standard for ICP (Sigma). A 0.6% HNO$_3$ solution was made (from a 65% solution, ACROS Organics) by diluting the acid in water. Next, the aforementioned standards were diluted to concentrations of 5, 10, 20, 30, 40, 50 and 70

ppm in the 0.6% HNO_3 solution. To comply with the calibration curve, the glass extracts were diluted five times with the 0.6% HNO_3 solution prior to analysis

3.2.2.6 *Surface features (BET/BJH)*

The surface area and pore volume parameters were determined by nitrogen adsorption/desorption isotherms at 77 K in a Belsorp Mini II Surface Area analyser. The samples were degassed at 200°C for 4 hours prior to measurement. The Brunauer-Emmett-Teller (BET) equation was used for specific surface area quantification whilst the Barret-Joyner-Halenda (BJH) approach was used for the mean pore size and pore volume determination.

3.2.2.7 *Scanning electron microscopy (SEM)*

The powdered samples were coated with a thin layer of gold suitable for examination of the surface and morphology of the particles in Secondary Electron mode. A JEOL JSM6490-LV Scanning Electron Microscope (SEM) fitted with an Oxford Instruments INCA Energy Dispersive X-ray Analysis system (EDA) was used for examination in accordance with in-house methods M24 and M25. Images were taken at different magnifications. Microanalysis results were tabulated on a semi-quantitative, normalised, elemental weight basis.

Light elements such as lithium and boron were not quantified by this analytical technique. Carbon is also omitted.

3.2.2.8 *TGA/DSC analyses*

The thermogravimetric analysis (TGA/DSC) was realised in a temperature range from 25°C to 500°C, under air as reactive gas and with a heating rate of 5°C/min. The starting material weight was 15 mg. The device used was the Thermogravimetric Analyzer Mettler Toledo TGA/DSC2.

3.2.3 Scaffold fabrication

3.2.3.1 *Glass milling*

To reduce particle size, the glass powders were milled using a Planetary Micro Mill PULVERISETTE 7 premium line by Fritsch. 100 g of 1mm ZrO_2-beads and 15g of glass powder were each placed into two zirconia-lined jars and sealed (zirconia-lined lid fitted with a polymer "O" ring). One cycle of milling was performed at 750 rpm for 5 min at room temperature. Subsequently, 15 g of isopropanol was added to each vessel and, after re-sealing, 5 cycles of milling at 750rpm for 5 min (each interrupted by an equal number of pauses of 10 min to reduce temperature build-up) were performed at room temperature. The wet glass powders were filtered using a 50μm sieve to separate the beads from the milled glass. The glasses were dried overnight at 37 °C and the particle size distribution was measured with a Malvern Mastersizer 3000. The size of the particles chosen for the scaffold preparation described in this article ranged between 0.1 and 10 μm.

3.2.3.2 *Scaffold elaboration*

Homogeneous collagen suspensions of 40 mgmL^{-1} were prepared by mixing the collagen fibres in ultra-pure water under continuous magnetic stirring. Then, glass particles were added to the collagen suspensions at a 1:1 wt ratio. After 5 min of vigorous stirring, the homogeneous mixtures were loaded into Petri dishes, frozen using liquid nitrogen and lyophilized under vacuum for 2 days. Finally, the scaffolds were chemically cross-linked overnight using 20 mM of N-(3-(dimethylamino)propyl)-N'-ethylcarbodiimide hydrochloride (EDC) and 8 mM of N-hydroxysuccinimide (NHS) in 80:20 (vol%) ethanol/deionized water. Afterwards, the scaffolds were rinsed with ethanol and deionized water (80:20 ratio) for three times and dried in an oven at 37°C for 24h.

To improve the solubilization of the collagen fibres, some samples were prepared in which 0.02 N of acetic acid (AcOH) was added to the collagen suspension. In addition, to improve the link between the fibres and the glass particles, same scaffolds were prepared with the

concentration of the crosslinker increased by 10 times. In the end, four batches were prepared as follows:

- Batch 1: without AcOH and 1X of crosslinkers (the control)
- Batch 2: with AcOH and 1X of crosslinkers
- Batch 3: without AcOH and 10X of crosslinkers
- Batch 4: with AcOH and 10X of crosslinkers

The four groups were submitted for compression testing

3.2.4 Scaffold characterization

3.2.4.1 *Mechanical test: compression*

All specimens (n=4 for each batch) were held at ambient temperature and humidity. Each specimen in turn was placed on a powder compaction test fixture of bore diameter 30 mm in an Instron universal testing machine. The loaded sample fixture was placed on the 5 kN capacity load cell platen. The load cell was tared before the loading piston was placed on the sample. Once the loading piston was positioned, a preload of 5 N was applied. The crosshead was adjusted to bring the loading piston into contact with the upper platen. The position measurement was then tared using the Bluehill software and the test initiated.

The test parameters were:

Crosshead speed = 1 mm/min

Output statistics:

Load in N at 2 mm extension F(2)

Position change in mm at 250N X(250)

3.2.4.2 *Surface features (BET/BJH)*

The surface area and pore volume parameters of the collagen-based scaffold were determined by nitrogen adsorption/desorption isotherms at 77 K in a Belsorp Mini II Surface area analyser. The sample was subjected to prolonged degassing at 40°C prior to measurement. The Brunauer-Emmett-Teller (BET) equation was used for the specific surface

area quantification while Barrett-Joyner-Halenda (BJH) was used for mean pore size and pore volume determination.

3.2.4.3 *pH measurement in water*

170 mg of collagen-based scaffolds were soaked in 20 mL of ultra-pure water and monitored for pH. The soaked scaffolds were sealed in a Falcon tube and left shaking (120rpm) in an incubator-shaker at 37 °C for 2, 6, 24, 48, 168, and 504 hours. For each time point, to remove debris, the solutions were filtered twice using a 0.2μm filter; the conditioned waters were collected in clean tubes and the pH measured using a Hanna pH-meter.

3.2.4.4 *Inductively coupled plasma (ICP) coupled with mass spectroscopy*

After recording the pH, the same solutions described in the section 2.2.4.3 were subjected to ICP analysis. Before performing the analysis on the samples, a calibration curve was made in the same way as for the glass particles alone, as described in the section 2.2.2.4. To fit the calibration curve, the scaffold extracts were diluted twenty times with the 0.6% HNO_3 solution and the diluted samples were used for the analysis.

3.2.4.5 *SBF test*

170 mg of the scaffolds were soaked in 20 mL of simulated body fluid[89] (SBF) for 1 and 3 weeks at 37 °C, 120 rpm. For each time point, the solutions were filtered twice using a 0.2μm filter. The media were subjected to immediate pH measurement, whereas the scaffolds were dried 24h at 60 °C prior to further analysis.

3.2.4.6 *SEM/EDX*

The scaffold samples were analysed, "as received", using SEM in low vacuum mode without any conductive coating. A JEOL JSM6490-LV Scanning Electron Microscope (SEM) fitted with an Oxford Instruments INCA Energy Dispersive X-ray Analysis system (EDA) was

used for examination in accordance with in-house methods M24 and M25. SEM imaging of the scaffold/ fibrous samples was conducted using Backscattered Electron Imaging; using this imaging mode the brightness of a given feature is proportional to its mean atomic number. Images were taken at different magnifications. Microanalysis results are tabulated on a semi-quantitative, normalised, elemental weight basis. Light elements such as lithium and boron are not quantified by this analytical technique. Carbon is also omitted.

The EDX spectra of the scaffolds before and after SBF immersion were collected for 100s at a primary beam energy of 15 keV and at a working distance of 10mm.

3.2.4.7   Cytocompatibility assay

3.2.4.7.1   Cells seeding

Human gingival fibroblasts (hGFs) were used to assess the cytocompatibility of the collagen-based scaffolds containing Sr-doped melt-quenched derived phosphate glasses (18.4 mm of diameter x 9.8 of height for a total of 0.45 g each).

Cells at passage 6 were defrosted and placed into two 75 cm^2 Corning® CellBIND® Surface cell culture flasks to let them grow. During this period the complete DMEM medium (10% FBS and 1% Pens-Strep) was changed every 2 days. When cells reached a confluence of about 90%, they were harvested by trypsinization with 0.25% trypsin without EDTA incubated for 3 min at 37 °C. After, the trypsin reaction was stopped by adding complete medium and cells were collected by centrifugation at 1200 rpm for 5 min. Cells were seeded at a density of 10^5 cells/scaffold by applying 300 µL of cell suspension on the samples at 37°C for 20 minutes. This step ensured that cells penetrated the scaffolds without felling in the gaps between the scaffolds and the walls of the wells. Afterwards, 2 mL of medium was added to cover the samples. As control, hGFs were seeded in an empty well at the concentration of 10^5 cells/well in a 12-well plate.

Cells viability was checked after 2, 4 and 7 days by using AlamarBlue. Briefly, the dye was added to each well at the dilution of 1:10 and left to incubate overnight at 37 °C. The following morning, a drop of 100 µL of media containing the dye from each condition was placed in a flat bottom 96 well plate and the absorbance was checked without cover using NanoQuant infinite M200PRO microplate reader (by Tecan) setting 600 nm as reference wavelength and 570 nm as measurement wavelength. The calculated difference between measurement and reference was used to compare the cell viability between the control and the samples.

After the measurement, the scaffolds and the control were washed with PBS and a fresh medium was added.

The experiment was performed in duplicate.

3.2.5   Use of Factorial Experimental Design (FED) in sol-gel composition optimisation

3.2.5.1   *Designing of experiments*

An article was published[90] in which a Zn-doped phosphate glass ceramic was produced by a sol–gel method in which a mixture of 40% EtOH and 60% EG (by volume) was used as the reaction medium. Inspired by the paper, the Design Expert "Statease" factorial experimental design software package was used to create a series of experiments in which the impact of (i) temperature, (ii) EtOH:EG ratio and (iii) time of the sol-gel reaction on final material properties could be appraised. For each of the three variables, ranges were imposed: for the volume ratio the window was from 100% EtOH and 0% EG to 0% EtOH and 100% EG; for the temperature under reflux the range was from 60 to 100 °C; the time under reflux was varied between 2 to 6 days. Having set these parameters, the software was used to create a restricted number (11) of representative experiments to run (the output-fig. 4). Based on the outcome from the trials, the FED software was used to calculate which variable (or variable combinations) were most influential on the chosen outcomes. Four responses were considered: phase, yield, colour and composition. A different weighting was assigned to each

of them according to their importance: the phase was chosen as the most critical parameter followed by yield, composition and colour. The final desirability plot combines the four outcomes. Having set preferred ranges for each outcome the desirability plot shows the variable combinations delivering the best desirability.

3.2.5.2 *Experimental setup*

To begin, EtOH and EG were mixed in a three-neck round-bottom flasks. Subsequently, the ethyl-P precursor was added to the blend and left stirring for about 10 min to ensure a homogeneous mix. Afterwards, NaAc was added and left stirring for 1h. The last precursor, CaAc, was then added and the flasks sealed. The flasks were kept sealed under constant stirring for 24h at room temperature before being immersed in the water thermal bath. At this point a condenser was attached. The temperature of the thermal bath and the time under reflux were chosen in agreement with the FED outputs.

Immediately after the reactions were completed, the wet gels were filtered using a 500mL VWR® Vacuum Filtration Systems with 0.20 µm pore size of the membrane. The materials obtained were collected in glass Petri dishes and calcined in an electric kiln at the following setting: ramp 1℃/min up to 250℃ and holding for 15min.

Runs*	EG/EtOH (mL %)	Temperature with reflux (℃)	Days
1	60/40	100	6
2	100/0	100	6
3	80/20	80	4
4	60/40	60	2
5	100/0	60	6
6	100/0	100	2
7	100/0	60	2
8	60/40	100	2
9	60/40	60	6
10	80/20	80	4
11	60/40	100	4

*All the experiments are left stirring for 24 hours at room temperature before applying the condenser
Yield fix at 20g

Figure 4 Experiments generated by the FED software

4 Results

4.1 Review article: Sol-gel bioglasses in dental and periodontal regeneration: a systematic review

Vincenzo Farano, Jean-Christophe Maurin, Nina Attik, Phil Jackson, Brigitte Grosgogeat, Kerstin Gritsch (Accepted: 19 June 2018)

Objectives: Bioglasses have been widely used in tissue engineering, in particular, for mineralized tissues regeneration. Indeed, they are known for their osteoconductive and osteoinductive properties. Thus, bioglasses seem to be interesting for the regeneration and repair of dental mineralized and periodontal tissues. Several bioglasses have been synthesized whose properties depend on the composition and the synthesis method. The two main methods of elaboration are melt-quench and sol-gel. The latter seems to be promising, allowing the incorporation of bioactive molecules and the control of the porosity. In order to elaborate a new material for dental tissue remineralization, we wanted to have an overview of the literature concerning sol-gel bioglasses applications in dentistry. Thus, the aim of this study is to review the current state of the art of the effects of bioactive glasses produced by sol-gel on cells for dental and periodontal regeneration. The study also discusses associated antibacterial properties. In addition, the methodology and the type of cells used in the included articles to investigate those effects was exanimated in order to underline common points and suggest guidelines.

Methods: The research was performed by consulting three databases (PubMed, ScienceDirect and Web of Science) to identify relevant published literature using the following terms (in Title/Abstract): ((((Bioglass*) OR glass*)) AND (((((dent*) OR odonto*) OR tooth) OR teeth) OR periodont*)) AND ((sol-gel) OR mesoporous). The research was performed considering five years' window time (from 01/01/2012 to 31/08/2017) and not language restriction was imposed. The Preferred Reporting Items for Systematic Reviews and the Meta Analyses (PRISMA) statement was used as a guideline for the review methodology.

Results and Discussions: From an initial 244 articles, after duplicates removal, rejection based on title and abstract and, then full text and addition of articles coming from other sources, 52 papers were included in the manuscript. From those, only 13 have proved both the ability of bioglasses (BGs) to differentiate dental cells at genetic level and their ability of triggering cell-mediated mineralization, but only 6 of them showed, along with cells, the antibacterial properties of the glasses. This review shows that sol-gel bioactive glasses are not toxic, can sustain cell proliferation and differentiation at a genetic level and can keep the bacterial

population under control. The versatility and the advantages of the sol-gel technique have been demonstrated in terms of applications (coating film, carrier, etc.) and in tailoring the composition to make it more specific in their effects and closer to the real structure of tissues (bioscaffolds). Moreover, the importance of using primary cells instead of cell lines and performing genome analysis was emphasises. Furthermore, by putting together all the data coming from the included studies, an ideal material and a standard protocol are proposed.

Sol-gel bioglasses in dental and periodontal regeneration: a systematic review

Vincenzo Farano [1,2], Jean-Christophe Maurin [1,2,3], Nina Attik [2] Phil Jackson [4], Brigitte Grosgogeat [1,2,3], Kerstin Gritsch* [1,2,3]

[1]Université Lyon, Université Claude Bernard Lyon 1, CNRS, Laboratoire des Multimatériaux et Interfaces, Villeurbanne, France
[2]Faculté d'Odontologie, Université Claude Bernard Lyon 1, Lyon, France
[3]Service d'Odontologie, Hospices Civils de Lyon, Lyon, France
[4]Lucideon Limited, Queens Road, Penkhull, Stoke-on- Trent, Staffordshire, ST4 7LQ, United Kingdom
*Corresponding author: kerstin.gritsch@univ-lyon1.fr

Abstract: Due to their osteoconductive and osteoinductive abilities, bioglasses (BGs) have attracted attention in tissue engineering, especially for mineralized tissue. The aim of this study is to review the current state of the art on the effects of bioglasses produced by sol-gel on cells for dental and periodontal regeneration. The study also discusses associated antibacterial properties.

The research was performed by considering the Preferred Reporting Items for Systematic Reviews and the Meta Analyses (PRISMA) statement. The research ranged five years' window time (from 01/01/2012 to 31/08/2017) and the relevant studies were identified based on the inclusion/exclusion criteria.

45 articles were selected from 244 initial returns, plus 7 further articles coming from other sources were selected for the same pourpose. From this systematic study, it is revealed that only 13 out of the 52 articles have proved both the ability of bioglasses to differentiate dental cells at genetic level and their ability of triggering cell-mediated mineralization, but only 6 of them showed, along with cells, the antibacterial properties of the glasses. This review shows that sol-gel bioglasses are not toxic, can sustain cell proliferation and differentiation at a genetic level and, can keep the bacterial population under control. Moreover, a standard methodology and an ideal material are suggested.

Key words: Bioglass, sol-gel, Dental cells, Periodontal, Antibacterial

INTRODUCTION

The first bioglasses were defined as a hard, amorphous and biocompatible silica oxide-based inorganic polymers that elicit a specific biological response at the surface which results in turn in the formation of a bond between the tissues and the material [1]. Other bioglasses were developed such as phosphate-based bioglasses but silica oxide-based bioglasses are still the most studied. The composition of bioglasses usually contain oxides of Si, Ca, P and sometimes Na; the leaching of these ions into the media could elicit cell responses and explain their bioactivity [2]. More recently, metallic ions (e.g., Cu2+, Co^{2+}) have been incorporated to bioactives glasses in order to promote angiogenesis [3]. Thus, bioglasses have been widely studied during the last decade as supporting materials for tissue engineering and tooth remineralization [4, 5]. Indeed, when their surface is soaked in a fluid, it undergoes complex ion exchange reactions with the medium leading to the formation of some salt precipitation and, with time, to the deposition of a hydroxyapatite (HA) layer. This mechanism can explain the strong ability of bioglasses to bind bones. Moreover, this layer plays an important role in favouring cells migration and adhesion. In addition to this, by the same mechanism of ion exchange, biogactive glasses have been shown to regulate gene expression and promote cells differentiation, two important steps in tissue restauration technology [6]. Bioglasses can be produced mostly by melt-quenching and sol-gel routes [7]: in the first case oxides (or alternative precursors such as carbonates or nitrates) are melted together and rapidly quenched to create the amorphous network; the second is a chemical approach where the

1

precursors polymerize at room temperature to form the glass network [8]. As the melt-quench technology has the drawbacks of high temperature processing and a dense network, the sol-gel route has been extensively researched as an alternative over the last few years. One of the advantages of the sol-gel compared with melt-quench is the high porosity achievable that create a higher surface area and improved cellular response. Indeed, the porous structure of the network provides a better support for cell adhesion, migration and growth [9]. Moreover, the porosity may work as a guide for blood vessels invasion and nutrient diffusion to the target [6]. The sol-gel technique allows the incorporation of important therapeutic ions as Sr [10], Mg [11, 12] or Li [13]; moreover, these sol-gel derived bioglasses have been shown to regulate gene expression [14, 15], protein synthesis and cell-mediated mineralization. It offers also the possibility to mix the glassy amorphous phase with some crystals to obtain combined materials with improved and joint mechanical properties. Furthermore, the sol-gel reaction achieved at room temperature allows the in-situ incorporation of biocompatible and resorbable polymers; also, the porous structure can be loaded with biological molecules for a local sustained release of growth factors [16]. Recently, surfactants have been added to the sol-gel reaction to generate a more ordered porous structure in order to better control ion dissolution/exchange with the surrounding environment. These mechanisms are essential for the restoration and regeneration of hard tissues, because they underlie the hydroxyapatite layer formation [17].

One of the main steps in tissue engineering is the identification and activation of adult stem cells. Dental pulp harbours a great variety of different cell types. Among them, a population of adult pulp stem cells have been identified [18]. These dental pulp stem cells have been proved to possess the ability to differentiate in odontoblast-like cells and secrete a mineralized extracellular matrix. Equally, inside the periodontal tissue mesenchymal-like cells with adult stem cell characteristics have been identified and have been shown to be able to differentiate in periodontal ligament fibroblast cells [19]. Hence, the main role for bioglasses in tooth and periodontal regeneration is the activation of those cells to produce a new natural dentin and periodontal ligament fibres.

An ideal material for tooth tissue engineering [20] and periodontal regeneration [21] should sustain and promote cells proliferation, differentiation, should have mechanical properties resembling the target tissues [22] and have antibacterial/bacteriostatic properties.

Sol-gel bioglasses seem to counteract bacterial growth and this task can be improved by loading them with antibiotics or doping with bactericidal ions like silver to avoid the emergence of resistant strains [23].

Bacteria and their metabolic products, especially lactic acid and proteolytic enzymes, are the main cause of caries in humans. By dropping the mouth pH below a critical value (5.5), the dissolution of enamel [24] and so the progressive loss of HA leading to the tooth decay is triggered. Bacteria are also responsible for periodontitis [25]. Nowadays, the main therapies involve the replacement of the damaged tissues; however, the current trend in dentistry is to preserve as much as possible the natural organ and regenerate the lost parts of the teeth and their components. In this context, tissue engineering is an emerging field which is based on the combination of stem cells, grow factors, vascularization and biomaterials.

Sol-gel derived bioglasses, due to their intriguing cell properties have been incorporated as fillers in scaffold for tooth and periodontal regeneration.

Keeping this scope, the aim of this systematic review is to address the state of the art of the effects of sol-gel bioglasses on cells, their possible antibacterial properties and their use in tooth and periodontal regeneration by assessing their biological behaviour.

METHOD

The Preferred Reporting Items for Systematic Reviews and Meta Analyses (PRISMA - fig. 1) has been used as a guideline throughout the manuscript [26].

The electronic search of the literature was conducted on PubMed, ScienceDirect and Web of Science with the following terms (in Title/Abstract):

Bioglass* OR glass*
AND
dent* OR odonto* OR tooth OR teeth OR periodont*
AND
sol-gel OR mesoporous

Data restrictions were applied from 01/01/2012 to 31/08/2017 corresponding to the major publication period about this topic. No language restriction was applied. Review articles and short communications were excluded. To be included, the papers had to meet the following criteria:

1. Studies including bioglasses produced by a sol-gel technique
2. Studies assessing biological effects of bioglasses on dental or periodontal cells or cell types relevant to dental or periodontal tissues.

The titles and abstracts were marked off independently by two reviewers. The full texts of all the abstracts in accordance with the inclusion criteria, were collected and reviewed (by consensus). In addition, the bibliographies of the considered papers was scanned to identify additional missing relevant articles. Again, the consensus between the two reviewers was reached to determine which studies met the inclusion criteria.

The quality of *in vitro* study (table 1) was evaluated considering the ratio between the size of the samples and the number of biological tests performed in response to sol-gel bioglasses and the presence of a control group.

RESULTS

Study selection

A total of 244 articles were found through the electronic research. After the duplicate removal, 178 papers were recorded and 7 came from other sources (for a total of 185). 118 articles were rejected based on title and abstract. The full text of the resulting 67 papers was screened. Subsequently, 15 papers more were excluded as they did not meet the inclusion criteria: 3 articles were excluded because considered ceramics rather than bioglasses [27–29], 7 articles did not perform any cells test at all [30–36], 4 articles used complete Si-glass [37–40] and one 1 Zr nanoparticles [41]. The bibliography of the 45 selected articles were analysed to identify and include other relevant publications that may have been missed during the electronic research: 7 additional studies were thus identified and included in this review. At the end, a total of 52 papers were included in the current manuscript. The composition of sol-gel bioglasses, the precursors and the methods used for their synthesis were listed in the table 2.

The analysis was performed to list the effect of sol-gel bioglasses on cells to address their possible application in dental restoration, periodontal regeneration and to investigate their potential antibacterial effects.

Effects of bioglasses on cells

Amongst the 52 papers, 11 have studied pure bioglasses [42–52], 23 have assessed doped-glasses [53–75] and 18 have used composite materials [76–93].

3

PURE BIOGLASSES

Dental pulp stem cells (DPSCs)

4 studies have investigated the effects of pure bioglasses (understood as glasses without dopant) produced by sol-gel processing on DPSCs. Four important characteristics affecting the material properties have been considered: dissolution/composition [49], surface properties [47] and particle size [48, 51]. The results have confirmed that bioglasses were not toxic and nano size in the range between 160 and 20 nm was preferred due to the associated increased surface area (from about 28 m^2 g^{-1} for the particles in meso-range up to 63 m^2 g^{-1} or even 400 m^2 g^{-1} for the nano-range glass particles). In addition, nano-BGs improved the cell-mineralization ability and regulated odontogenic related genes expression (DSPP1-dentin sialophosphoprotein, DMP1-dentin matrix protein and col1-collagen).

Periodontal ligaments cells (PDLCs)

2 papers [44, 52] have studied the effect of pure bioglasses for periodontal regeneration using PDLCs. Wu, et al. [52] proved that Ca-Si nano particles (100 nm) had no cytotoxicity and their ionic extract (ranging between 12.5 and 100 mg mL^{-1}) could induce and stimulate cell differentiation through enhancing osteopontin (OPN), alcalin phosphatase (ALP) and osteocalcin (OCN) gene expression. X. Cheng, et al. synthesized quaternized mono-dispersed bioactive nanospheres by sol-gel with different methacrylate salts linked at the surface. By studying the effect of the extract on PDLCs, they found no cytotoxicity and cells viability after 1, 3 and 7 days of treatment. In addition, the efficiency of the material was studied in vivo using Sprague-Dawley (SD) mice with periodontal defects. They found that after 4 weeks from the implantation, the serum level of inflammatory markers decreased.

Other cells

5 articles have used different cells to study the effect of sol-gel pure bioglasses for tissue engineering. Amongst them, 2 studies [42, 50] have found that nano scale particles (between 37 and 74 nm) were more effective than meso-scale equivalents in promoting cells growth and proliferation on bone mesenchymal stem cells (BMSCs) and unrestricted somatic stem cells (USSCs) respectively.

In addition, bioglasses were used to trigger cells differentiation in other ways. For instance, they were used as a carrier to delivery siRNA [46], or as a thin film to cover sheets of Ti6A14V titanium alloy for improved cell adhesion [43, 45].

Doped glasses

Silver (Ag) has been reported in 7 selected articles. 4 of them [55, 56, 63, 71] have examined the effect of adding Ag to sol-gel bioglasses on DPSCs. 3 studies [55, 56, 71] agreed that Ag (2.1 wt%) had a toxic effect only when it was present with a high concentration (whose extract is undiluted or diluted 1:2) and that it retained its action even when the glasses were mixed (30:70 50:50 glass: extracellular metrix (ECM) wt ratio) with organic polymers. The remaining [63] proved that 5 mol% of Ag are not toxic even if cells are directly exposed to the doped glass.

2 articles [57, 70] have studied the effect of Ag-BG on BMSCs. The first has concluded that the way Ag is incorporated determines the toxicity: adsorption being more toxic than templating. The second study proved that Ag exercised its action even after HA crystal growth.

1 article [54] has used NIH3T3 cells: the Ag-glass thin film covering a Ti-disk has shown no cytotoxic effect and was able to support cell growth.

4 papers [53, 68, 69, 74] have assessed the effect of zinc (Zn) on DPSCs. These 4 studies have proved that Zn was not toxic for cells and supported cells growth/viability in a time-dependent manner after 7-

4

14 days of exposition. Moreover, it was proved to promote cell proliferation and differentiation by increasing odontogenesis-related markers expression after 7 and 14 days.

The effects of Mg-BGs have been studied in 3 articles [58–60]. Their results have demonstrated that: the doped glasses were not toxic on Chinese hamster ovary cells (Cho) and strmal cells (ST2).

The effects of copper (Cu) have been considered in 2 publications [69, 73]. Only 1 article used DPSC [69]. However, both studies have shown that the presence of Cu significantly enhances cell proliferation and differentiation at earlier time points (between 3 and 7 days of exposure).

3 articles [62, 64, 72] have studied the effects of increasing strontium (Sr) in a sol-gel glass system: 1 on PDLCs [72], 1 on DPSCs [62] and 1 on BMSCs [64]. Sr (6 or 10 mol%) promoted cells viability and proliferation in a time dependent manner (14 days). In addition, osteogenesis/cementogenesis-related gene expression was enhanced. In addition, Lee et al. 2017 [64] loaded the Sr-doped glass with phenamil. A synergism between Sr and Phenamil was found in activating a (tribbles homolog 3) Trb3-dependent BMP (bone morphogenetic protein) signalling pathway. 2 articles [64, 75] have explored the possibility to use Sr-BG in vivo. It demonstrated that Sr-MBG scaffolds led to greater new bone formation in Wistar rats and SD mice with periodontal defects. In addition, the synergic effect was proved to happen also in vivo.

1 paper [61] took into consideration the effects of varying the concentration of Li on PDLCs. Li-MBGs were not cytotoxic and provided a proper support for cell growth and differentiation in a concentration-dependent manner (from 2 to 5 mol%) by activating the *Wnt* pathway.

1 study [66] investigated the effect of the presence of zirconium (Zr) in a glass or glass/ceramic (GC) system on MG63 osteoblasts-like cells. GC strongly improved cell metabolism in a time dependent manner (within 6 days) compared with Zr-free GC, pure glass and Zr-G.

1 article [65] was published on the effect of a glass doped with magnetic iron on BMSCs. It was indicated that bone cells easily adhered and proliferated onto the magnetic glass surface by prolonging the time exposure (up to 6 days).

For further details see table 3.

COMBINED MATERIALS

18 articles have combined pure bioglasses with other materials using a sol-gel technique. Amongst them, in particular, 13 papers mixed bioglasses with organic polymers and 5 papers used ceramics.

5 articles [76, 85, 86, 88, 90] studied the effect of mixing bioglasses with organic polymers on DPSCs. Nadeem, et al. 2016 [88] have mixed type-A porcine gelatine with 10 wt% bioglass to obtain a biodegradable scaffold for bone regeneration. The safety of the material and its ability to sustain cell adhesion and proliferation was proved by SEM and H&E staining. Extensive studies undertaken by Bae, et al. 2012, Tiejun, et al. 2013 and Kim, et al. 2014 [76, 86, 90] have demonstrated the ability of gelatine/collagen-bioglass scaffolds to sustain and promote odontogenic differentiation of DPSCs when they are in contact with the material. These 3 authors concorded on the non-toxicity of the scaffolds and their ability to support cell attachment and proliferation; moreover, they showed the cell-mediated mineral nodule formation and the up-regulation of key genes like OCN, DSPP, DMP-1, Col-1, ALP and integrins. Kim, et al. 2017 [85] mixed glasses with chitosan (CHT) founding that serial dilutions (from 1:2 to 1:16) of the extract were not toxic after one day of treatment.

6 articles have studied the effects of bioglass-based combined materials on PDLCs: specifically, 4 mixed bioglasses with organic polymers, 2 mixed bioglasses with ceramics. The first 4 articles showed that by mixing sol-gel bioglasses with organic biopolymers such as 10 wt% polycaprolactone (PCL) and gelatine [82], 3 wt% alginate [92] or chitosan [87] it was possible to improve PDLFs-material interaction. The other 2 articles showed that by combining bioglasses with leucite [80] or porcelain (66.7

5

wt%) [77], the PDLFs activity resulting was significantly enhanced. An advanced study on periodontal regeneration by gene therapy was carried on by Zhang, et al. 2015 [93]. They have used a bioglass/silk scaffold containing adPDGF-B and adBMP7. The developed system has been shown to repair periodontal defects in beagle dogs.

3 articles [77, 80, 83] confirmed the benefits of mixing an amorphous phase (sol-gel derived bioglass) with a crystal phase on gingival fibroblasts (GFs).

6 additional papers [78, 79, 81, 84, 89, 91] have studied the effects of different combined materials on other cell types. Coating Ti disks with a Si-Ca/PCL6 scaffold [78] or combining bioglasses with forsterite [91] or leucite [89] enhanced the proliferation of NIH3T3, human osteoblast-like cells and rat derived osteoblasts respectively. As well mixing glasses with CHT/PEG (polyethylene glycol) ratio [84], calcium phosphate [81] or PEG (0, 6, 12, 24, 50 wt%) dip-coat Ti4 [79] promoted proliferation and cell differentiation of human fibroblasts, NIH 3T3 and C3H10T1/2 in a concentration and time dependent manner.

1 study [67] took into consideration the possibility that some components of dental composite could be toxic. Combining silica calcium phosphate glasses and bisphenol A glycidyl methacrylate (BisGMA)/triethylene glycol dimethacrylate (TEGDMA), the authors proved that both the concentrated extract of the composite immediately after light curing as well as direct contact to the materials killed cells. However, if the materials were washed after light curing, the toxicity of both the extracts and direct exposure disappeared. The article concluded that the toxicity is due to the residual unpolymerized monomers.

ANTIBACTERIAL PROPERTIES

In total, 12 articles (see table 4) showed both good cell biocompatibility and bactericidal properties: of those, 7 considered silver; 1 magnesium; 1 copper; 2 the possibility to use BGs as carriers for antibiotic delivery; 1 functionalized the surface with metacrilate salts.

From the analysis of these studies, Ag-doped glasses (2.1 wt%) presented a better antibacterial property on a great variety of clinically relevant microorganisms. Wang, et al. 2015 [71] and Chatzistavrou, et al. 2014 and 2016 [55, 56] showed that silver kept its antibacterial action even when the Ag-BGs were mixed with different organic polymers: *S. mutans*, *L. casei*, *E. coli* and *E. faecalis* were respectively proved to be highly sensitive to the presence of Ag. Fan, et al. 2014 [57] proved that the bactericidal action of Ag was independent of the way by which the Ag was incorporated into the glass: *E. faecalis* was completely and equally killed both when the Ag was incorporated by absorption and when it was incorporating by template. Catauro, et al. 2015 [54] showed that the bactericidal action of Ag-doped glass against *S. aureus* was concentration-dependent. Lee, et al. 2017 [63] studied the antibacterial effect of Ag-doped glass on *E. coli, E. faecalis, S. oralis* and *S. mutans*. They founded that the Ag-free glass was unable to kill any of those bacteria, and that the efficiency of the Ag-doped glass was strain specific: using three different concentrations (40, 80, 160 µg/mL) they found that *E. coli* and *S. oralis* were the most sensitive to the doping agent; whereas, *S. faecalis* was killed only when exposed to the highest concentration. *S. mutans* was shown to be highly resistant. The addition of tetracycline (TC) or chlorohexidine equally killed both *S. faecalis* and *S. mutans*.

The study of Tian, et al. 2016 [70] has proved that silver glasses can kill both *S. aureus* and *E. coli* even when the materials were covered by a layer of HA and independently on the crystals orientation.

Fooladi, et al. 2012 [58] incorporated magnesium (Mg) in a sol-gel based phosphate calcium silicate glass. *S. aureus*, *E. coli* and *P. aeruginosa* were exposed to different concentrations of the glass by-product: the extracts were particularly effective against *E. coli* whereas a highly concentrated extract (1000 – 250 mg mL^{-1}) was necessary to kill *P. aeruginosa* (the most resistant between the three tested strains); *S. aureus* showed intermediate sensitivity.

6

1
2
3
4
5
6
7
8
9
10
11
12
13
14
15
16
17
18
19
20
21
22
23
24
25
26
27
28
29
30
31
32
33
34
35
36
37
38
39
40
41
42
43
44
45
46
47
48
49
50
51
52
53
54
55
56
57
58
59
60

Copper was used as a doping agent by Wu, et al. 2013 [73]: only the glass with the highest Cu content (5 mol%) could kill *E coli*.

Considering the works of Wu, et al. and Liu, et al. [52, 65], it is possible to conclude that neither the pure bioglasses nor the magnetic ones possessed any antibacterial potentiality when tested on *E. coli* and *S. epidermidis*. However, they were proved to be excellent carriers for antibiotics such as ampicillin and gentamicin respectively.

Cheng, et al. 2017 [44] proved that the antibacterial activity of any bioglass may be enhanced by functionalizing the surface with some antibacterial agents (metacrilate salts in this case). It was found that all the tested materials (20mg/well) retained the antibacterial activity within 24hrs after the incubation against all the strains (*E. faecalis, S. mutans* and *S. sanguis*). SBG-HA retained it up to 28th day.

DISCUSSION
On the cell types
The aim of this review was to assess advances made in the use of sol-gel derived bioglasses to positively impact on dental pulp cells and periodontal tissues as well as providing bactericidal properties. Considering this scope, it is interesting to note that, despite using dental related key words, out of the 52 articles included in this manuscript, only 30 used dental related cells (DPSCs, PLSCs and GFs) either from rats, mice or humans. 9 articles appeared with BMSCs, 1 using rat-derived osteoblast cells, 1 human osteoblast-like cells and 13 articles involved other cells, mainly MG63 and NIH3T3.

Moreover, it should be pointed out that only 19 studies (of which 13 were strictly related to dental cells) have analysed the effects of the materials at a genetic level by using primary cells and not cell lines which were selected only to check the cytotoxicity of the bioglasses. Hence, it is evident that to study cell-material interaction and be as close as possible to the reality, the choice of appropriate cell type is crucial. It is known that cell lines may act differently with respect to primary cells, so primary cells from the targeted tissue should be the preferred choice prefer rather than cell lines [94]. In particular, it seems that DPSCs might be a good model to study bioglasses for tooth restoration and PDLFs for periodontal tissue regeneration.

On the methodology
To study the effects of the materials on cells, the following methods were the most used: MTT test and AlamarBlue assay to measure cell viability; staining methods (Alizarin red or von Kossa) for cell-mediated mineralization; RT-qPCR to assess the regulatory role of bioglasses on some key genes; and ALP activity as a further marker of differentiation.

The reliability of the methodology used to prove the effectiveness of the material is as important as the choice of the appropriate cell type. The methods can be qualitative or quantitative: in the first case, a visualization approach employing microscope techniques is used; the second aims for a quantifiable measurement of the phenomenon under study. Studying the genes expressed by the cells placed in contact with glasses, is essential to evaluate their ability to promote and to sustain cell differentiation, two steps necessary for tissue repair. Consequently, if it is possible to prove that sol-gel derived bioglasses are able, by dissolving their ions in the media, to sustain cell growth and proliferation, the only studies reporting a gene expression analysis allow to conclude on the actual effectiveness of bioglasses in triggering cells differentiation [42, 51, 52, 63, 64, 68, 81].

It is well-known that proteins may have a different turnover and a different time line expression compared to their mRNAs. Moreover, proteins often need to undergo post-translational modifications that convert an inactive form to an active one. Western blot (WB) offers also the possibility to visualize and study in detail the role of proteins involved in the differentiation process. Of the short-listed papers

7

investigated in this review, only 6 [42, 51, 64, 73, 74, 86] used WB showing an increase of proteins content in the cytosol due to the action of the glasses. This approach completes genomic analysis and allows to explore signaling pathways as MAPK and canonical and non-canonical Wnt signaling. All these data suggest that a deeper proteomic approach could provide a better knowledge of the molecular mechanisms regulating the metabolism of proteins involved in cell differentiation.

Considering these studies all together, a methodology could be suggested allowing a complete evaluation of the effects of any bioglass on cells. An interesting approach would be to combine cytotoxicity assay, gene analysis (especially DMP-1, ALP, DSPP, OCN, OPN and Col1), ALP activity associated to a more qualitative analysis like chromatic staining (alizarin red or Von Kossa). Microscopy techniques and WB could be also used to add strength to the study.

On the composition and technique versatility

The current review highlights that sol-gel bioglasses placed in direct contact with cells or their ion extracts are not cytotoxic. However, there is a limit of dose based on glass composition that cells can tolerate after which they start to suffer. In addition, it is possible to notice that their action is mainly time dependent and, in some cases, both dose and time dependent. It can also be observed that by doping the glass it is possible to improve cell response and to tailor the material to provoke a specific effect. For example, Cu was added to trigger angiogenesis [69, 73], Li [61] or Sr [62, 64, 72] to activate the *wnt*/β-catenin canonical pathway; Zn [53, 68, 69, 74] was proved to play an active role in sustaining and promoting dental pulp regeneration; Mg [58–60] seems to ensure a real improvement of cells proliferation especially when it is incorporated in bioscaffolds; Zr [66] has high corrosion resistance and a remarkable ability for being bonded directly to the bone (a property called osteointegration) and providing biocompatibility and antiallergenic properties; magnetic Fe [65] was used to improve several cellular aspects such as adhesion, proliferation and differentiation.

Within a tissue cells reside in a complex structure made by ECM proteins, water, ions and other elements. The intricate 3D network provides for cells growth and interaction. To mimic that structure and to reproduce as close as possible the real conditions, bioglasses fabricated by sol-gel can be mixed with different polymers to form a scaffold with a 3D structure and interconnected wormholes. In addition, they can be combined with minerals to create glass ceramics with improved mechanical and bioactive properties.

Glasses produced by sol-gel can be also used to make thin films in order to cover substrates like titanium [43, 45] or to form substrate for HA growth [70]. The surface particles can be chemically modified [47] to change the surface charge in order to control directly glass particle-to-cell interaction/internalization/repulsion. This review underlines as well that sol-gel bioglasses, because of their porosity, can be used as carriers for an advanced regeneration therapy: gene therapy by siRNA [46], or using modified virus [93].

All together these results show and prove the great versatility of the sol-gel technique, the different potential applications of the materials and their effectiveness in dental restoration and periodontal tissue regeneration.

On the antibacterial properties

More than 500 different species of bacteria live in a mouth. They comprise both Gram positive and Gram-negative bacteria. The relative equilibrium between a healthy flora and unhealthy one makes the difference between a healthy mouth and a diseased one. Moreover, besides being the main cause of caries lesion and periodontal inflammation, bacteria are also responsible for the secondary caries and the failure of dental restorations. Thus, a material able to control bacterial population could decrease this risk. Ag is a well-known antibacterial agent, and in this review, it is shown as Ag can be

8

successfully incorporated into a sol-gel glass network. Moreover, Ag retains its action even when the glass is mixed with polymers [55, 56, 71], is used as coating agent [54] or is incorporated within a layer of HA growth [70]. Other ions could have bactericidal properties, example being Cu [73] and Mg [58]. In addition, to control bacterial population, bioglasses can be loaded with antibiotics [52, 65]. However, the use of antibiotics instead of Ag may cause the presence of antibiotic-resistant strains. To avoid this, if necessary, the bactericidal effect of the bioglasses could be improved by functionalizing the surface with non-antibiotics antibacterial agents [44].

It is also possible to notice that the antibacterial efficiency of the glass depends not only on the composition [54] but also on the bacterial strain used [56, 58, 63]: some bacteria are more resistant than others. It is possible distinguish sensitive (*E. Coli*), resistant (*E. faecalis*) and intermediate (*P. aeruginosa* and *S. mutans*) bacteria types.

Concerning test methodology, CFU was the most commonly used procedure to assess the eventual antibacterial activity of sol-gel bioglasses. Other approaches like ESEM imagine analysis or crystal violet were used as supporting data.

A good material should combine both cell differentiation ability and antibacterial properties. Only 5 articles have studied both cell effect at a genetic level and antibacterial properties of the same material and it appears that doping bioglasses with therapeutic ions and incorporating them in a biocomposite using polymers could be the right strategy. It might be reasonable to conclude that a double doped sol-gel glass, with Sr and Ag (for instance), in association with a polymer, to make scaffolds, could represent a preferred approach for novel products.

CONCLUSION

The effects of sol-gel derived bioglasses on dental cells and their eventual antibacterial properties for dental restoration and periodontal regeneration applications have been discussed in this systematic review. Moreover, the versatility and the advantages of the sol-gel technique have been demonstrated in terms of method of incorporation (coating film, carrier, etc.) and in tailoring the composition to make it (a) more specific in its effect (doping) and (b) a closer reproduction of the real structure of the tissue (bioscaffolds).

The issue of primary cells vs cell line has been addressed and a possible standard set of experiments to fully test the sol-gel glass effectiveness has been suggested. Furthermore, the possibility to have an ideal material that can combine both tissue regeneration capacity and antibacterial properties has been suggested.

ACKNOWLEDGEMENTS

REFERENCES

1. Cao W, Hench L L. Bioactive materials. Ceramics International 1996 22:493–507.

2. Alves E G L, Serakides R, Rosado I R, Pereira M M, Ocarino N M, Oliveira H P, Góes A M, Rezende C M F. Effect of the ionic product of bioglass 60s on osteoblastic activity in canines. BMC Veterinary Research 2015 11:247.

3. Kargozar S, Baino F, Hamzehlou S, Hill R G, Mozafari M. Bioactive Glasses: Sprouting Angiogenesis in Tissue Engineering. Trends Biotechnol 2018 36:430–444.

4. Baino F, Verné E. Production and characterization of glass-ceramic materials for potential use in dental applications: thermal and mechanical properties, microstructure, and in vitro bioactivity. Applied Sciences 2017 7:1330.

5. Baino F, Fiume E, Miola M, Verné E. Bioactive sol-gel glasses: Processing, properties, and applications. International Journal of Applied Ceramic Technology 2018 15:841–860.

6. Rahaman M N, Day D E, Bal B S, Fu Q, Jung S B, Bonewald L F, Tomsia A P. Bioactive glass in tissue engineering. Acta Biomater 2011 7:2355–2373.

7. Kaur G, Pickrell G, Sriranganathan N, Kumar V, Homa D. Review and the state of the art: Sol-gel and melt quenched bioactive glasses for tissue engineering. J. Biomed. Mater. Res. Part B Appl. Biomater. 2016 104:1248–1275.

8. Jones J R. Reprint of: Review of bioactive glass: From Hench to hybrids. Acta Biomater 2015 23 Suppl: S53–82.

9. Owens G J, Singh R K, Foroutan F, Alqaysi M, Han C-M, Mahapatra C, Kim H-W, Knowles J C. Sol–gel based materials for biomedical applications. Progress in Materials Science 2016 77:1–79.

10. Taherkhani S, Moztarzadeh F. Influence of strontium on the structure and biological properties of sol–gel-derived mesoporous bioactive glass (MBG) powder. J Sol-Gel Sci Technol 2016 78:539–549.

11. Ma J, Chen C Z, Wang D G, Hu J H. Synthesis, characterization and in vitro bioactivity of magnesium-doped sol–gel glass and glass-ceramics. Ceramics International 2011 37:1637–1644.

12. Vallet-Regí M, Salinas A J, Román J, Gil M. Effect of magnesium content on the in vitro bioactivity of CaO-MgO-SiO2-P2O5 sol-gel glasses. J. Mater. Chem. 1999 9:515–518.

13. Maçon A L B, Jacquemin M, Page S J, Li S, Bertazzo S, Stevens M M, Hanna J V, Jones J R. Lithium-silicate sol–gel bioactive glass and the effect of lithium precursor on structure–property relationships. J Sol-Gel Sci Technol 2017 81:84–94.

14. Hattar S, Loty S, Gaisser D, Berdal A, Sautier J-M. Effects of 58S sol-gel glasses on the temporal expression of bone markers during mouse osteoblastic differentiation. J Biomed Mater Res A 2006 76:811–819.

15. Jell G, Stevens M M. Gene activation by bioactive glasses. J Mater Sci Mater Med 2006 17:997–1002.

16. Wu C, Chang J. Mesoporous bioactive glasses: structure characteristics, drug/growth factor delivery and bone regeneration application. Interface Focus 2012 2:292–306.

17. Greenspan D C. Bioactive glass: mechanism of bone bonding. Tandläkartidningen Årk 1999 91:1–32.

18. Bansal R, Jain A. Current overview on dental stem cells applications in regenerative dentistry. J Nat Sci Biol Med 2015 6:29–34.

10

19. Pejcic A, Kojovic D, Mirkovic D, Minic I. Stem Cells for Periodontal Regeneration. Balkan J Med Genet 2013 16:7–12.

20. Sharma S, Srivastava D, Grover S, Sharma V. Biomaterials in Tooth Tissue Engineering: A Review. J Clin Diagn Res 2014 8:309–315.

21. Shue L, Yufeng Z, Mony U. Biomaterials for periodontal regeneration. Biomatter 2012 2:271–277.

22. Kinney J H, Habelitz S, Marshall S J, Marshall G W. The importance of intrafibrillar mineralization of collagen on the mechanical properties of dentin. J Dent Res 2003 82:957–961.

23. Rai M, Deshmukh S, Ingle A, Gade A. Silver nanoparticles: the powerful nanoweapon against multidrug-resistant bacteria. Journal of Applied Microbiology 2012 112:841–852.

24. West N X, Joiner A. Enamel mineral loss. J Dent 2014 42 Suppl 1:S2–11.

25. Nath S G, Raveendran R. Microbial dysbiosis in periodontitis. J Indian Soc Periodontol 2013 17:543–545.

26. Moher D, Liberati A, Tetzlaff J, Altman D G, PRISMA G. Preferred reporting items for systematic reviews and meta-analyses: the PRISMA statement. Ann. Intern. Med. 2009 151:264–269, W64.

27. Wu C, Han P, Xu M, Zhang X, Zhou Y, Xue G, Chang J, Xiao Y. Nagelschmidtite bioceramics with osteostimulation properties: material chemistry activating osteogenic genes and WNT signalling pathway of human bone marrow stromal cells. Journal of Materials Chemistry B 2013 1:876–885.

28. Wu C, Chen L, Chang J, Wei L, Chen D, Zhang Y. Porous nagelschmidtite bioceramic scaffolds with improved in vitro and in vivo cementogenesis for periodontal tissue engineering. RSC Advances 2013 3:17843–17850.

29. Zhou Y, Wu C, Xiao Y. The stimulation of proliferation and differentiation of periodontal ligament cells by the ionic products from Ca7Si2P2O16 bioceramics. Acta Biomater 2012 8:2307–2316.

30. Fan W, Wu D, Ma T, Fan B. Ag-loaded mesoporous bioactive glasses against Enterococcus faecalis biofilm in root canal of human teeth. Dent Mater J 2015 34:54–60.

31. Hyun H K, Salehi S, Ferracane J L. Biofilm formation affects surface properties of novel bioactive glass-containing composites. Dent Mater 2015 31:1599–1608.

32. Kattan H, Chatzistavrou X, Boynton J, Dennison J, Yaman P, Papagerakis P. Physical Properties of an Ag-Doped Bioactive Flowable Composite Resin. Materials 2015 8:4668–4678.

33. Massa M A, Covarrubias C, Bittner M, Fuentevilla I A, Capetillo P, Von Marttens A, Carvajal J C. Synthesis of new antibacterial composite coating for titanium based on highly ordered nanoporous silica and silver nanoparticles. Mater Sci Eng C Mater Biol Appl 2014 45:146–153.

34. Salehi S, Davis H B, Ferracane J L, Mitchell J C. Sol-gel-derived bioactive glasses demonstrate antimicrobial effects on common oral bacteria. Am J Dent 2015 28:111–115.

35. Thampi V V A, Prabhu M, Kavitha K, Manivasakan P, Prabu P, Rajendran V, Shankar S, Kulandaivelu P. Hydroxyapatite, alumina/zirconia, and nanobioactive glass cement for tooth-restoring applications. Ceramics International 2014 40:14355–14365.

36. Zhang J F, Wu R, Fan Y, Liao S, Wang Y, Wen Z T, Xu X. Antibacterial dental composites with chlorhexidine and mesoporous silica. J Dent Res 2014 93:1283–1289.

37. Catauro M, Bollino F, Papale F, Gallicchio M, Pacifico S. Influence of the polymer amount on bioactivity and biocompatibility of SiO2/PEG hybrid materials synthesized by sol-gel technique. Mater Sci Eng C Mater Biol Appl 2015 48:548–555.

38. Catauro M, Bollino F, Papale F, Ferrara C, Mustarelli P. Silica–polyethylene glycol hybrids synthesized by sol–gel: biocompatibility improvement of titanium implants by coating. Materials Science and Engineering: C 2015 55:118–125.

39. Catauro M, Renella R A, Papale F, Vecchio Ciprioti S. Investigation of bioactivity, biocompatibility and thermal behavior of sol-gel silica glass containing a high PEG percentage. Materials Science & Engineering. C, Materials for Biological Applications

11

71

Mater Sci Eng C Mater Biol Appl 2016 61:51–55.

40. Chiang Y C, Lin H P, Chang H H, Cheng Y W, Tang H Y, Yen W C, Lin P Y, Chang K W, Lin C P. A mesoporous silica biomaterial for dental biomimetic crystallization. ACS Nano 2014 8:12502–12513.

41. Catauro M, Bollino F, Papale F. Preparation, characterization, and biological properties of organic–inorganic nanocomposite coatings on titanium substrates prepared by sol–gel. Journal of Biomedical … 2014

42. Ajita J, Saravanan S, Selvamurugan N. Effect of size of bioactive glass nanoparticles on mesenchymal stem cell proliferation for dental and orthopedic applications. Materials Science and Engineering: C 2015 53:142–149.

43. Catauro M, Papale F, Bollino F. Coatings of titanium substrates with xCaO · (1 - x)SiO2 sol-gel materials: characterization, bioactivity and biocompatibility evaluation. Mater Sci Eng C Mater Biol Appl 2016 58:846–851.

44. Cheng X, Qu T, Ma C, Xiang D, Yu Q, Liu X. Bioactive mono-dispersed nanospheres with long-term antibacterial effects for endodontic sealing. J Mater Chem B Mater Biol Med 2017 5:1195–1204.

45. Covarrubias C, Mattmann M, Von Marttens A A, Caviedes P, Arriagada C, Valenzuela F A, Pablo Rodriguez J, Corral C. Osseointegration properties of titanium dental implants modified with a nanostructured coating based on ordered porous silica and bioactive glass nanoparticles. APPLIED SURFACE SCIENCE 2016 363:286–295.

46. El-Fiqi A, Kim T-H, Kim M, Eltohamy M, Won J-E, Lee E-J, Kim H-W. Capacity of mesoporous bioactive glass nanoparticles to deliver therapeutic molecules. Nanoscale 2012 4:7475–7488.

47. Lee J H, Kang M S, Mahapatra C, Kim H W. Effect of Aminated Mesoporous Bioactive Glass Nanoparticles on the Differentiation of Dental Pulp Stem Cells. PLoS One 2016 11:e0150727.

48. Li Y, Liang Q, Lin C, Li X, Chen X, Hu Q. Facile synthesis and characterization of novel rapid-setting spherical sub-micron bioactive glasses cements and their biocompatibility in vitro. Mater Sci Eng C Mater Biol Appl 2017 75:646–652.

49. Mi S-s, Dong Y-m, Gao X-j. [Effects of ionic-dissolution of sol-gel bioactive glasses on human dental pulp cells]. Beijing Da Xue Xue Bao 2012 44:39–42.

50. Tavakolizadeh A, Ahmadian M, Fathi M, Doostmohammadi A, Seyedjafari E, Ardeshirylajimi A. Investigation of Osteoinductive Effects of Different Compositions of Bioactive Glass Nanoparticles for Bone Tissue Engineering. ASAIO J. 2016

51. Wang S, Gao X, Gong W, Zhang Z, Chen X, Dong Y. Odontogenic differentiation and dentin formation of dental pulp cells under nanobioactive glass induction. Acta Biomater 2014 10:2792–2803.

52. Wu C, Chang J, Fan W. Bioactive mesoporous calcium–silicate nanoparticles with excellent mineralization ability, osteostimulation, drug-delivery and antibacterial properties for filling apex roots of teeth. J. Mater. Chem. 2012 22:16801–16809.

53. Bakopoulou A, Papachristou E, Bousnaki M, Hadjichristou C, Kontonasaki E, Theocharidou A, Papadopoulou L, Kantiranis N, Zachariadis G, Leyhausen G, Geurtsen W, Koidis P. Human treated dentin matrices combined with Zn-doped, Mg-based bioceramic scaffolds and human dental pulp stem cells towards targeted dentin regeneration. Dent Mater 2016 32:e159–175.

54. Catauro M, Bollino F, Papale F, Vecchio Ciprioti S. Investigation on bioactivity, biocompatibility, thermal behavior and antibacterial properties of calcium silicate glass coatings containing Ag. JOURNAL OF NON-CRYSTALLINE SOLIDS 2015 422:16–22.

55. Chatzistavrou X, Fenno J C, Faulk D, Badylak S, Kasuga T, Boccaccini A R, Papagerakis P. Fabrication and characterization of bioactive and antibacterial composites for dental applications. Acta Biomater 2014 10:3723–3732.

12

56. Chatzistavrou X, Rao R R, Caldwell D J, Peterson A W, McAlpin B, Wang Y-Y, Zheng L, Christopher Fenno J, Stegemann J P, Papagerakis P. Collagen/fibrin microbeads as a delivery system for Ag-doped bioactive glass and DPSCs for potential applications in dentistry. Journal of Non-Crystalline Solids 2016 432, Part A:143–149.

57. Fan W, Wu D, Tay F R, Ma T, Wu Y, Fan B. Effects of adsorbed and templated nanosilver in mesoporous calcium-silicate nanoparticles on inhibition of bacteria colonization of dentin. Int J Nanomedicine 2014 9:5217–5230.

58. Fooladi A A I, Hosseini H M, Hafezi F, Hosseinnejad F, Nourani M R. Sol-gel-derived bioactive glass containing SiO2-MgO-CaO-P2O5 as an antibacterial scaffold. J Biomed Mater Res A 2013 101:1582–1587.

59. Goudouri O-M, Kontonasaki E, Chrissafis K, Zinn K, Hoppe A, Detsch R, Paraskevopoulos K M, Boccaccini A R. Towards the synthesis of an Mg-containing silicate glass–ceramic to be used as a scaffold for cementum/alveolar bone regeneration. Ceramics International 2014 10 Part B:16287–16298.

60. Goudouri O-M, Vogel C, Grünewald A, Detsch R, Kontonasaki E, Boccaccini A R. Sol-gel processing of novel bioactive Mg-containing silicate scaffolds for alveolar bone regeneration. J Biomater Appl 2016 30:740–749.

61. Han P, Wu C, Chang J, Xiao Y. The cementogenic differentiation of periodontal ligament cells via the activation of Wnt/β-catenin signalling pathway by Li+ ions released from bioactive scaffolds. Biomaterials 2012 33:6370–6379.

62. Hu Q, Jiang W, Chen X, Li Y, Liang Q. The effects of Sr concentration on physicochemical properties, bioactivity and biocompatibility of sub-micron bioactive glasses spheres. Advanced Powder Technology 2017 28:2713–2722.

63. Lee J-H, El-Fiqi A, Mandakhbayar N, Lee H-H, Kim H-W. Drug/ion co-delivery multi-functional nanocarrier to regenerate infected tissue defect. Biomaterials 2017 142:62–76.

64. Lee J-H, Mandakhbayar N, El-Fiqi A, Kim H-W. Intracellular co-delivery of Sr ion and phenamil drug through mesoporous bioglass nanocarriers synergizes BMP signaling and tissue mineralization. Acta Biomater 2017 60:93–108.

65. Liu Y-Z, Li Y, Yu X-B, Liu L-N, Zhu Z-A, Guo Y-P. Drug delivery property, bactericidal property and cytocompatibility of magnetic mesoporous bioactive glass. Mater Sci Eng C Mater Biol Appl 2014 41:196–205.

66. Montazerian M, Yekta B E, Marghussian V K, Bellani C F, Siqueira R L, Zanotto E D. Bioactivity and cell proliferation in radiopaque gel-derived CaO–P2O5–SiO2–ZrO2 glass and glass–ceramic powders. Materials Science and Engineering: C 2015 55:436–447.

67. Salehi S, Gwinner F, Mitchell J C, Pfeifer C, Ferracane J L. Cytotoxicity of resin composites containing bioactive glass fillers. Dent Mater 2015 31:195–203.

68. Theocharidou A, Bakopoulou A, Kontonasaki E, Papachristou E, Hadjichristou C, Bousnaki M, Theodorou G, Papadopoulou L, Kantiranis N, Paraskevopoulos K, Koidis P. Odontogenic differentiation and biomineralization potential of dental pulp stem cells inside Mg-based bioceramic scaffolds under low-level laser treatment. Lasers Med Sci 2017 32:201–210.

69. Theodorou G S, Kontonasaki E, Theocharidou A, Bakopoulou A, Bousnaki M, Hadjichristou C, Papachristou E, Papadopoulou L, Kantiranis N A, Chrissafis K, Paraskevopoulos K M, Koidis P T. Sol-Gel Derived Mg-Based Ceramic Scaffolds Doped with Zinc or Copper Ions: Preliminary Results on Their Synthesis, Characterization, and Biocompatibility. International Journal of Biomaterials 2016 2016:e3858301.

13

70. Tian B, Chen W, Dong Y, Marymont J V, Lei, Yong, Ke Q, Guo Y, Zhu Z. Silver nanoparticle-loaded hydroxyapatite coating: structure, antibacterial properties, and capacity for osteogenic induction in vitro. RSC ADVANCES 2016 6:8549–8562.

71. Wang Y-Y, Chatzistavrou X, Faulk D, Badylak S, Zheng L, Papagerakis S, Ge L, Liu H, Papagerakis P. Biological and bactericidal properties of Ag-doped bioactive glass in a natural extracellular matrix hydrogel with potential application in dentistry. Eur Cell Mater 2015 29:342–355.

72. Wu C, Zhou Y, Lin C, Chang J, Xiao Y. Strontium-containing mesoporous bioactive glass scaffolds with improved osteogenic/cementogenic differentiation of periodontal ligament cells for periodontal tissue engineering. Acta Biomater 2012 8:3805–3815.

73. Wu C, Zhou Y, Xu M, Han P, Chen L, Chang J, Xiao Y. Copper-containing mesoporous bioactive glass scaffolds with multifunctional properties of angiogenesis capacity, osteostimulation and antibacterial activity. Biomaterials 2013 34:422–433.

74. Zhang J, Park Y-D, Bae W-J, El-Fiqi A, Shin S-H, Lee E-J, Kim H-W, Kim E-C. Effects of bioactive cements incorporating zinc-bioglass nanoparticles on odontogenic and angiogenic potential of human dental pulp cells. J Biomater Appl 2015 29:954–964.

75. Zhang Y, Wei L, Wu C, Miron R J. Periodontal regeneration using strontium-loaded mesoporous bioactive glass scaffolds in osteoporotic rats. PloS One 2014 9:e104527.

76. Bae W-J, Min K-S, Kim J-J, Kim J-J, Kim H-W, Kim E-C. Odontogenic responses of human dental pulp cells to collagen/nanobioactive glass nanocomposites. Dent Mater 2012 28:1271–1279.

77. Beketova A, Poulakis N, Bakopoulou A, Zorba T, Papadopoulou L, Christofilos D, Kantiranis N, Zachariadis G A, Kontonasaki E, Kourouklis G A, Paraskevopoulos K M, Koidis P. Inducing bioactivity of dental ceramic/bioactive glass composites by Nd:YAG laser. Dent Mater 2016 32:e284–e296.

78. Catauro M, Nunziante S P, Papale F, Bollino F. Preparation of 0.7 SiO2· 0.3 CaO/PCL hybrid layers via sol–gel dip coating for the surface modification of titanium implants: characterization, bioactivity and biocompatibilty evaluation. Journal of Sol-Gel Science and Technology 2015 76:241–250.

79. Catauro M, Papale F, Piccirillo G, Bollino F. PEG-based organic–inorganic hybrid coatings prepared by the sol–gel dip-coating process for biomedical applications. Polym Eng Sci 2017 57:478–484.

80. Chatzistavrou X, Tsigkou O, Amin H D, Paraskevopoulos K M, Salih V, Boccaccini A R. Sol–gel based fabrication and characterization of new bioactive glass–ceramic composites for dental applications. Journal of the European Ceramic Society 2012 32:3051–3061.

81. Dinesh Kumar S, Mohamed Abudhahir K, Selvamurugan N, Vimalraj S, Murugesan R, Srinivasan N, Moorthi A. Formulation and biological actions of nano-bioglass ceramic particles doped with Calcarea phosphorica for bone tissue engineering. Mater Sci Eng C Mater Biol Appl 2018 83:202–209.

82. El-Fiqi A, Kim J-H, Kim H-W. Osteoinductive fibrous scaffolds of biopolymer/mesoporous bioactive glass nanocarriers with excellent bioactivity and long-term delivery of osteogenic drug. ACS Appl Mater Interfaces 2015 7:1140–1152.

83. Goudouri O M, Kontonasaki E, Papadopoulou L, Kantiranis N, Lazaridis N K, Chrissafis K, Chatzistavrou X, Koidis P, Paraskevopoulos K M. Towards the synthesis of an experimental bioactive dental ceramic. Part I: Crystallinity characterization and bioactive behavior evaluation. Materials Chemistry and Physics 2014 145:125–134.

84. Haghighat A, Mehdikhani-Nahrkhalaji M, Reihany-Mohammadi A, Soltani-Dehnavi S, Eblaghian G. Novel Chitosan/Polyethylene Glycol/Bioactive glass Nanocomposite membrane for Guided Tissue/Bone Regeneration. Int. J. Adv. Biotechnol. Res. 2017 8:787–800.

14

85. Kim D-A, Lee J-H, Jun S-K, Kim H-W, Eltohamy M, Lee H-H. Sol-gel-derived bioactive glass nanoparticle-incorporated glass ionomer cement with or without chitosan for enhanced mechanical and biomineralization properties. Dent Mater 2017 33:805–817.

86. Kim G-H, Park Y-D, Lee S-Y, El-Fiqi A, Kim J-J, Lee E-J, Kim H-W, Kim E-C. Odontogenic stimulation of human dental pulp cells with bioactive nanocomposite fiber. J Biomater Appl 2015 29:854–866.

87. Mota J, Yu N, Caridade S G, Luz G M, Gomes M E, Reis R L, Jansen J A, Walboomers X F, Mano J F. Chitosan/bioactive glass nanoparticle composite membranes for periodontal regeneration. Acta Biomater 2012 8:4173–4180.

88. Nadeem D, Kiamehr M, Yang X, Su B. Fabrication and in vitro evaluation of a sponge-like bioactive-glass/gelatin composite scaffold for bone tissue engineering. Mater Sci Eng C Mater Biol Appl 2013 33:2669–2678.

89. Nezafati N, Moztarzadeh F, Hesaraki S, Moztarzadeh Z, Mozafari M. Biological response of a recently developed nanocomposite based on calcium phosphate cement and sol–gel derived bioactive glass fibers as substitution of bone tissues. Ceramics International 2013 39:289–297.

90. Qu T, Liu X. Nano-Structured Gelatin/Bioactive Glass Hybrid Scaffolds for the Enhancement of Odontogenic Differentiation of Human Dental Pulp Stem Cells. J Mater Chem B Mater Biol Med 2013 1:4764–4772.

91. Saqaei M, Fathi M, Edris H, Mortazavi V. Preparation and biocompatibility evaluation of bioactive glass-forsterite nanocomposite powder for oral bone defects treatment applications. Mater Sci Eng C Mater Biol Appl 2015 56:409–416.

92. Srinivasan S, Jayasree R, Chennazhi K P, Nair S V, Jayakumar R. Biocompatible alginate/nano bioactive glass ceramic composite scaffolds for periodontal tissue regeneration. Carbohydrate Polymers 2012 87:274–283.

93. Zhang Y, Miron R J, Li S, Shi B, Sculean A, Cheng X. Novel MesoPorous BioGlass/silk scaffold containing adPDGF-B and adBMP7 for the repair of periodontal defects in beagle dogs. J. Clin. Periodontol. 2015 42:262–271.

94. Anselme K, Davidson P, Popa A M, Giazzon M, Liley M, Ploux L. The interaction of cells and bacteria with surfaces structured at the nanometre scale. Acta Biomater 2010 6:3824–3846.

FIGURE 1. Study flow for the systematic review as described in the PRISMA statement.

TABLE 1. Quality evaluation of the included studies

Studies	Size of samples	Control group	Number of biological tests performed	Quality evaluation
Wang, et al. 2015 [71]	1	Yes	4	+++
Chatzistavrou, et al. 2014[55]	2	Yes	2	++
Catauro, et al. 2015[54]	4	Yes	2	+
Tian, et al. 2016[70]	1	Yes	5	+++
Fan, et al. 2014[57]	2	Yes	2	++
Chatzistavrou, et al. 2016 [56]	1	Yes	2	++
Lee, et al. 2017 [63]	3	Yes	11	+++
Zhang, et al. 2015[74]	4	Yes	6	++
Theodorou, et al. 2016 [69]	2	Yes	1	+
Bakopoulou, et al. 2016 [53]	1	Yes	6	+++
Theocharidou, et al. 2017 [68]	4	Yes	6	++
Fooladi, et al. 2012 [58]	1	Yes	3	+++
Goudouri, et al. 2014 [59]	5	Yes	2	+
Goudouri, et al. 2016 [60]	1	Yes	3	++
Wu, et al. 2013 [73]	3	Yes	4	++
Wu, et al. 2012 [72]	3	Yes	3	++
Hu, et al. 2017[62]	3	Yes	3	++
Lee, et al. 2017 [64]	2	Yes	7	+++
Salehi, et al. 2015 [67]	8	Yes	1	+
Han, et al. 2012 [61]	3	Yes	5	+++
Liu, et al. 2014 [65]	3	Yes	5	+++
Montazerian, et al. 2015 [66]	4	Yes	1	+
Mi, et al. 2012 [49]	3	Yes	2	+
Lee, et al. 2016 [47]	1	Yes	5	+++
Wang, et al. 2014 [51]	2	Yes	8	+++
Li, et al. 2017 [48]	4	Yes	2	+
Wu, et al, 2012 [52]	1	Yes	4	+++
Cheng, et al. 2017 [44]	4	Yes	3	+
El-Fiqi, et al. 2012 [46]	2	Yes	4	+++
Ajita, et al. 2015[42]	3	Yes	5	+++
Covarrubias, et al. 2016 [45]	1	Yes	3	+++
Catauro, et al, 2016 [43]	5	Yes	1	+
Tavakolizadeh, et al. 2016 [50]	3	Yes	3	++
Nadeem, et al. 2013 [88]	1	Yes	3	+++
Qu, et al. 2013 [90]	4	Yes	6	++
Kim, et al. 2014 [86]	2	Yes	5	++
Kim, et al. 2017 [85]	3	Yes	2	++

1

Bae, at al. 2012 [76]	2	Yes	4	++
Mota, et al. 2012 [87]	2	Yes	5	+++
El-Fiqi, et al. 2015 [82]	4	Yes	7	++
Srinivasan, et al. 2012 [92]	3	Yes	3	++
Beketova, et al. 2016 [77]	4	Yes	2	+
Chatzistavrou, et al. 2012 [80]	2	Yes	3	++
Goudouri, et, al. 2014 [83]	2	Yes	1	+
Haghighat, et al. 2017 [84]	2	Yes	2	++
Catauro, at al. 2015 [78]	5	Yes	1	+
Saqaei, et al. 2015 [91]	3	Yes	1	+
Nezafati, et al. 2013 [89]	2	Yes	2	++
Catauro, et al. 2017 [79]	5	Yes	1	+
Dinesh Kumar, et al. 2017 [81]	1	Yes	4	+++
Zhang, et al. 2014 [75]	2	Yes	2	++
Zhang, et al. 2015 [93]	4	Yes	7	+++

Quality of the study : (+) low, (++) middle and (+++) high

TABLE 2. Details of the sol-gel bioglasses synthezised in the included studies

Studies	Glass composition	Precursor type	Sol-Gel process
Wang, et al. 2015 [71]	SiO₂ 58.6- CaO 24.9- P₂O₅ 7.2 Al₂O₃ 4.2-Na₂O 1.5-K₂O 1.5-Ag₂O 2.1 wt. %	Tetraethoxysilane (TEOS), triethylphosphate (TEP), aluminium nitrate nonahydrate, potassium nitrate, sodium nitrate, calcium nitrate tetrahydrate, silver nitrate	- mix of the sol–gel precursors in DI water and nitric acid - the final solution was converted to a gel by drying at 180 °C - the stabilization was performed by heat treatment up to 700 °C
Chatzistavrou, et al. 2014 [55]	SiO₂ 58.6- CaO 24.9- P₂O₅ 7.2 Al₂O₃ 4.2-Na₂O 1.5-K₂O 1.5-Ag₂O 2.1 wt. %	Tetraethoxysilane (TEOS), triethylphosphate (TEP), aluminium nitrate nonahydrate, potassium nitrate, sodium nitrate, calcium nitrate tetrahydrate, silver nitrate	- mix of the sol–gel precursors in DI water and nitric acid - the final solution was converted to a gel by drying at 180 °C - the stabilization was performed by heat treatment up to 700 °C
Catauro, et al. 2015 [54]	(in mol%): 70% of SiO₂, 30% of CaO and x% of Ag₂O, with 0.08 ≤ x ≤ 0.27	Tetraethoxysilane (TEOS), calcium nitrate tetrahydrate, silver nitrate	- mix of the sol–gel precursors under constant stirring into an ethanol (EtOH) and distilled water solution. - nitric acid was then added as catalyst.
Tian, et al. 2016 [70]	CaO–SiO2–P₂O₅	Tetraethoxysilane (TEOS), triethylphosphate (TEP), calcium nitrate tetrahydrate	- Sol-gel precursors were dissolved into ethanol and nitric acid solution (1 mol). - the mixtures were stirred for 4 h at 40° C and then aged at 50° C to form the sol. - Ti–6Al–4V substrate was dipped into the Sol and then withdrawn at a rate of 1 mm s_1, followed by calcination at 400° C for 1 h.
Fan, et al. 2014 [57]	Ca-Si-Ag	Tetraethoxysilane (TEOS), calcium nitrate tetrahydrate, silver nitrate	- cetyltrimethylammonium bromide (CTAB) and ammonium hydroxide were dissolved in deionized water - stirring for 30 minutes. - Sol-gel precursors were added with vigorous stirring for 3 hours

3

			- the collected products were dried at 60°C overnight and calcined at 550°C for 2 hours.
Chatzistavrou, et al. 2016 [56]	SiO$_2$ 58.6–CaO 24.9–P$_2$O$_5$ 7.2–Al$_2$O$_3$ 4.2–Na$_2$O 1.5–K$_2$O 1.5–Ag$_2$O 2.1 (wt.%)	Tetraethoxysilane (TEOS), triethylphosphate (TEP), aluminium nitrate nonahydrate, potassium nitrate, sodium nitrate and calcium nitrate tetrahydrate, silver nitrate	- mix of the sol–gel precursors in water and nitric acid - the final solution was converted to a gel by drying at 180 °C, while the stabilization was performed by heat treatment up to 700 °C.
Lee, et al. 2017 [63]	85SiO$_2$ – (15- x) CaO – x Ag$_2$O glass composition (x = 0 and 5 wt%)	Calcium nitrate tetrahydrate, TEOS, silver nitrate	Prepared by the ultrasound-assisted sol-gel method using PEG, Ca, and Ag solubilized in 150 ml of anhydrous methanol and at pH 12.5 adjusted using NH$_4$OH. - Polyethylene glycol (PEG) was dissolved in absolute methanol at pH 12.5 - Ca and Zn precursors were added.
Zhang, et al. 2015 [74]	85SiO$_2$-15CaO 85SiO$_2$-13CaO-2ZnO 85SiO$_2$-10CaO-5ZnO (mol%)	Tetraethyl orthosilicate, calcium nitrate tetrahydrate, zinc nitrate hexahydrate	- TEOS was diluted in absolute methanol and was then added dropwise to the Ca/Zn solution. - during mixing, high-power ultra-sonication was applied for 20 min. - after stirring for 24 h, and drying overnight, the gel was thermal treated at 600° C for 5 h.
Theodorou, et al. 2016 [69]	60 SiO$_2$ – 30 CaO – 7.5 MgO – 2.5 ZnO 60 SiO$_2$ – 30 CaO – 7.5 MgO – 2.5 CuO (wt%)	TEOS, calcium nitrate, magnesium nitrate hexahydrate, zinc nitrate hexahydrate or cupric nitrate hemi-pentahydrate	- the glass precursors were added to a mixture of ultrapure H$_2$O and HNO$_3$ (2N) for 30 min at 60°C. - the samples were retrieved from the sol-gel and squeezed to remove the excess of sol from the pores - the samples left to dry out for at least 12 h.
Bakopoulou, et al. 2016 [53]	SiO$_2$= 60, MgO = 7.5, CaO = 30, ZnO = 2.5 (wt%)	Tetraorthosilicate (TEOS) calcium nitrate tetrahydrate, magnesium	- the glass precursors were added to a mixture of ultrapure H$_2$O and HNO$_3$ (2N) for 30 min at 60° C - the samples were left to dry out

4

		nitrate hexahydrate, zinc nitrate hexahydrate	for at least 12 h.
Theocharidou, et al. 2017 [68]	SiO_2 = 60, MgO = 7.5, CaO = 30, and ZnO = 2.5 in wt%	Tetraorthosilicate (TEOS) calcium nitrate tetrahydrate, magnesium nitrate hexahydrate, zinc nitrate hexahydrate	- the sol-gel precursors were mixed in distilled H_2O and 2 HNNO$_3$ for 5h at room temperature - the solution was transferred in a furnace of 60° C for 1 day - it was dried at 120° C for 2 days to produce the xerogel.
Fooladi, et al. 2012 [58]	SiO_2, MgO, CaO, P_2O_5	TEOS, TEP, calcium nitrate, magnesium nitrate hexahydrate	- TEOS was added to 0.1 M HNO3 followed by TEP, calcium nitrate and magnesium nitrate and stirred for 1 h at room temperature - the gel was first dried at 70° C for 3 days and then at 120° C for 2 days. - to stabilize the glass structure, the product was heated at 700° C for 24 h.
Goudouri, et al. 2014 [59]	SiO 70, CaO 30 SiO 70, CaO 10, MgO 20 SiO 70, CaO 20, MgO 10 SiO 60, CaO 30, MgO 10 SiO 50, CaO 30, MgO 20 (mol%)	TEOS, calcium nitrate, magnesium nitrate hexahydrate	- mix of the precursors in water and 2 N HNO$_3$. - aging, drying and chemical stabilization of the prepared sols were carried out in a muffle furnace.
Goudouri, et al. 2016 [60]	(in mol%) 60SiO$_2$-30CaO-10MgO	TEOS, calcium nitrate, magnesium nitrate hexahydrate	- mix of the precursors in deionized water and 2 M HNO$_3$ - after complete dissolution, polyurethane sponges were immersed in the solution for 5 min before drying at room temperature (RT) for 24 h. - aging, drying, and chemical stabilization of the prepared scaffolds were carried out in a muffle furnace - the final stabilization temperature was selected to be

5

Wu, et al. 2013 [73]	Cu 0/Ca 15/P 5/Si 80 Cu 1/Ca 14/P 5/Si 80 Cu 2/Ca 13/P 5/Si 80 Cu 5/Ca 10/P 5/Si 80 (molar ratio)	TEOS, calcium nitrate, TEP, $CuCl_2$	860 °C. - P123 TEOS, Ca, Cu, and TEP, were dissolved in ethanol and 0.5 M HCl at room temperature for 24 h. - the dry samples were calcined at 650° C for 5 h.
Wu, et al. 2012 [72]	Sr 0/Ca 15/P 5/Si 80 Sr 2.5/Ca 14/P 5/Si 77.5 Sr 5/Ca 13/P 5/Si 75 Sr 10/Ca 10/P 5/Si 70 (molar ratio)	TEOS, calcium nitrate, TEP, $SrCl_2$	- P123, sol-gel precursors and 0.5 M HCl were dissolved in ethanol and stirred at room temperature for 1 day - the dry samples were calcined at 700 °C for 5 h.
Hu, et al. 2017 [62]	Sr 0/Ca 16/P 4/Si 80 Sr 6/Ca 10/P 4/Si 80 Sr 15/Ca 1/P 4/Si 80 (mole %)	TEOS, calcium nitrate, TEP, strontium nitrate	- the precursors were mixed in deionized water (DW) and absolute ethanol for 30 min under stirring at 40 °C. - the sol was collected by filtration and rinsed - the sol was heated at 650 °C for 3 h (2 °C/min).
Lee, et al. 2017 [64]	85Si:10Ca:5Sr, mol%	TEOS, calcium nitrate, strontium nitrate	- the sol-gel precursors were dissolved in alkaline methanol (pH 12.5) and left for 24 h of stirring - the collected precipitate was dried at 70 °C overnight. - the organic template, PEG, was removed by calcination of the dried powder at 600 °C for 5 h in air.
Salehi, et al. 2015 [67]	65 mole% SiO_2, 31 mole% CaO, 1 mole% P_2O_5, 3 mole% F	TEOS, calcium methoxyethoxide, TEP	- the sol-gel solutions were prepared in a dry nitrogen environment - water vapor was introduced by aging them in a 100% humidity chamber at 37 °C - after mixing, the resulting glasses were aged for 3 weeks - the networks were stabilized in a furnace at 600 °C over 2 days.
Han, et al. 2012 [61]	Li/Ca/P/Si/ = 0/15/5/80 Li/Ca/P/Si/ = 2/13/5/80 Li/Ca/P/Si/ = 5/10/5/80 Mol%	TEOS, TEP, calcium nitrate and lithium chloride	For porous lithium-containing mesopore-bioglass (Li-MBG) scaffolds: - Li (0,2M – 5%) is incorporated into MBG using co-templates of non-ionic block polymer P123 (EO20-PO70-EO20) and

6

			polyurethane sponges - P123 is used to produce mesoporous structures (mesopore size: around 5 nm) - polyurethane sponges were used to create large pores (large pore size: 300-500 hundred micrometres) For MBG scaffolds: - The polyurethane 5% Li, P123 (Mw=5800), TEOS, Ca, Li, TEP and 0.5 M HCl were dissolved in ethanol and stirred at room temperature for 1 day - sponges (25 ppi) were cleaned and completely immersed into this solution for 10 min - The polyurethane sponges were transferred to a Petri dish to allow evaporating at room temperature for 12 h.
Liu, et al. 2014 [65]	$SiO_2:CaO:P_2O_5:Fe_3O_4 = 75:15:5:5$ Mol% $68SiO_2-27CaO-5P_2O_5$	TEOS, TEP, calcium nitrate and Fe_3O_4 nanoparticles	catalytic hydrolysis of calcium nitrate, tetraethyl orthosilicate, triethyl phosphate and Fe_3O_4 nanoparticles.
Montazerian, et al. 2015 [66]	$61SiO_2-24CaO-5P_2O_5-10ZrO_2$ (molar ratio)	TEOS, TEP, calcium nitrate zirconium oxynitrate	- the polymerization of the precursors was catalysed with a solution of 0.1 Mol·L^{-1} HNO$_3$ - the gels were dried for 3 days at 70 °C and for 1 day at 150 °C
Mi, et al. 2012 [49]	58S and 45S5	Article in Chinese	Article in Chinese - mix of the precursors in a solution containing water, ethanol, 2-ethoxyethanol hexadecyltrimethylammonium bromide (CTAB) and ammonia at room temperature
Lee, et al. 2016 [47]	$SiO_2:CaO=85:15$ in mol%	TEOS, calcium nitrate	- the precipitate was heated to 600°C at a rate of 1 °C/min for 5 hours - the surface was functionalized with– NH2 using 3% APTES at 80 °C for 24 hours dried at 80 °C in a vacuum for 24 h.
Wang, et al. 2014 [51]	Molar composition: 58% SiO_2, 33% CaO,	TEOS, calcium nitrate,	- the sol was produced by the hydrolysis of TEOS, TEP and

7

82

	9% P_2O_5	diammonium phosphate (DAP)	Ca in EtOH and HCl at 70 °C for 3 days - drying at 150 °C for 2 days - the gel was heated for 2 h at 700 °C.
Li, et al. 2017 [48]	40% SiO_2, 55% CaO, 5% P_2O_5 35% SiO_2, 55% CaO, 10% P_2O_5 40% SiO_2, 40% CaO, 20% P_2O_5 (mol%)	TEOS, TEP, Ca-nitrate	- modified sol-gel technique, where dodecylamine (DDA) served as both a catalyst and a template - DDA was dissolved in deionized water (DW) and absolute ethanol - the precursors were added to the above solutions with magnetically stirring at 40 °C for 3 h - the precipitate was collected and freeze-dried for 24 h - the glasses were heated at 650 °C for 3 h (2 °C/min).
Wu, et al, 2012 [52]	Ca-Si	TEOS, Ca-nitrate	- CTAB and NH_4OH were dissolved in double distilled H2O. - TEOS and Ca precursor were added with vigorous stirring for 3 h - the collected powder was dried at 60 C overnight and calcined at 550° C for 2 h
Cheng, et al. 2017 [44]	Ca-Si-P	TEOS, TEP, Ca-nitrate	- method using a CTAB-assistant sol-gel process - CTAB was dissolved in DW and 28% ammonia to form a solution - TEP, Ca and TEOS were added to the solution - the mixture was stirred magnetically for 24 h at room temperature - the gels were removed by calcination at 600 °C for 5 h at a ramping rate of 1 °C/min
El-Fiqi, et al. 2012 [46]	$85SiO_2/15CaO$ (mol%)	TEOS, Ca-nitrate tetrahydrate, 3-aminopropyl triethoxysilane (APTES)	BG nanoparticles were synthesized by an ultra-sound assisted base-catalysed sol–gel method using PEG and CTAB as templates.
Ajita, et al. 2015 [42]	$SiO_2:CaO:P_2O_5 = $ 45:40:15, mol%	TEOS, Ca-nitrate, diammonium hydrogen orthophosphate	- a first solution was prepared by dispersing Ca and TEOS in a mixture of ethanol and water (1:2) at room temperature

8

			- a second solution was prepared by mixing diammonium hydrogen orthophosphate and PEG in water under vigorous stirring - the 2 solutions were mixed - after 48 h of stirring and 24 h of aging at room temperature, the precipitate was dried at 60 °C for 8 h - calcination at 700 °C for 6 h with a temperature increase of 1 °C per minute
Covarrubias, et al. 2016 [45]	Molar composition: $58SiO_2$:$40CaO$:$5P_2O_5$	TEOS, TEP, Ca-nitrate tetrahydrate	- mix of the precursors in water, ethanol and ammonia - the mixture was stirred for 48 h and aged for 48 h at room temperature - the precipitate was separated by centrifugation (12,000 rpm) and calcined at 700°C for 3 h.
Catauro, et al, 2016 [43]	$xCaO \cdot (1-x)SiO_2$ ($0.0 < x < 0.60$) (mol%)	TEOS, Ca-nitrate	TEOS was mixed, under stirring, in ethanol, nitric acid and water, before adding the calcium.
Tavakolizadeh, et al. 2016 [50]	45S, 58S, and 63S compositions	TEOS, Ca-nitrate, TEP	mix of the precursors in water 2N HCl, and ethanol at room temperature for 30 min - the glasses were aged in an oven at 60°C for 48 h and at 130°C for 48 h. - the dried gel was calcined at 600 °C for 2 h.
Nadeem, et al. 2013 [88]	70S30C; 70% SiO_2, 30% CaO – mol%		Commercial sol–gel derived bioactive-glass powder (by Novathera Medcell, UK).
Qu, et al. 2013 [90]	Molar composition: 60% SiO_2, 36% CaO, 4% P_2O_5	TEOS, TEP, Ca-nitrate	- mix of TEOS, TEP and Ca were mixed in a solution composed of water, ethanol and citric acid for 5 h. - drying and calcination at 700°C for 3 h.
Kim, et al. 2014 [86]	Molar ratio: Si/Ca=85/15	TEOS, Ca-nitrate	BGN powders were synthesized by an ultra-sound-assisted base-catalysed sol-gel method where PEG was used as a template.
Kim, et al. 2017 [85]	85% SiO_2–15% CaO (mol%)	TEOS, Ca-nitrate	Spherical bioglass nanoparticles containing were synthesized via a base-catalysed sol–gel approach in the presence of templates.
Bae, at al. 2012 [76]	70% SiO_2–25% CaO–	TEOS, Ca-	For preparation of the bioactive

9

	5% P_2O_5 in mol%	nitrate, TEP	inorganic nanocomponent, electrospinning process was applied. - mix of the precursors in citric
Mota, et al. 2012 [87]	$SiO2:CaO:P_2O_5$ (mol.%) = 55:40:5	TEOS, calcium nitrate tetrahydrate, ammonium phosphate dibasic	acid, absolute ethanol and ammonium hydroxide - the PEG was used as the surfactant. - after drying, the glasses were sintered at 700 °C for 5 h.
El-Fiqi, et al. 2015 [82]	75%SiO_2/25%CaO (mol %)	TEOS, calcium nitrate tetrahydrate	The bioglasses were prepared using an ultrasound assisted base-catalysed sol−gel method.
Srinivasan, et al. 2012 [92]	$CaO-SiO_2-P_2O_5$	TEOS, calcium nitrate tetrahydrate, ammonium phosphate dibasic	- TEOS and Ca precursor were dissolved in a mixture of distilled water and ethanol - stirring at room temperature - TEOS and $NH_4H_2PO_4$ were added
Beketova, et al. 2016 [77]	SiO_2 60 wt%, CaO 36 wt% and P_2O_5 4 wt%	TEQS, TEP, calcium nitrate tetra-hydrate	- mix of distilled water, nitric acid, TEOS, TEP and calcium nitrate - the sol was sintered at 60 ◦C for 55h, - drying and heating at 700 ◦C for 18h
Chatzistavrou, et al. 2012 [80]	SiO_2-58, CaO-33, P_2O_5-9 in wt%	TEOS, TEP, Ca-nitrate tetra-hydrate	-mix of DI water, HCl, TEOS, TEP and calcium nitrate tetra-hydrate at 60°C for 55 h
Goudouri, et, al. 2014 [83]	% weight ratio: $SiO2:CaO:P_2O_5$ = 60:36:4	TEOS, TEP, Ca-nitrate tetra-hydrate	- mix of TEOS, nitric acid, TEP and calcium nitrate in 9.5 mL distilled H_2O. - the sol was placed inside a furnace and heated at 60 C - the gel was heated at 700° C
Haghighat, et al. 2017 [84]	45S5	TEOS, TEP, Ca-nitrate	- mix of TEOS ethanol, HCl and deionized water - TEP and calcium nitrate were added - stirring for 1 h, - aging at 60 ℃ for 52 h - drying for 48 h at130℃. - calcination of the dried for 1 h at 600℃
Catauro, at al. 2015 [78]	70SiO_2-30CaO, mol%	TEOS, calcium nitrate tetrahydrate	To prepare the inorganic matrix, a solution of calcium in ethanol was added to a mixture of TEOS, ethanol nitric acid and water.
Saqaei, et al. 2015 [91]	57.72% SiO_2, 35.09% CaO, 7.1% P_2O_5 in molar %	TEOS, Ca-nitrate, TEP	- TEOS was added to water containing 2 N HCl for 30 min under stirring. - TEP and calcium nitrate were

10

85

			incorporated. - the mixture was stirred for 1 h. and placed in an oven for aging treatment at 60 °C for 44 h. - the dried gel was calcined at a rate of 5 °C/min up to 600 °C for 1 h.
Nezafati, et al. 2013 [89]	SiO2–CaO–P$_2$O$_5$	TEOS, TEP, Ca-nitrate	- mix of TEOS, water, ethanol (2:1 for water/TEOS and 4:1 for ethanol/ TEOS), HCl (pH=1.5) - TEP and calcium nitrate was used to obtain the sol. - the fibre-shaped gel was produced by extruding the viscous gel through a thin syringe with needle's inside diameter of 0.01 mm - the fibres were then dried for 24h at 343 K - the fibres were heated to 973 K at the rate of 3 Kmin^{-1} - The fibres were sintered and stabilized at 973K for 24 h
Catauro, et al. 2017 [79]	Silica-based material	TEOS	- TEOS was used as precursor of the inorganic phase. - TEOS was added to a solution containing ethanol, distilled water, and nitric acid
Dinesh Kumar, et al. 2017 [81]	SiO$_2$:CaO:P$_2$O$_5$=55:40:5 Mol%	TEOS, Ca-nitrate, diammonium hydrogen orthophosphate	- a first solution was prepared by mixing and dispersing calcium nitrate and TEOS into a solution of ethanol and water - a second solution was prepared by mixing diammonium hydrogen orthophosphate with 2% of poly ethylene glycol and NH$_3$ (pH 10) - the 2 solutions were refluxed under stirring and aged for 24 h at room temperature. - the precipitate was dried under vacuum, lyophilized and calcined at 700 °C for 6 h.
Zhang, et al. 2014 [75]	Sr/Ca/P/Si/ = 5/15/5/75, molar ratio	TEOS, calcium nitrate tetrahydrate, strontium chloride, TEP	- dissolution of Sr, P123, TEOS, Ca, TEP, and 0.5 M HCl in ethanol - stirring at room temperature for 24 h - after driying, the samples were calcined at 700 °C for 5 h.
Zhang, et al. 2015 [93]	Molar ratio: Si/Ca/P =	TEOS, calcium	- dissolution of pluronic P123

11

80/15/5	nitrate tetrahydrate, TEP	(Mw = 5800;), TEOS, Ca, TEP, and 0.5 M HCl in ethanol - stirred at room temperature for 1 day - the solution was introduced into a Petri dish for an evaporation-induced self-assembly process - calcination of the dry gel at 700° C for 5 h.	

APTES: (3-Aminopropyl) triethoxysilane; BGs: bioglasses; CTAB: cetyltrimethylammonium bromide; DDA: dodecylamine; DW: deionized water; EtOH: ethanol; GC: glass ceramic; MBG: mesoporous bioactive glass; PEG: polyethylene glycol; TEOS: Tetraethoxysilane; TEP: triethylphosphate

TABLE 3. Further details of studies examining the effects of doped-glasses on cells

Doping agents	Cell type	Effect	Expected	Reference articles
Ag	DPSC	Undiluted extract was slightly toxic, enhanced cell mineralization and DMP-1, ALP, DSPP and RUNX2 gene expression	No cytotoxicity	Wang, et al. 2015 [71]
	DPSC	Ag-BG/ECM ratio mattered more than extract dilution		Chatzistavrou, et al. 2014 [55]
	NIH3T3	Lowest concentration of Ag (from 0.08 up to 0.27 mol%) showed highest cell viability		Catauro, et al. 2015 [54]
	BMSC	Cristal orientations affected cells attachment and growth, enhanced cell mineralization, ALP activity and Col1, OPN and OCN gene expression		Tian, et al. 2016 [70]
	BMSC	Ag by adsorption was more cytotoxic than by templating		Fan, et al. 2014 [57]
	DPSC	Differentiating on BG-Ag with polymer		Chatzistavrou, et al. 2016 [56]
	DPSC	Deferrization in odontoblasts after 7 and 21 days of exposure at 160µg/mL by DMP and DSPP enhanced gene expression. ALP and Alizarin red stain proved mineral deposition after one week		Lee, et al. 2017 [63]
	DPSC	Highest effect after 14 days: it enhanced cell mineralization, ALP activity and DMP-1, DSPP, integrins and angiogenetic genes.		Zhang, et al. 2015 [74]
	DPSC	Highest proliferation after 7 days		Theodorou, et al. 2016 [69]
Zn	DPSC	No toxicity was showed up to day 12: it enhanced ALP activity and DSPP, BMP-2, ALP, OCN, RUNX2 gene expression	No cytotoxicity and time dependent enhanced cell attachment, growth and mineralization	Bakopoulou, et al. 2016 [53]
	DPSC	The bioceramic was not toxic for cells after 4 days of exposure and was proved to promote cell proliferation and differentiation by increasing odontogenetic-related markers BMP-2, DSPP, Osx and Runx2 after 7 and 14 days. ALP activity was significantly increased at 3 and 7 days and newly formed Ca-P tissue was formed on the		Theocharidou, et al. 2017 [68]

13

		SC/DPSC complexes after 28 days of culture		
Mg	Cho	No significant difference was detected between test and control: none cytotoxicity was found		Fooladi, et al. 2012 [58]
	ST2	No significant difference was noticed between material and control: no cytotoxicity was found	No cytotoxicity	Goudouri, et al. 2014 [59]
	ST2	Mitochondrial and LDH activity values of coated scaffolds were higher than values of noncoated ones; EG coated scaffolds presented highest cell viability.		Goudouri, et al. 2016 [60]
Cu	DPSC	Time dependence response, cells viability improved after 3 days	No cytotoxicity, expression of angiogenetic related genes	Theodorou, et al. 2016 [69]
	BMSC	Best performance for direct contact after 7 days with no differences between the glasses. For the extract 12.5mg/mL seemed to be the limit. It enhanced ALP activity and ALP, OPN and OCN gene expression		Wu, et al. 2013 [73]
	PDLC	Time dependence response and no cytotoxicity: it enhanced ALP activity and ALP, RUNX2, Col1m OPN and CEMP1 gene expression	No cytotoxicity and activation of *wnt* pathway	Wu, et al. 2012 [72]
Sr	DPSC	The Sr-SBG extracts (1mg/mL) promoted significantly cell viability after 3 days. The best performer was the one with 6mol% of Sr and the ALP activity was found increased after 7 and 14 days. New mineralized tissues were secreted after 21 days.	No cytotoxicity	Hu, et al. 2017 [62]
	BMSC	The co-delivered system (up to 320µg/mL) enhanced differentiation and maturation of cells by significantly increasing expression of osteo/odontogenic genes, alkaline phosphatase activity, and mineralization of cells after 14 and 21 days: the stimulation is a result of a synergism of Sr and Phenamil, through a Trb3-dependent BMP signalling pathway. In vivo, the osseous-dentinal hard tissue formation is significantly stimulated by the Sr/Phenamil delivery.	No cytotoxicity and bone development pathway activation	Lee, et al. 2017 [64]
F	OD-21	Toxicity of composite depended on extract dilution, time curing, and pre-extraction.	Cytotoxicity composition independent	Salehi, et al. 2015 [67]

14

89

Li	PDLC	It enhanced cell proliferation, mineralization and ALP activity, improved ALP, OCN, CEMP1, OPN, and *wnt* related gene expression	No cytotoxicity, activation of *wnt* pathway	Han, et al. 2012 [61]
Magnetic iron	BMSC	Cell viability enhanced after 7 days	Time dependence	Liu, et al. 2014 [65]
Zr	MG63	GC-Zr enhanced cells proliferation after 6 days	Time dependence no cytotoxicity	Montazerian, et al. 2015 [66]

15

90

TABLE 4. Summary of studies examining the antibacterial effect of sol-gel glasses

Glass system	Dopant	Additional components	Bacterial strains	Tests	Effects	Reference articles
Si-Ca-P	Ag	ECM	*Streptococcus mutans* *Lactobacillus casei*	CFU counting for direct contact	No colonies were found in the presence of Ag-BG/ECM (10mg/mL)	Wang, et al. 2015 [71]
Si-Ca-P	Ag	ECM	*Escherichia coli* *Enterococcus faecalis*	CFU counting for direct contact	No colonies were found in the presence of BG and BG 50/50 (5mg)	Chatzistavrou, et al. 2014 [55]
Si-Ca-P	Ag	Collagen/fibrin	*Escherichia coli* *Streptococcus mutans* *Enterococcus faecalis*	CFU counting for direct contact	Antibacterial effect was strongly enhanced by the Ag (2.5 mg/ml): *E. faecalis* more resistant	Chatzistavrou, et al. 2016 [56]
Si-Ca	Ag	Titanium coating	*Staphylococcus aureus*	ESEM image analysis	Antibacterial activity of the film increased by increasing Ag content (8 mm diameter discs)	Catauro, et al. 2015 [54]
Si-Ca-P	Ag	HAC	*Staphylococcus aureus* *Escherichia coli*	CFU counting for direct contact	No bacteria were found on Ag substrate	Tian, et al. 2016 [70]
Si-Ca	Ag		*Enterococcus faecalis*	CFU counting for direct contact	The Ag-MCSNs-A and Ag-MCSNs-T showed better antibacterial properties than the MCSNs (20 mg/mL of Ag-MCSN suspension)	Fan, et al. 2014 [57]

16

91

Si-Ca	Ag		*Escherichia coli* *Enterococcus faecalis* *Streptococcus oralis* *Streptococcus mutans*	PrestoBlue assay and CFU counting for direct contact	They found that the Ag-free glass was unable to kill any of those bacteria. Ag-doped glass efficiency was strain specific and concentration dependent (40, 80, 160 µg/mL): E. coli and *S. oralis* were the most sensitive; whereas, *S. faecalis* was killed only when exposed to the highest concentration. *S. mutans* was shown to be highly resistant. The addition of tetracycline or chlorohexidine equally killed both *S. faecalis* and *S. mutans*.	Lee, et al. 2017 [63]
Si-Ca-P	Mg		*Staphylococcus aureus,* *Escherichia coli* *Pseudomonas aeruginosa*	MBC and MIC determination of glass particles	Antibacterial activity was detected for high concentrated extract (including 1000, 500, 250, 125, 62.5, 31.25, 15.62, 7.81, 3.9, and 1.59	Fooladi, et al. 2012 [58]

17

Si-Ca-P	Cu	*Escherichia coli*	Counting of number of living bacteria	mg/mL): it was less effective on *S. aureus* and more on *E. coli* 5Cu-MBG) (scaffolds with the size of 5 x 5 x 5 mm in 5 mL) showed high antibacterial activity over time	Wu, et al. 2013 [73]
Si-Ca		*Escherichia coli*	Counting of number of bacteria	None antibacterial property of the glass was detected, but good drug delivery system for AMP (25 mg MCS particles soaked in 5 mg mL-1 ampicillin-PBS)	Wu, et al. 2012 [52]
Si-Ca-P	Fe3O4	*Staphylococcus epidermidis*	CLSM imagine analyses, Cristal violet, Spread plate method	None antibacterial property of the glass was detected, but good drug delivery system for GENT (15 mm discs were soaked in 0, 1, 2, 4, 8, 16, 32, 64, 128, 256, 512, or 1024 µg/mL GENT)	Liu, et al. 2014 [65]
Si-Ca-P	Functionali	*Enterococcus*	DCT method	All the tested	Cheng, et al.

18

| zed with methacrylat e salts | *faecalis Streptococcus mutans Streptococcus sanguis* | and CFU counting | materials (20mg/well) retained the antibacterial activity within 24hrs after the incubation against all the strains. SBG-HA retained it up to 28th day. | 2017 [44] |

AMP : ampicillin; BG: bioglass; CFU : colony forming unit ; DCT : distal tip cell; ECM : extracellular matrix ; ESEM: environmental scanning electron microscope ; GENT: gentamicin; HAC : hydroxyapatite cement ; MBC : minimum bactericidal concentration; MCSNs : mesoporous calcium-silicate nanoparticles; MIC: minimum inhibitory concentration; MBG : mesoporous bioactiveglass;
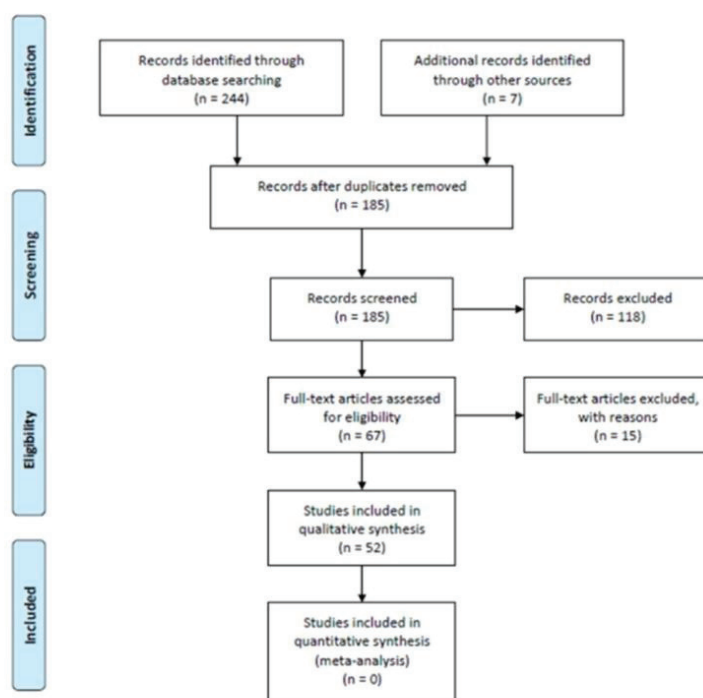
19

94

1
2
3
4
5
6
7
8
9
10
11
12
13
14
15
16
17
18
19
20
21
22
23
24
25
26
27
28
29
30
31
32
33
34
35
36
37
38
39
40
41
42
43
44
45
46
47
48
49
50
51
52
53
54
55
56
57
58
59
60

FIGURE 1. Study flow for the systematic review as described in the PRISMA statement.

66x66mm (220 x 220 DPI)

95

4.2 Research article: Bioactivity evaluation of collagen-based scaffolds containing a series of Sr-doped melt-quench derived phosphate-based glasses

Vincenzo Farano, Mark Cresswell, Kerstin Gritsch, Phil Jackson, Nina Attik, Brigitte Grosgogeat, Jean-Christophe Maurin (Accepted: 18 June 2018)

Objectives: Due to their osteoconductive and osteoinductive properties, BGs have been widely used in tissue engineering. However, the effects of a long-term exposure to such resistant materials are still debated. Phosphate-based glasses have been attracting attention due to their possible medical applications arising from unique dissolution characteristics in the human body leading to the possibility of new tissue regeneration. The two main methods of elaboration are melt-quench and sol-gel. However, due to the challenges that the sol-gel route provides, the MQ technique remains the favourite route for those materials. In this study, the effects of increasing Sr concentration at the expense of Ca on phase and solubility in water of a series of Sr-doped PBGs made by melt-quench technique is reported. Afterwards, to mimic the natural 3D structure of tissues, Sr-doped PBG particles were incorporated in collagen based-scaffolds. The influence that the interaction between collagen fibres could have had on the dissolution properties of those particles compare with the row glasses was investigated. The HA formability of such composite materials was tested by soaking the scaffolds in SBF for one and three weeks.

Methods: The series of S-doped glass with composition $(P_2O_5)53–(CaO)(32-x)–(Na_2O)15–(SrO)x$, where x = 0, 5, 10 or 15 (mol%) was made by melt-quench technique. The phase was analysed by XRD. To study the dissolution behaviour, the glass particles were soaked in UPW at the concentration of 1mg/mL for several weeks. After, the conditioned media were filtrated and diluted 5 times before the analysis. The glass particles ranging between 0.1 and 10 μm were incorporated into collagen scaffolds at 1:1 wt ratio by freeze-drying and crosslinked using EDC and NHS. Their dissolution kinetics was studied by soaking 170 mg of collagen-based scaffolds in 20 mL of ultra-pure water. To test the HA formability, 170 mg of scaffolds were soaked in 20 mL of simulated body fluid. After drying, the soaked scaffolds were submitted to SEM/EDX analysis.

Results and Discussions: It was found that Sr did not act as a nucleation sites for crystal growth. However, it influenced the dissolution kinetics of the glasses: by increasing the concentration of Sr in the glass composition, the rate the glass dissolved reduces. It was find as well that the collagen fibres interact with the glass by-products (pyrophosphates and Na

97

ions) altering the dissolution profiles of the glasses. Furthermore, the EDX analysis revealed the presence of deposits rich in Ca and P on the surface of the scaffolds after soaking them in SBF. The Ca/P ratio of such precipitate was 1.68 (mol%) in good agreement with the HA ratio being 1.67 (mol%). For those reasons, their possible application in restorative dentistry is proposed.

BIOMATERIALS SYNTHESIS AND CHARACTERIZATION

Original Research

Bioactivity evaluation of collagen-based scaffolds containing a series of Sr-doped melt-quench derived phosphate-based glasses

Vincenzo Farano[1,2] · Mark Cresswell[3] · Kerstin Gritsch[1,2,4] · Phil Jackson[3] · Nina Attik[2] · Brigitte Grosgogeat[1,2,4] · Jean-Christophe Maurin[1,2,4]

Abstract

Phosphate-based glasses have been attracting attention due to their possible medical applications arising from unique dissolution characteristics in the human body leading to the possibility of new tissue regeneration. In this study, the leaching kinetics of a series of melt-quenched Sr-doped phosphate glasses are presented. Regardless of the presence of Sr, all the glasses have an initial linear and sustained release of the ions followed by a plateau. To guarantee proper nutritional support to the growing tissue during regeneration and to mimic the 3-dimensional architecture of tissues, organic scaffold systems have been developed. However, their poor mechanical strength has limited their application. To overcome this problem, cross-linkers can be used although this then limits the solubility of the materials. To succeed in dealing with such a limitation, in this paper, by freeze-drying, the aforementioned soluble melt-quenched phosphate glasses were combined as powders with collagen fibres from bovine achilles tendon to make degradable scaffolds. The scaffolds were characterized by SEM, EDX and BET. Changes to the dissolution behaviour of the glasses arising from the presence of collagen interacting with the ions leached were reported. Furthermore, the ability of the scaffolds to induce hydroxyapatite (HA) formation was evaluated: one the elaborated scaffold could grow an HA-like layer after a week in SBF. Based on the results obtained, a possible application in restorative dentistry is proposed for one or more materials.

Graphical Abstract
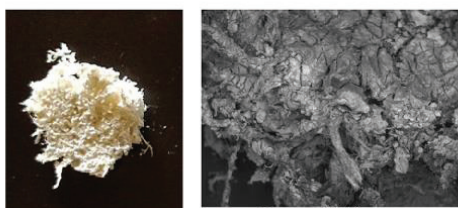
✉ Jean-Christophe Maurin
  jean-christophe.maurin@univ-lyon1.fr

1   Université Claude Bernard Lyon 1, CNRS, Laboratoire des
    Multimatériaux et Interfaces, Université Lyon,
    Villeurbanne, France

2   Faculté d'Odontologie, Université Claude Bernard Lyon 1,
    Lyon, France

3   Lucideon Limited, Queens Road, Penkhull, Stoke-on-Trent,
    Staffordshire ST4 7LQ, UK

4   Service d'Odontologie, Hospices Civils de Lyon, Lyon, France

1 Introduction

Since Professor. L. Hench proposed the first bioactive glass material in 1969 [1, 2], the majority of the glasses and glass-ceramics that have been researched for medical applications have been based on a silica network. However, due to their low and slow solubility in human body fluids they are mainly used as long-term implants for tissue restoration. Nowadays the trend is to develop bioactive materials that can fully dissolve in biological solutions to be subsequently

⌐Ø Springer

99

$Q^3 \nu(P{=}O){=}1390 \text{ cm}^{-1}$ $Q^2 \nu(PO_2){=}1180 \text{ cm}^{-1}$

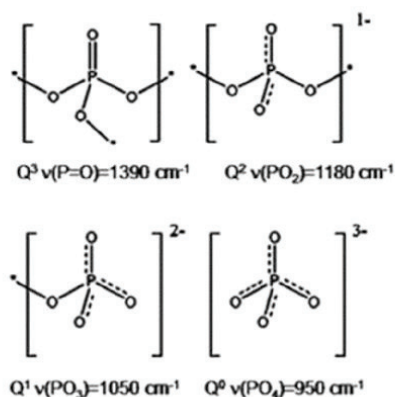$Q^1 \nu(PO_3){=}1050 \text{ cm}^{-1}$ $Q^0 \nu(PO_4){=}950 \text{ cm}^{-1}$

Fig. 1 Phosphate structure in the glasses, as defined by the Qi terminology

totally replaced by new regenerated tissue. These materials are classified as bioresorbable [3].

Phosphate-based glasses (PBGs) represent an interesting class of biomaterials because of their unique property to fully dissolve in aqueous solutions [4, 5]. More interesting, by adding modifier oxides (e.g. CaO and Na_2O) it is possible to control and tailor the dissolution rate of the glass network in agreement with the targeted tissue and its rate of turnover [6]. Moreover, the oxide and anionic species present in glasses from the ternary system P_5O_2-CaO-Na_2O are naturally present in the human body thus avoiding eventual inflammatory responses [7, 8] and making them biocompatible. Furthermore, they can be used as a drug delivery system [9] or doped with ions for triggering important biological functions [10], enhancing cytocompatibility [11] or exerting antibacterial function [12]

In recent times, strontium has attracted a lot of attention as a glass doping agent for its interesting therapeutic properties. It has been shown to promote new bone formation by triggering the differentiation of bone marrow stromal cells (BMSCs) in osteoblasts through the activation of ERK1/2 and the Wnt pathway. In addition, due to its high similarity with Ca (especially in term of size and charge), it can activate Ca-dependent signals like, for instance, the CaSR downstream signalling pathways resulting in osteoclasts apoptosis and bone resorption reduction [13]. Moreover, as Sr-ranelate, it has been shown to be effective in treating osteoporosis [14]. Furthermore, silica-based glasses doped with Sr have already been shown to promote cell differentiation and proliferation [15].

The basic unit in the phosphate glass network is the tetrahedral entity $(PO_4)^{3-}$, possessing three potential sharing (or bridging) oxygens. Based on the covalent oxygen bonds, phosphate is present in different anion forms

classified in agreement with the Q^i terminology, where "i" represents the number of bridging oxygens (i.e. P–O–P bonds). The Fig. 1 (adapted from [16]) shows the phosphate ions in the different conformations: Q^0 is the orthophosphate, Q^1 the pyrophosphate, Q^2 the metaphosphate and Q^3 the ultraphosphate configuration.

The main route to produce PBGs is by melt-quenching (MQ), however, the high temperature represents a drawback because bioactive molecules cannot be incorporated at such high temperatures. An alternative way is the sol–gel method (SG). This low temperature process allows for a more homogenous material with improved textural features and for incorporating bioactives during the synthesis [17]. On the other hand, phosphate glass sol–gel processing is more demanding than for silicates: despite the basic unit in the glass network being tetrahedral, as for silica $(SiO_4)^{4-}$, the monophosphate is not as good a network former as silica [18] due to different chemical behaviour in solution [19]; in addition, much less work has been done on the sol–gel synthesis of phosphates compare with silicates.

More recently, attempts to understand the organization of the atoms in the fused phosphate glass networks have been made using molecular dynamic (MD) methods [20–22]. A ternary metaphosphate glass is dominated by Q^2 units connected by corners, as chains or rings, terminating by Q^1 or branched Q^3 tetrahedra. The modifiers, Na and Ca, coordinate with their non-bridging oxygen (NBO) nearest neighbours by forming corners or edge-shearing tetrahedra acting as bridges and connecting the chains.

In order to demonstrate changes in the glass structure associated with the two different processing techniques, comparison studies between sol–gel (SG_- and melt quench (MQ)-derived phosphate-based glasses with the same composition have been performed [23–26]. Despite some variations in density and prominence of the Q^2 units (due to the organics, temperature and network densification), all the studies agree (based on FTIR and NMR analysis) that, at the atomic scale, both structures are almost identical except for the greater presence of the OH groups which terminate the SG glass chains reducing the connectivity.

In the last few years, tissue engineering has offered new possibilities to repair damaged tissues. One of those contemplates the opportunity to use scaffolds (SCFs) for tissue regeneration [27]. An ideal scaffold should be biocompatible, promote cell adhesion and ideally differentiation at the genetic level, have mechanical properties matching those of the host tissue, bond to the host tissue, possess a degree of porosity that can allow the spread of nutrients and oxygen to the regenerating tissue and, finally, have the same turnover as the target tissue (bio-resorbable).

Collagen 1 (Col1) is one of the most frequently represented proteins in all human tissues and naturally offers a support for cell adhesion and differentiation. When used to

make scaffolds, Col1 fibrils pack into randomly orientated fibres to form an interconnected porous network that in turn results in a sponge-like material. For these reasons, Col1 is one of the most commonly used naturally based materials to produce scaffolds for tissue engineering. However, these scaffolds suffer from weak mechanical properties. A conventional method of improving the mechanical properties relies on chemical cross-linking, which could compromise degradation and biological function [28].

To overcome this problem, in this study, a series of soluble Sr-doped melt-quenched derived phosphate-based glasses were added to the collagen scaffolds. The aim was to evaluate the HA formability of the combined scaffolds by soaking them in SBF. Prior, the glasses were characterized by XRF, XRD and FTIR. In addition, the effect of increasing Sr at the expense of Ca on the dissolution behaviour of the glass series was studied. Furthermore, the impact that incorporating glass powders in the scaffolds and using cross-linkers has on the solubility properties of the glasses was studied. In the end, a possible application in dentistry for one or more scaffold materials was proposed based on the results obtained.

2 Materials and methods

2.1 Materials

For the MQ preparation, the following raw materials were used: calcium carbonate ($CaCO_3$), sodium carbonate (Na_2CO^3), strontium carbonate ($SrCO^3$) and mono-ammonium phosphate ($NH_4H_2PO_4$). Melting was undertaken in quartz crucibles (QZ-crucible).

For the scaffold preparation, collagen fibres from bovine achilles tendon (Sigma), N-(3-(dimethylamino)propyl)-N′-ethylcarbodiimide hydrochloride (EDC, Sigma) and N-hydroxysuccinimide (NHS, Sigma) were used.

2.2 Synthesis of melt-quenched glasses

The melt-quenched glasses were prepared as follows. A batch calculation was performed to determine the wt% of the raw materials needed to deliver the final target oxide formulation (P_2O_5)53–(CaO)(32-x)–(Na_2O)15–(SrO)x, where x = 0, 5, 10 or 15. The raw materials were weighed out and manually mixed to generate a homogeneous blend. The QZ-crucible was pre-heated at 1150 °C and the mixed powder was poured in little by little. When all the powder was in the crucible, the temperature was raised up to 1250 °C for about 4 h to allow a proper homogenisation. After 4 h, the molten mixtures were quickly quenched on a steel plate. After quenching, the obtained glass was milled to a particle size ranging between 20 and 200 μm using a TEMA Mill machinery model T 750 k.

2.3 Glass characterization

2.3.1 Semi-quantitative X-ray fluorescence (XRF)

This analysis was performed using a Panalytical Axios XRF Spectrometer. A small amount of material was smeared onto a filter paper and presented to the XRF spectrometer. The analysis was run using the preinstalled semi-quantitative XRF package.

2.3.2 X-ray diffraction (XRD)

This analysis was performed using a Bruker D8 Advance run in Bragg-Brentano para-focussing mode. Copper K alpha radiation was used throughout. A fixed divergence slit of 0.3 degrees was used, with a fixed 3 degree receiving slit employed prior to the detector. A Lynxeye 1-d detector was used covering a 3-degree two theta window. 192 channels were simultaneously collecting the data. A 0.02-degree step size was used from 5 to 65 degrees two thetas with a dwell time per step of 0.5 s. A 20-micron thick nickel foil was used to monochromat the copper K Alpha X-ray beam. The samples were continuously rotated with respect to omega at a rate of 15 times per minute throughout the data collecting procedure. Bruker Diffrac Eva was used to examine the collected diffraction trace.

2.3.3 Fourier Transform Infrared Spectroscopy (FTIR)

The infrared transmittance spectra were recorded using an SAFAS Monaco IR700. The analytical software used was SAFAS SP2000. The glass powders were placed in the centre of the sample holder (on the prism) and a pressure of 12 kg was applied before measuring. The infrared spectra were recorded in the range from 4000 to 600 cm^{-1} in transmission mode.

2.3.4 pH measurement

The ground glass powders were weighed to create a suspension concentration of 1 mg/mL: specifically, 25 mg of powder were soaked in 25 mL of ultra-pure water. The system (powder + water) was sealed in a Falcon tube and left shaking in an incubator-shaker at 37 °C, 120 rpm for 2, 6, 24, 48, 168, and 504 h. For each time point, to remove the glass particles, the solutions were filtered twice using a 0.2 μm filter; the conditioned waters were collected in clean tubes and the pH measured using a Hanna pH-meter.

2.3.5 Inductively coupled plasma (ICP)

After recording the pH, the solutions created as described in the Section 2.3.4 were sent for ICP analysis. Before
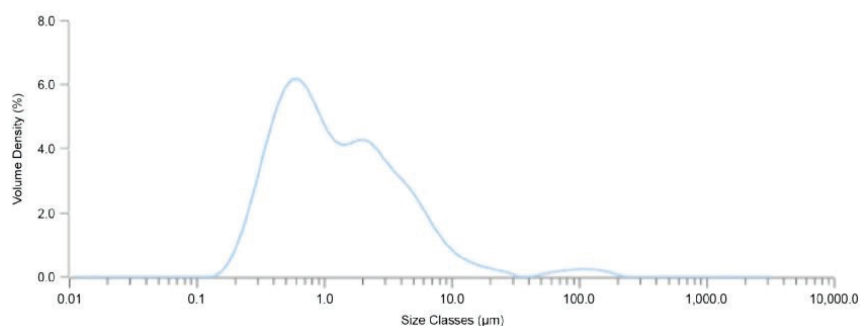
101

Fig. 2 Size distribution of the glass particles used for the scaffold elaboration

performing the analysis on the samples, a calibration curve was made using the following ICP standards: phosphorus standard for ICP (Sigma), sodium standard for ICP (Sigma), strontium standard for ICP and calcium standard for ICP (Sigma). A 0.6% HNO_3 solution was made (form a 65% solution, ACROS Organics) by diluting the acid in water. After, the standards were diluted to concentrations of 5, 10, 20, 30, 40, 50 and 70 ppm in the 0.6% HNO_3 solution. To comply with the calibration curve, the glass extracts were diluted five times with the 0.6% HNO_3 solution and the diluted samples were used for the analysis.

2.4 Scaffold fabrication

2.4.1 Glass milling

To further reduce the particle size, the glass powders were milled on using a Planetary Micro Mill PULVERISETTE 7 premium line by Fritsch. 100 g of 1 mm ZrO_2-beads and 15 g of glass powder were each sealed into the two vessels. One cycle of milling was performed at 750 rpm for 5 min at room temperature. Subsequently, 15 g of isopropanol was added to each vessel and, after sealing, 5 cycles of milling at 750 rpm for 5 min each interrupted by an equal number of pauses of 10 min respectively were performed at room temperature. The wet glass powders were filtered using a 50 μm sieve to separate the beads from the milled glass. The glasses were dried overnight at 37 °C and the particle size distribution was measured with a Mastersizer 3000. The size of the particles chosen for the scaffold preparation described in this article ranged between 0.1 and 10 μm (as shown in Fig. 2).

2.4.2 Scaffold elaboration

Homogeneous collagen suspensions of 40 mg mL^{-1} were prepared by mixing the collagen fibres in ultra-pure water

under continuous magnetic stirring. Then, glass particles were added to the collagen suspensions at a 1:1 wt ratio. After 5 min of vigorous stirring, the homogeneous mixtures were loaded into Petri dishes, frozen using liquid nitrogen and lyophilized under vacuum for 2 days. Finally, the scaffolds were chemically cross-linked overnight using 20 mM of EDC and 8 mM of NHS in 80:20 (vol%) ethanol/ deionized water. After, the scaffolds were rinsed with ethanol and deionized water (80:20 ratio) for three times and dried in an oven at 37 °C for 24 h.

2.5 Scaffold characterization

2.5.1 Brunauer-Emmett-Teller (BET)

The surface area and pore volume parameters of the collagen-based scaffolds were determined by nitrogen adsorption/desorption isotherms at 77 K in a Belsorp Mini II Surface area analyser. The sample was subjected to prolonged degassing at 40 °C prior to measurement. The Brunauer-Emmett-Teller (BET) equation was used for the specific surface area and pore volume quantification while Barrett-Joyner-Halenda (BJH) was used for mean pore size determination.

2.5.2 pH measurement in water

170 mg of collagen-based scaffolds were soaked in 20 mL of ultra-pure water and monitored for pH as mentioned previously (Section 2.3.4) for the raw glasses.

2.5.3 ICP

After recording the pH, the same solutions were subjected to ICP analysis. Before performing the analysis on the samples, a calibration curve was made as for the glass particles alone. To fit the calibration curve, the scaffold

extracts were diluted twenty times with the 0.6% HNO_3 solution and the diluted samples were used for the analysis.

2.5.4 SBF test

170 mg of the scaffolds were soaked in 20 mL of simulated body fluid [29] (SBF) for 1 and 3 weeks at 37 °C, 120 rpm. For each time point, the solutions were filtered twice using a 0.2 μm filter. The media were subjected to immediate pH measurement, whereas the scaffolds were dried 24 h at 60 °C prior to analysis.

2.5.5 SEM-EDX

The scaffold samples were observed, "as received", in SEM in low vacuum mode without any conductive coating. A JEOL JSM6490-LV Scanning Electron Microscope (SEM) fitted with an Oxford Instruments INCA Energy Dispersive X-ray Analysis system (EDA) was used for examination in accordance with in-house methods M24 and M25.

SEM imaging of the scaffold was conducted using Backscattered Electron Imaging; using this imaging mode the brightness of a given feature is proportional to its mean atomic number. Images were taken at different magnifications.

Microanalysis results are tabulated on a semi-quantitative, normalised, elemental weight basis. Light elements such as lithium and boron are not quantified by this analytical technique. Carbon is also omitted.

The EDX spectra of the scaffolds before and after SBF immersion were collected for 100 s at a primary beam energy of 15 keV and at a working distance of 10 mm.

3 Results

3.1 Characterization of the glasses

3.1.1 Composition (XRF)

Four MQ glasses were produced by fixing the P and Na content and varying systematically the Ca to Sr ratio: with an increase in Sr, the Ca decreased by an equivalent amount. This ensured the alkali to alkaline earth ratio remained constant.

Table 1 shows the actual compositions of the MQ glasses. It is possible to notice that the incorporation of the Sr succeeded and that with the increase of Sr the Ca content decreased. In addition, the yields were not disturbed while the Sr increased.

Considered together, these results show that the melt-quench technique is a reliable and consistent processing

Table 1 Real compositions of the MQ-glasses obtained by XRF

Name	Mol%				Yield (%)
	P_2O_5	CaO	Na_2O	SrO	
PBG/Sr0	51	34	15	0	81
PBG/Sr5	52	28	14	5	80
PBG/Sr10	54	20	16	9	80
PBG/Sr15	53	18	13	15	82

method to incorporate Sr in the Ca-Na-P based glass system.

3.1.2 Phase (XRD)

The XRD patterns of all the MQ glasses (Fig. 3) showed a broad peak indicating that the materials are totally amorphous. The presence of Sr as dopant did not compromise the amorphous structure of the glasses elaborated.

3.1.3 Structure (FTIR)

Further information on the structure of the glasses and on the nature of the bonds can be gained from the infrared analysis. Figure 4 reports the FTIR spectra of the glasses prepared by melt-quench. The peaks are assigned as previously described by Brow, R. et al 2000 [30]. The assignments are listed in Table 2 and, where possible, the associated Q state is given.

The spectra of the glass samples have the characteristic finger print region of the phosphate glass network ranging from 1260 to 620 cm^{-1}. In all spectra, the typical bands of the POP bonds can be recognized both in symmetric and asymmetric configuration. In addition, the asymmetric and symmetric $(PO_3)^{2-}$ can be detected. Furthermore, the $(PO_2)^-$ in asymmetric arrangement can be distinguished for all the tested glasses. All the spectra contain Q^1 and Q^2 units: Q^1 for the symmetric and asymmetric $(PO_3)^{2-}$ and Q^2 for the asymmetric POP and $(PO_2)^-$

Considering those findings, it is possible to conclude that increasing Sr at the expense of Ca did not alter the structure of the glass network.

3.1.4 pH measurement

Figure 5 shows the pH variation over time. After 2 h of incubation, the pH dropped to an average of 3.5 ± 0.03. After this time, the pH continued to decrease up to 2.92 for the following 48 h for all the tested glasses. Subsequently, the pH remained stable through the next three weeks of the experiment.

The reduction of the pH was driven by phosphorous leaching. The pH changes were correlated with the
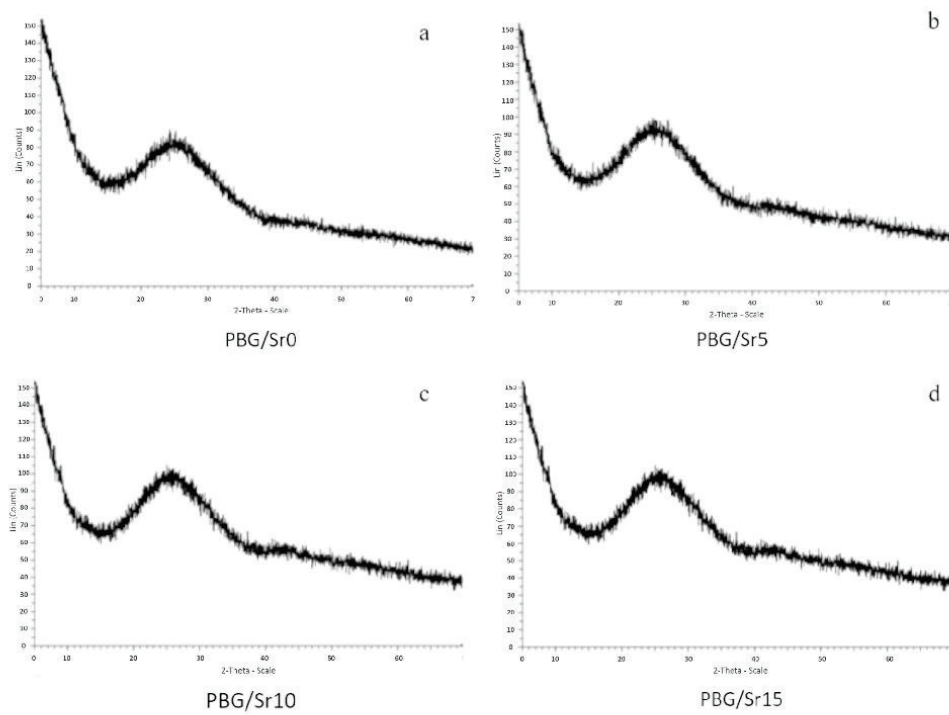
Fig. 3 XRD graphs of Sr-doped melt-quenched glasses: PBG/SrO **a**, PBG/Sr5 **b**, PBG/Sr1O **c**, PBG/Sr15 **d**
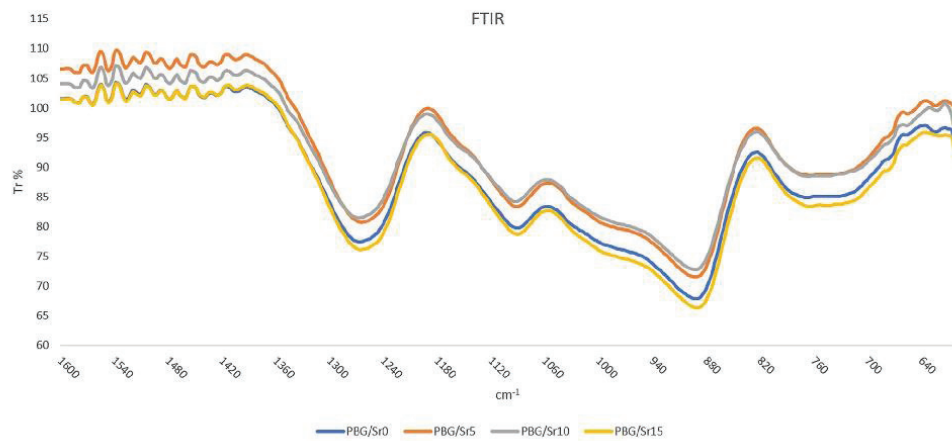

Fig. 4 Infra-red spectra in the range 1600–4000 cm^{-1} of the MQ glasses

104

phosphate release data (chapter 3.5.1): the pH dropped during the leaching phase but not during the plateau phase.

The presence of Sr in the glass composition did not influence the acidification of the medium.

Considering all those findings, it is possible to conclude that the acidification of the medium was Sr-independent.

3.1.5 Dissolution

All the Sr-doped phosphate glasses were found to degrade in water (Fig. 6). Globally, the MQ glasses showed a linear degradation during the first 24 h for all the four ions; after this, a plateau phase was reached. The concentration of the ions in the water reflected their content in the glass formulation: the leached phosphate had the highest value which is to be expected given its high mol% loading in the glass. This also explains the acidic pH values. In the same way, an inverse relationship between Sr and Ca was found depending on their relative concentration. In addition, the ion content influenced the release kinetics of the four ions during the linear part: P had the highest rate followed by Ca, Na and Sr.

Analysing in more depth the release kinetics of both Na and P (that are fixed in the composition) it is possible to notice that, in fact, the growing presence of strontium affected the dissolution of the glasses. By increasing the

concentration of Sr it seems that their degradation levels decreased. The dissolution behaviour of the glasses showed not so much difference between PBG/Sr0 and PBG/Sr5 but as the Sr increased, it became more and more significant (going from PBG/Sr5 to PBG/Sr15).

Considered together, the results show that replacing Ca with Sr does not affect the dissolution profile of the glasses, but the rate of dissolution was inversely proportional to the presence of Sr.

3.2 Characterization of the Scaffolds

3.2.1 Scaffolds morphology

From the SEM pictures (Fig. 7), it is possible to see that the Col1 fibres were arranged to make an interconnected matrix with the glass particles dispersed within and attached to the fibres (Fig. 7, white arrows). In addition, connecting wormholes were visible across the whole structure.

No real differences in the morphology and micro-structural organization were detected between the tested scaffolds.

Considering Fig. 8a, the scaffolds appear as a hard and white matrix, grainy to the touch. A random organization of the fibres with interconnected voids was visible.

From this, it is possible to conclude that replacing Ca with Sr did not affect the macroscopic organisation of the scaffolds.

3.2.2 BET

Since no variations in the structure were identified among the samples, SCF/Sr0 was chosen as reference to analyse the surface feature and physical parameters.

Figure 8b shows the isotherm plot of the scaffold SCF/Sr0. This track is indicative of type IV(a) hysteresis typical

Table 2 Infrared peaks position (cm^{-1}) and Q status assignment of the observed bands of the melt-quenched glass samples

Name	s(POP)	νs(POP)	νas(POP)/Q^2	νas(PO$_3$)$^{2-}$/Q^1	νas(PO$_2$)$^{-}$/Q^2
PBG/Sr0	624	768	890	1090	1266
PBG/Sr5	624	764	892	1092	1264
PBG/Sr10	622	766	892	1092	1266
PBG/Sr15	622	768	890	1090	1262

Fig. 5 pH variation of the water during three weeks of incubation of PBGs

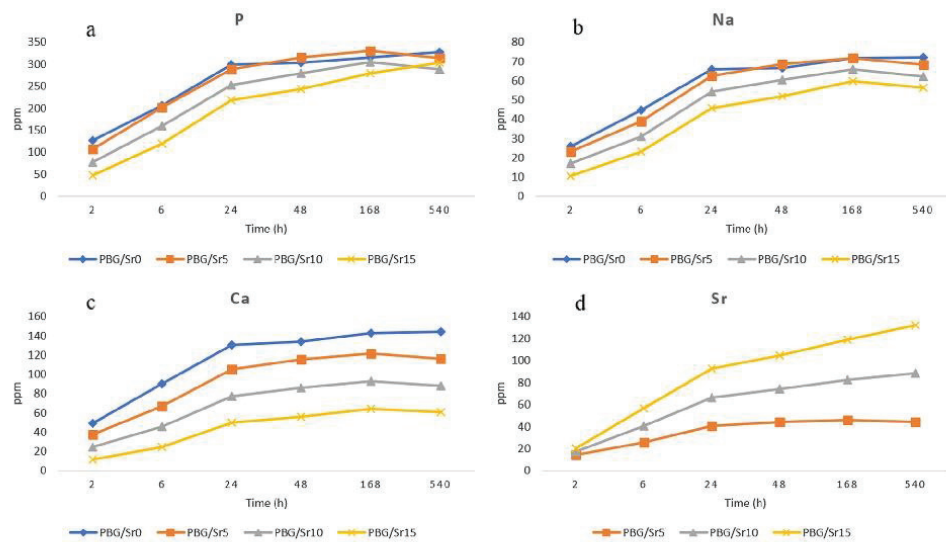Water pH measurement

Springer
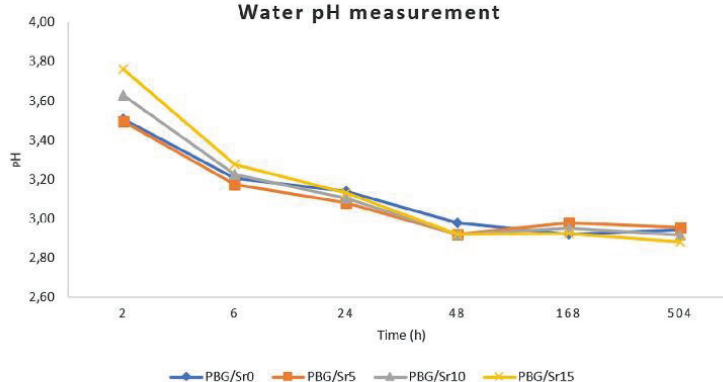
Fig. 6 Cumulative release (ppm) of P **a**, Na **b**, Ca **c** and Sr **d** ions in function of time (h) for the phosphate glasses
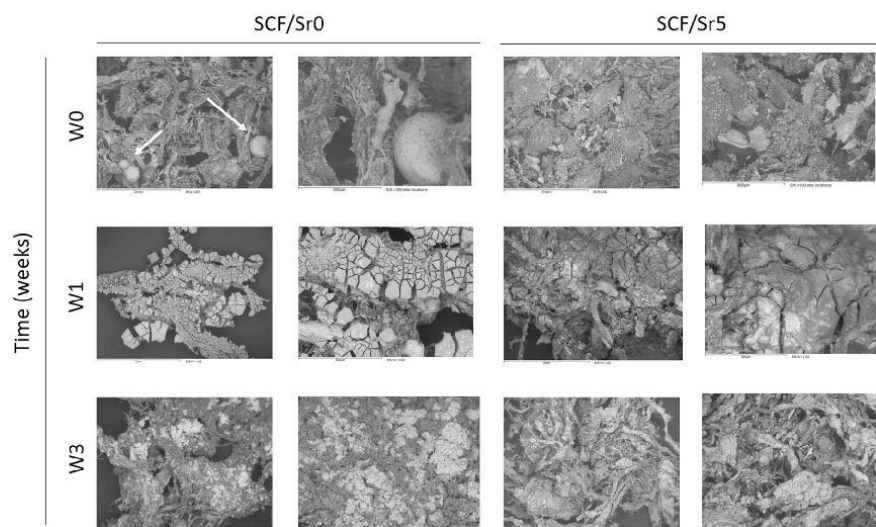

Fig. 7 SEM imagines at different magnitudes of the scaffolds before (W0) and after (W1 and W3) SBF immersion. Glass particles are visible (white arrows) attached at the body of the collagen fibres

of mesoporous materials [31]. This result corroborates the SEM imagines where interconnected porous are visible.

The surface feature parameters are reported in Table 3.

3.2.3 pH in water

Figure 9a shows that the pH associated with the water of the soaked scaffolds decreased linearly through the experiment

106
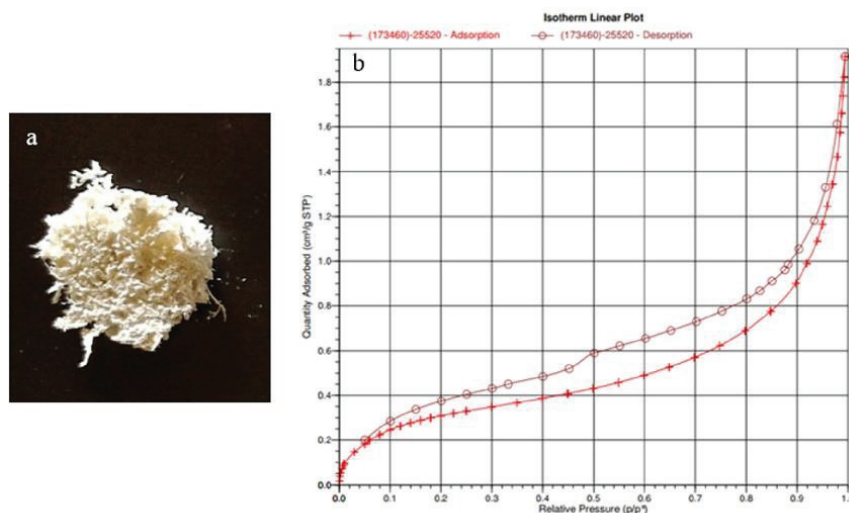
Fig. 8 Picture of the SCF/Sr0 scaffold at natural size **a**. Adsorption and desorption isotherm loop of the SCF/Sr0 sample **b**

Table 3 Surface feature of the scaffold SCF/Sr0

Surface area	Pore volume	Pore size
$1.2129 \ m^2/g$	$0.002691 \ cm^3/g$	13.0733 nm

for all the tested scaffolds. The scaffold combined with the SCF/Sr0 glass had the highest pH, whereas the scaffolds combined with SCF/Sr15 showed the lowest pH. By comparing those pH data with the equivalent data for the glass particles alone, it is possible to conclude that the presence of Col influenced the acidification of the medium. In other words, the fibres influenced the dissolution behaviour of the glasses.

3.2.4 pH in SBF

The pH of the SBF (Fig. 9b) containing the scaffolds dropped after one and three weeks. A constant and linear decrease was recorded both for SCF/Sr0 and SCF/Sr5 scaffolds. For the SCF/Sr10 scaffold the change in pH between week 1 and week 3 was less significant. The SCF/Sr15 showed a constant pH between week 1 and week 3.

3.2.5 Dissolution

The glasses combined with Col fibres were found to degrade in water (Fig. 10). Consideration of the dissolution kinetics of the ions reveals that all the incorporated glasses degraded linearly during the first 6 h of the experiment,

whereupon they reached a plateau. The concentration of the ions in water reflected their relative content in the composition: P reached the highest concentration and an inverse relationship between Ca and Sr was found.

Deeper analysis of the dissolution trends for Na and P reveals a non-obvious trend. In both cases, the SCF/Sr10 scaffolds released, at each time point, more Na and P than the other glasses. The release from the other glasses decreased in the order SCF/Sr5, SCF/Sr15 then SCF/Sr0.

Considered together these results indicate that the presence of the collagen influences the dissolution kinetics of the glass particles by interacting with them or with the ionic species released.

3.2.6 EDX

The scaffolds were immersed in SBF to test their ability to induce surface HA precipitation and the influence of collagen and/or Sr on this process.

EDX performed before immersion (Fig. 11, first line) showed a Ca/P ratio compatible with that expected for the glass. The EDX profiles (Fig. 11) of the scaffold specimens recorded after one and three weeks of SBF immersion showed augmented peaks for Ca and P. SEM images (Fig. 7) taken at the same time points showed the presence of a Ca-P enriched layer formed onto all the tested scaffolds.

Considering that the Ca/P in HA is 1.67 (mol%), noteworthy are the specimens SCF/Sr0 and SCF/Sr5: the first
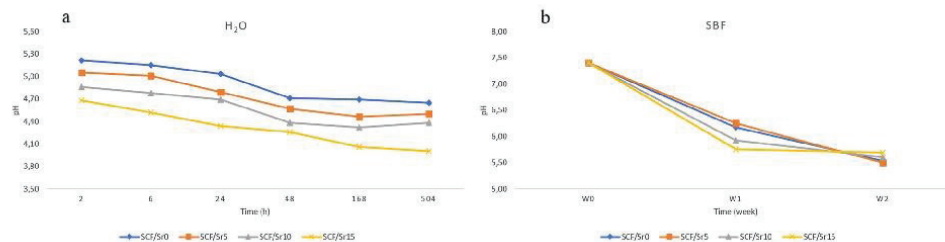
Fig. 9 pH variation of the water **a** and SBF **b** during three weeks of incubation of the tested scaffolds
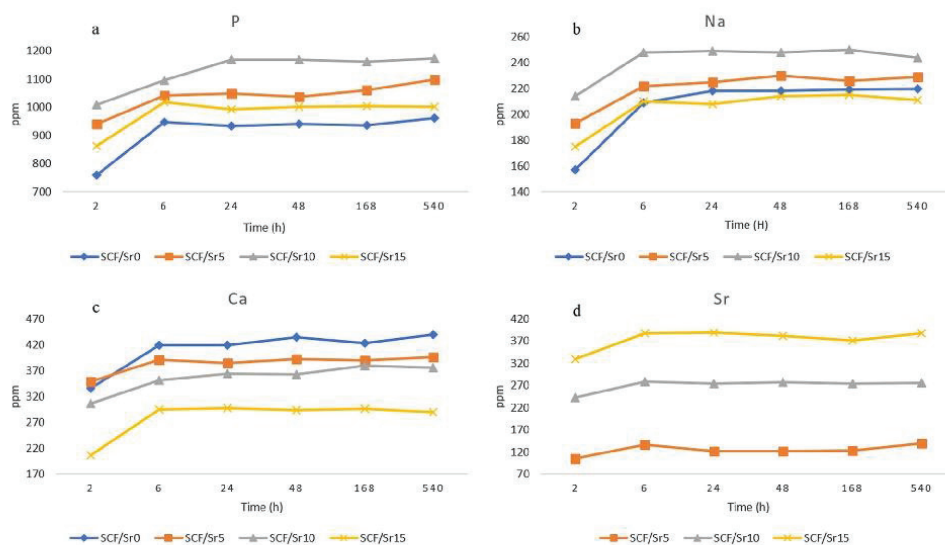

Fig. 10 Cumulative release (ppm) in function of time (h) of P **a**, Na **b**, Ca **c** and Sr **d** ions from the tested scaffolds embedded in water for three weeks

has a precipitate layer with a Ca/P ratio of 1.38 (molar) after three weeks of immersion; the second delivers 1.68 (molar) after one week.

All together those results show that all the samples can trigger the precipitation and growth of a Ca-P rich layer on their surface when immersed in SBF. Especially promising is sample SCF/Sr5 because its precipitate layer Ca/P ratio matches that of HA after just one week.

4 Discussion

4.1 Glasses

In this study, four phosphate-based glasses were produced by melt-quench. The glasses were systematically doped

with Sr at the expense of Ca: as the Sr concentration in the glass composition increased, the Ca concentration was reduced by an equivalent amount. P and Na were kept constant. By doing this the alkali to alkaline earth ratio remained unchanged in the formulation. The glasses were characterized for their structural properties by XRD, XRF, FTIR and ICP analysis of dissolution aliquots was used to determine their relative degradation kinetics in water.

The XRF analysis (Table 1) showed that the real composition of the glasses was in good agreement with the expected one and that Sr was successfully incorporated in the glasses. It is evident that the growing presence of Sr did not affect the extent to which actual compositions matched the target composition. In addition, the alkali to alkaline earth ratio was maintained through the series. The relative chemical similarity between Ca and Sr could explain why
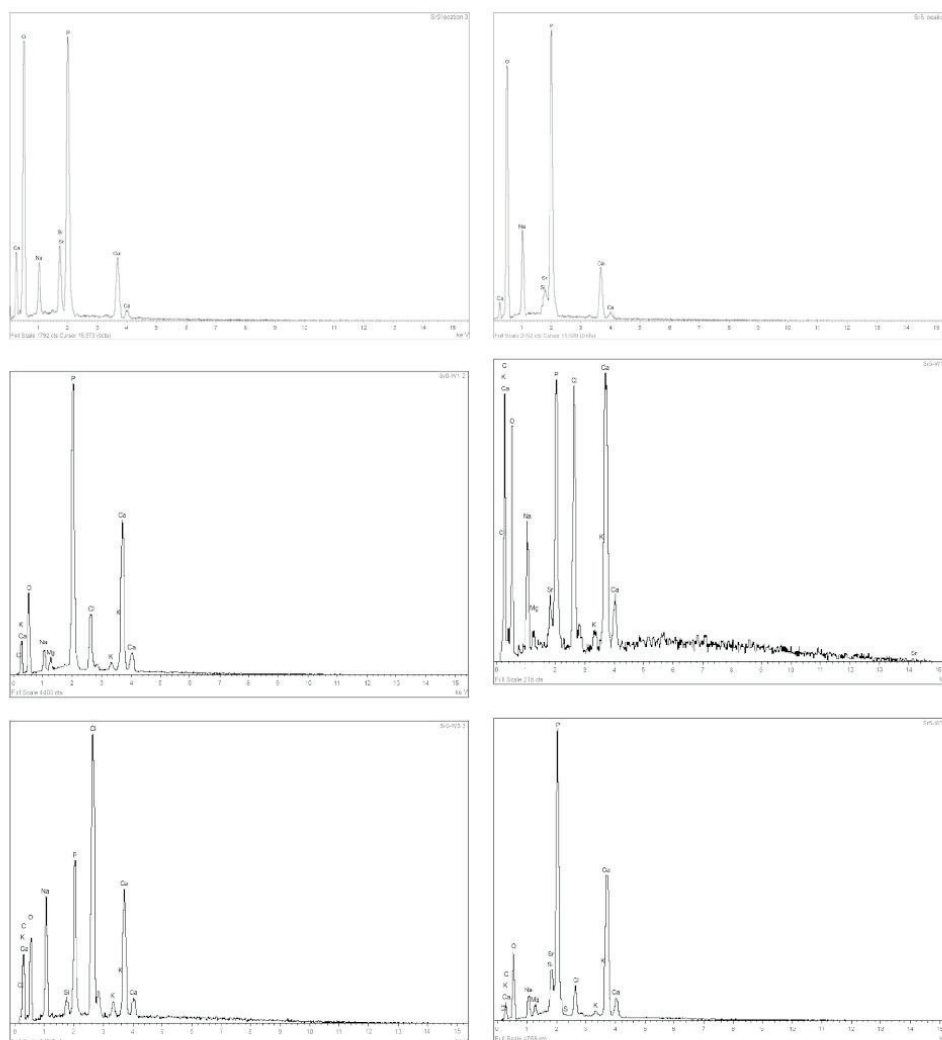
Fig. 11 EDX profiles of the scaffolds before (W0) and after (W1 and W3) SBF immersion

the incorporation of Sr did not perturb the composition of the glasses: the systematically substitution of Ca with Sr succeeded and the other two elements (Na and P) remined fixed across the 4 glasses hitting the target.

The XRD analysis (Fig. 3) showed that all glasses were amorphous. Sr did not act as a nucleation sites for crystal growth.

The network structure of the tested glasses and the nature of their bonding was investigated by FTIR (Fig. 4). The network structure of the four glasses was dominated by endless Q^2 phosphate chains and did not present any significant variation with increasing strontium. The atomic radius of the two ions is 197 and 215 ρm respectively for Ca and Sr. In addition, it has been proved that Sr similarly to Ca tends to be located more in the bulk of the glass rather than at the surface [32]. Those two factors, size similarity and analogous preferred position, could explain why Sr did not have a significant impact on the structural properties of

the glasses. Furthermore, they all have the same P content, and this can contribute the structures are similar.

An interesting observation came from the dissolution test performed in ultra-pure water. By analysing the variations of the pH (Fig. 5) during the experiment, no correlation was found between the Sr content and reduction in pH. From the ion leaching kinetics of the four glasses (Fig. 6), it possible to see that all glasses degraded linearly during the first 24 h of experiment independently of the Sr content. This sustained release of the ions over time indicates a compact and dense network.

The dissolution of both Ca and Sr ions reflected their reciprocal content in the composition; whereas, a deeper analysis of the first 24 h of P and Na revealed the influence of Sr on the dissolution rate. Both P and Na dissolved in water inversely to an increase of Sr in the glass. This finding could be explained considering the coordination number (CN) of the two alkaline earth elements: Ca has a CN equal to 7, Sr's CN is 7.5 [33]. This slight difference could be enough to increase the glass network density and connectivity to generate the differences seen in the glass dissolution rate. This fits with the current accepted mechanism of phosphate glass network dissolution where at first Na and protons are exchanged at the interface. A higher network connectivity therefore entails a slower exchange reaction speed and a more stable glass, indeed, the glass with the highest Sr never reached a real plateau.

4.2 Scaffolds

SEM images (Fig. 7) reveals that all the scaffolds had a randomly oriented microstructure due to the casual disposition of the fibres during the casting. Glass particles were attached to the body of the fibres (Fig. 7 white arrows) and randomly dispersed within the matrix. No changes are evident in the scaffold structures due to the growing presence of Sr because no interesting variations were noticed in the organisation of the glass networks. For this reason, the SCF/Sr0 scaffold was chosen as a representative sample to run a BET analysis (Fig. 8a). The hysteresis loop measured is typical of mesoporous materials and could be explained by considering the typical random organization of the fibres that generates voids and interconnected channels through the whole structure of the scaffold. This could be a really useful property for this material because it may guarantee both a proper 3D support for cells, close to real conditions, and allow the diffusion of oxygen and nutrients to the tissue to sustain growth and regeneration.

To better understand how the scaffolds may behave in aqueous environments, their dissolution kinetics were studied. The analysis of the variations of the aqueous phase pH (Fig. 9a) the scaffolds were embedded in revealed a surprising order throughout the series: there seemed to be an inverse relationship between Sr content in the glasses and pH decrease. The dissolution behaviour of the glass particles incorporated in the Col fibres showed (Fig. 10) a linear degradation rate during the first 6 h of the time course independent of the presence of the organic polymer. Noteworthy was the particular order in both Na and P dissolution rates from the scaffolds when compared with the equivalent raw glasses featuring in each scaffold. Such a sequence (decreasing rate in the order SCF/Sr10, SCF/Sr5, SCF/Sr15 then SCF/Sr0) becomes explainable when considering the study of A. Weinstock et al, on the ion-binding ability of the reconstructed collagen [34]. When in water, the side chains of amino acid residues are fully protonated generating an excess of positive charges that attract pyrophosphates. This in turn, generates additional negative charges that need to be balanced by attracting Na but not Sr or Ca ions. The only source of those ions are the dissolving glass particles: the collagen interacts with the ions coming from the dissolving particles removing those from the medium, the pyrophosphates first then the Na ions. This explains why both the Na and P graphs exhibit the same trends. The progression can be explained considering that when Sr is incorporated in the glass there is an increase in Q^1 (and Q^3) species in the glass structure [35]. It is possible to speculate that when Sr reaches 10 mol% a maximum level of Q^1 is reached in the glass.

To test the bioactivity of the scaffolds through the formation of an HA layer, all the scaffolds were immersed in SBF for one and three weeks. By comparing the SEM imagines (Fig. 7) before and after, it is possible to see a deposit layer formed on the surface of all the tasted samples. The EDX analysis (Fig. 11) revealed that such deposits were rich in Ca and P. Considering the Ca/P ratio in HA as being 1.67 (mol%), the samples SCF/Sr0 and SCF/Sr5 showed the most promising results. SCF/Sr0 formed a layer in which the Ca to P ratio was just 1.38 (mol%) after three weeks; whereas, SCF/Sr5 generated, after one week, a deposit which ratio was 1.68 (mol%) that matches the HA one. It possible to argue that for the SCF/Sr0 scaffold maybe more time in SBF would have been necessary to generate the apatite-like layer. Whereas, the case of the SCF/Sr5 could be explained considering that it has been reported that Sr enhances HA formability [36] by increasing the Ca absorption at the earlier stages [37]. However, and this can be the explanation for the other scaffolds, it has been described [38] that above a certain concentration of Sr or Sr/Ca ratio, the octacalcium phosphate precursor phase is unable to form which ultimately retards the formation of a hydroxycarbonate like phase.

The development of those strata could be explained with the ion exchanging mechanism [39]. During the dissolution of the network, ions from the glass (especially Ca and Na) are exchanged with the ions in the media (protons), this

creates a reactive hydrated layer at the surface where the concentration of ions reaches the saturation level. Those ions interact and precipitate on the surface of the materials. In addition, in the case of phosphate glasses, P_2O_5 is also released into the medium. Part of it hydrates forming PO_4H_2 and both were shown to facilitate HA formation in SBF [40, 41]. The scaffold SCF/Sr5 optimizes the condition needed for the growth of an HA layer after one week in the SBF. Due to this, SCF/Sr5 was identified as a promising bioresorbable scaffold with desirable bioactivity (HA formability in human fluid) for future application in regenerative medicine.

5 Conclusions

The aim of this study was to evaluate the bioactivity of organic/inorganic bioresorbable scaffolds. A new series of Sr-doped phosphate-based glasses was produced by the melt-quench technique. The materials obtained were proved to be the reliable in terms of composition, phase and structure. The glasses had a well-defined dissolution profile in ultrapure water: an initially sustained release followed by a plateau. Subsequently, the glasses were combined as powders with collagen fibres to make biodegradable scaffolds. Their characterization using different techniques showed the presence of an interconnected porous structure and revealed the degradable nature of the materials. The bioactivity of the scaffolds as HA formability was tested by soaking them in SBF. A thick Ca-P rich layer was detected on the surface of all the tested scaffolds. In one sample, the Ca/P ratio of the deposited layer matched that of HA. For all those reasons, its possible application in restorative dentistry is proposed.

Compliance with ethical standards

Conflict of interest The authors declare that they have no conflict of interest.

References

1. Hench LL, Clark AE, Schaake HF. Effects of microstructure on the radiation stability of amorphous semiconductors. J Non-Cryst Solids. 1972;8–10:837–43.
2. Hench LL, Splinter RJ, Allen WC, Greenlee TK. Bonding mechanisms at the interface of ceramic prosthetic materials. J Biomed Mater Res. 1971;5:117–41.
3. Knowles JC. Phosphate based glasses for biomedical applications. J Mater Chem. 2003;13:2395–401.
4. Gao H, Tan T, Wang D. Dissolution mechanism and release kinetics of phosphate controlled release glasses in aqueous medium. J Control Release. 2004;96:29–36.
5. Bunker BC, Arnold GW, Wilder JA. Phosphate glass dissolution in aqueous solutions. J Non-Cryst Solids. 1984;64:291–316.
6. Franks K, Abrahams I, Knowles JC. Development of soluble glasses for biomedical use Part I: in vitro solubility measurement. J Mater Sci Mater Med. 2000;11:609–14.
7. Kesisoglou A, Knowles JC, Olsen I. Effects of phosphate-based glasses on T lymphocytes in vitro. J Mater Sci Mater Med. 2002;13:1189–92.
8. Ozaki T. [An experimental study on the biological safety of calcium phosphate glass ceramics]. Nihon Seikeigeka Gakkai Zasshi. 1990;64:1215–25.
9. Pickup DM, Newport RJ, Knowles JC. Sol-gel phosphate-based glass for drug delivery applications. J Biomater Appl. 2012;26:613–22.
10. Sahdev R, Ansari TI, Higham SM, Valappil SP. Potential use of gallium-doped phosphate-based glass material for periodontitis treatment. J Biomater Appl. 2015;30:85–92.
11. Salih V, Franks K, James M, Hastings GW, Knowles JC, Olsen I. Development of soluble glasses for biomedical use Part II: the biological response of human osteoblast cell lines to phosphate-based soluble glasses. J Mater Sci Mater Med. 2000;11:615–20.
12. Ahmed I, Ready D, Wilson M, Knowles JC. Antimicrobial effect of silver-doped phosphate-based glasses. J Biomed Mater Res A. 2006;79:618–26.
13. Saidak Z, Marie PJ. Strontium signaling: molecular mechanisms and therapeutic implications in osteoporosis. Pharmacol Ther. 2012;136:216–26.
14. Pors Nielsen S. The biological role of strontium. Bone . 2004;35:583–8.
15. Wu C, Zhou Y, Lin C, Chang J, Xiao Y. Strontium-containing mesoporous bioactive glass scaffolds with improved osteogenic/cementogenic differentiation of periodontal ligament cells for periodontal tissue engineering. Acta Biomater. 2012;8:3805–15.
16. Gobbo JP, de Faria DLA, Martinelli JR. Inertization of small-scale chemical wastes using iron phosphate glass. Quím Nova. 2014;37:1058–62.
17. Zha J, Roggendorf H. Sol–gel science, the physics and chemistry of sol–gel processing. In: Brinker CJ, Scherer GW, editors. Boston: Academic Press; 1990. xiv, 908 pp., bound—ISBN 0-12-134970-5. Adv Mater. 1991;3:522–522.
18. Abou Neel E, Pickup D, Valappil S, Newport R, Knowles J. Bioactive functional materials: a perspective on phosphate-based glasses. J Mater Chem. 2009;19:690-701.
19. Averbuch-Pouchot DA. Topics in Phosphate Chemistry. [Internet]. Singapore: World Scientific Publishing Company; 1996. http://public.eblib.com/choice/publicfullrecord.aspx?p=1214750.
20. Ruiz Hernandez SE, Ainsworth RI, de Leeuw NH. Molecular dynamics simulations of bio-active phosphate-based glass surfaces. J Non-Cryst Solids. 2016;451:131–7.
21. Hermansen C, Mauro JC, Yue Y. A model for phosphate glass topology considering the modifying ion sub-network. J Chem Phys. 2014;140:154501.
22. Al Hasni B, Martin RA, Storey C, Mountjoy G, Pickup DM, Newport RJ. Molecular dynamics modelling of sodium and calcium metaphosphate glasses for biomaterial applications. Phys Chem Glasses. 2016;57:245–53.
23. Pickup DM, Guerry P, Moss RM, Knowles JC, Smith ME, Newport RJ. New sol-gel synthesis of a (CaO)(0.3)(Na2O)(0.2)(P2O5)(0.5) bioresorbable glass and its structural characterisation. J Mater Chem. 2007;17:4777–84.

24. Carta D, Pickup D, Newport R, Knowles J, Smith ME, Drake KO. Structural studies of bioactive sol-gel phosphate based glasses. Phys Chem Glasses. 2005;46:365–71.

25. Carta D, Pickup DM, Knowles JC, Ahmed I, Smith ME, Newport RJ. A structural study of sol–gel and melt-quenched phosphate-based glasses. J Non-Cryst Solids. 2007;353:1759–65.

26. Qiu D, Martin RA, Knowles JC, Smith ME, Newport RJ. A comparative study of the structure of sodium borophosphates made by sol-gel and melt-quench methods. J Non-Cryst Solids. 2010;356:490–4.

27. Bose S, Roy M, Bandyopadhyay A. Recent advances in bone tissue engineering scaffolds. Trends Biotechnol. 2012;30:546–54.

28. Charulatha V, Rajaram A. Influence of different crosslinking treatments on the physical properties of collagen membranes. Biomaterials. 2003;24:759–67.

29. Kokubo T, Takadama H. How useful is SBF in predicting in vivo bone bioactivity? Biomaterials. 2006;27:2907–15.

30. Brow RK. Review: the structure of simple phosphate glasses. J Non-Cryst Solids. 2000;263–264:1–28.

31. Thommes M, Kaneko K, Neimark AV, Olivier JP, Rodriguez-Reinoso F, Rouquerol J, et al. Physisorption of gases, with special reference to the evaluation of surface area and pore size distribution (IUPAC Technical Report). Pure Appl Chem. 2015;87:1051–69.

32. Pires R, Abrahams I, Nunes TG, Hawkes GE. Non-random cation distribution in sodium–strontium–phosphate glasses. J Non-Cryst Solids. 2004;337:1–8.

33. Christie JK, de Leeuw NH. Effect of strontium inclusion on the bioactivity of phosphate-based glasses. J Mater Sci. 2017;52:9014–22.

34. Weinstock A, King PC, Wuthier RE. The ion-binding characteristics of reconstituted collagen. Biochem J. 1967;102:983–8.

35. Abou Neel EA, Chrzanowski W, Pickup DM, O'Dell LA, Mordan NJ, Newport RJ, et al. Structure and properties of strontium-doped phosphate-based glasses. J R Soc Interface. 2009;6:435–46.

36. Fredholm YC, Karpukhina N, Brauer DS, Jones JR, Law RV, Hill RG. Influence of strontium for calcium substitution in bioactive glasses on degradation, ion release and apatite formation. J R Soc Interface. 2012;9:880–9.

37. Lindahl C, Engqvist H, Xia W. Effect of strontium ions on the early formation of biomimetic apatite on single crystalline rutile. Appl Surf Sci. 2013;266:199–204.

38. Sriranganathan D, Kanwal N, Hing KA, Hill RG. Strontium substituted bioactive glasses for tissue engineered scaffolds: the importance of octacalcium phosphate. J Mater Sci Mater Med. 2016;27. https://www.ncbi.nlm.nih.gov/pmc/articles/PMC4690837/.

39. Islam MT, Felfel RM, Abou Neel EA, Grant DM, Ahmed I, Hossain KMZ. Bioactive calcium phosphate–based glasses and ceramics and their biomedical applications: a review. J Tissue Eng. 2017;8. https://www.ncbi.nlm.nih.gov/pmc/articles/PMC5524250/.

40. Kasuga T, Hattori T, Niinomi M. Phosphate glasses and glass-ceramics for biomedical applications. Phosphorus Res Bull. 2012;26:8–15.

41. Kokubo T, Kim H-M, Kawashita M. Novel bioactive materials with different mechanical properties. Biomaterials. 2003;24:2161–75.

4.3 Complementary results

4.3.1 Sol-gel glasses

4.3.1.1 *Effect of increasing Calcium (Ca) content*

Objectives: Ca content is the parameter that affects the behaviour of fused phosphate glasses the most. In this section the effects of increasing Ca at the expense of Na in a series of sol-gel derived phosphate-based glasses (P_2O_5 53% - CaO (24+x)% - Na_2O (23-x)% with x=0, 8, 16 – mol%) are described.

Methods: For this set of experiments, the glasses were synthesized as follows. Under constant stirring, Bt/P was added dropwise to NaOMe and left mixing for 1h. Afterwards, the Ca precursor (Ca-methoxyethoxide – CME) was added dropwise. Composition, phase and surface features were characterized in agreement with the manual of the instruments.

Results and discussions: The results indicate that the phosphate network evolves from a 3D-network of phosphate chains linked by Ca to a more disordered system of separated phosphate chains as Ca progressively reduces (or Na increases).

4.3.1.1.1 Composition and yield

Table 1 shows the actual composition (in mol%) of the SG glasses. The SG glasses were deficient in P, suggesting losses for volatilisation. Interestingly, the missing percentage of both P and Ca in the samples has been gained by the Na. This perhaps suggests the sodium precursor reacted into the P/Ca/Na oxide structure more readily. Moreover, the table shows the relative yield of the preparations: there is potential for unreacted precursors.

Table 1. Actual composition (mol%) and yield of the phosphate-based glasses prepared by sol-gel

Name	P_2O_5	CaO	Na_2O	Yield (%)
PBG-C24	49	24	27	77
PBG-C32	49	30	21	50
PBG-C40	49	38	13	37

4.3.1.1.2 Phase

The XRD patterns of the tested glasses (fig. 5) showed a broad peak indicating that the materials were totally amorphous despite the progressively increasing Ca levels that might be expected to encourage unwanted crystallisation. It demonstrates elegantly how the sol-gel technique gives products with high amorphous phase purity.
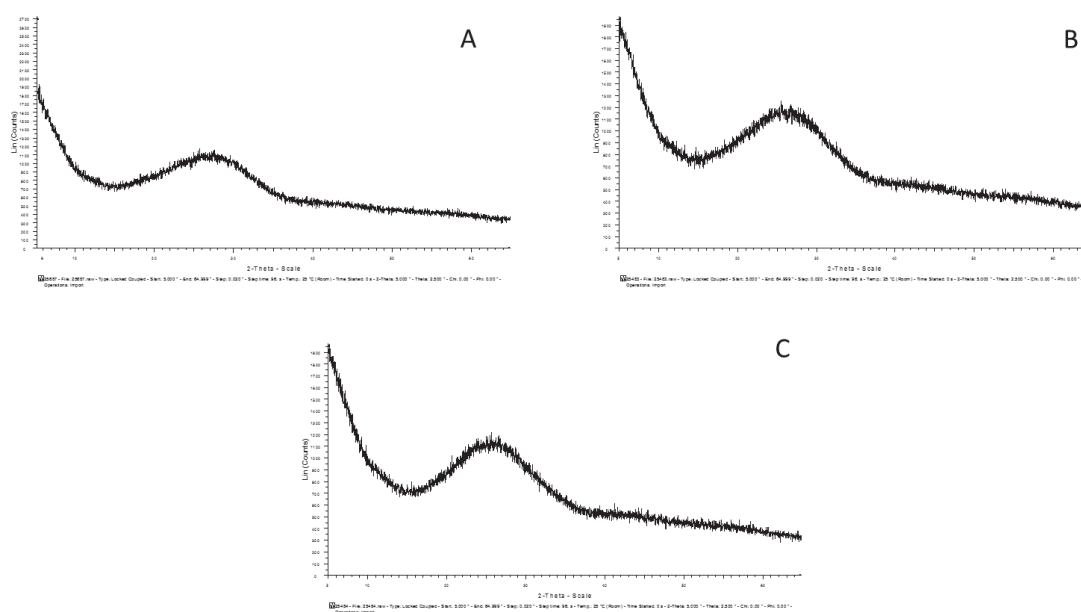

Figure 5. XRD graphs of C24 (A) C32 (B) and C40 (C) glasses

4.3.1.1.3 Structure

Further information on the structure and bonding can be gained from infrared analysis. Fig. 6 shows the FTIR spectra recorded for the glasses prepared by sol-gel techniques. The peaks were assigned as previously described[8]. The assignments are listed in table 2 and where possible, the associated Q state is assigned.
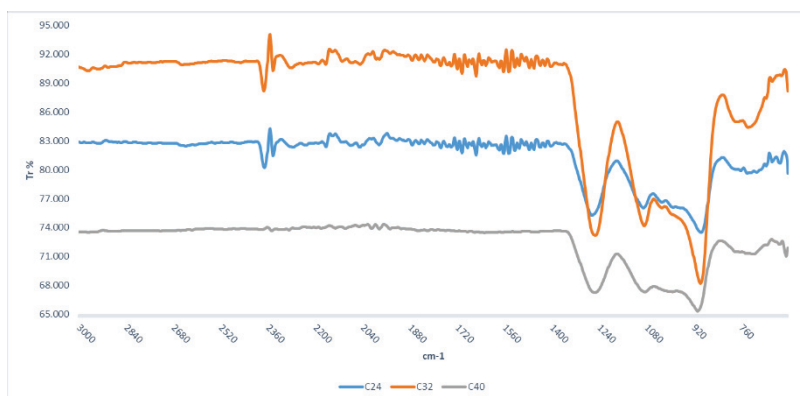
Figure 6. Infra-red spectra in the range 600-3000 cm^{-1}

The spectra of the sol-gel samples reveal the characteristic bands associated with P-O-P bonding: for the C24 glass the peaks were identified at 708 cm^{-1}, 762 cm^{-1} and 896 cm^{-1}; for the C32 glass the POP bonding peaks were recognized at 705 cm^{-1}, 776 cm^{-1} and 898 cm^{-1}; for the C40 the same peaks were assigned to 702 cm^{-1}, 720 cm^{-1} and 908 cm^{-1}. In all the three cases the first peaks represent the POP bond in symmetric configuration, whereas, the second and third peaks characterise the same bond in asymmetric mode. The pairs of peaks at 1028 cm^{-1} and 1090 cm^{-1}, 1028 cm^{-1} and 1088 cm^{-1} and 992 cm^{-1} and 1086 cm^{-1} were recognised and assigned to the $(PO_3)^{2-}$ bond in the symmetric and asymmetric state respectively for the first and second member of each pair. Further peaks at 1264 cm^{-1}, 1254 cm^{-1} and 1256 cm^{-1} belonging respectively to C24, C32 and C40 glass can be detected and assigned to the asymmetric $(PO_2)^-$ bond.

Table 2. Infrared peak positions (cm^{-1}) and Q assignment of the observed bands of sol-gel glass samples

Samples	Peaks (cm^{-1})/Q states					
	$v_{as}(PO_2)^-$/Q2	$v_{as}(PO_3)^{2-}$/Q1	$v_s(PO_3)^{2-}$/Q1	$v_{as}(POP)$/Q2	$v_s(POP)$	$v_s(POP)$
C24	1264	1090	1028	896	726	708
C32	1254	1088	1028	898	776	705
C40	1256	1086	992	908	720	702

All the spectra contain Q1 and Q2 units: especially, Q1 for the symmetric and asymmetric $(PO_3)^{2-}$ and Q2 for the asymmetric POP and $(PO_2)^-$ bond.

116

Based on the shape of the FTIR tracks and in agreement with the previous studies, it is possible to conclude that the atomic scale structure of the three glasses is similar consisting of long chains dominated by Q2 phosphate tetrahedrons.

4.3.1.1.4   pH measurement in water

Fig. 7 shows the pH variation after 24 hours of incubation in DI water. The pH dropped down to 3.27, 2.86 and 2.1 considering C24, C32 and C40 glass respectively. It is possible to notice that there is a correlation between the increase of Ca content and the reduction in pH.
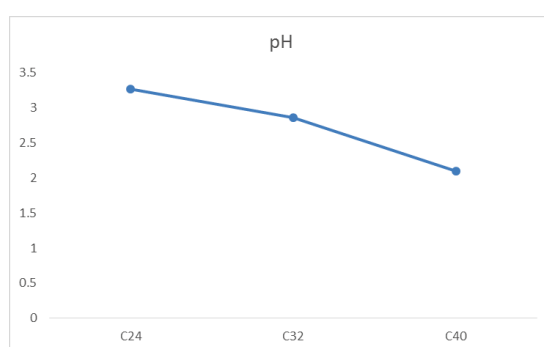
Figure 7. pH variation of the water as a function of Ca increment after 24 hours of incubation

4.3.1.1.5   Surface features

For the tested glasses, the BET analysis gave a type II hysteresis (fig. 8) typical of nonporous adsorbents[91].
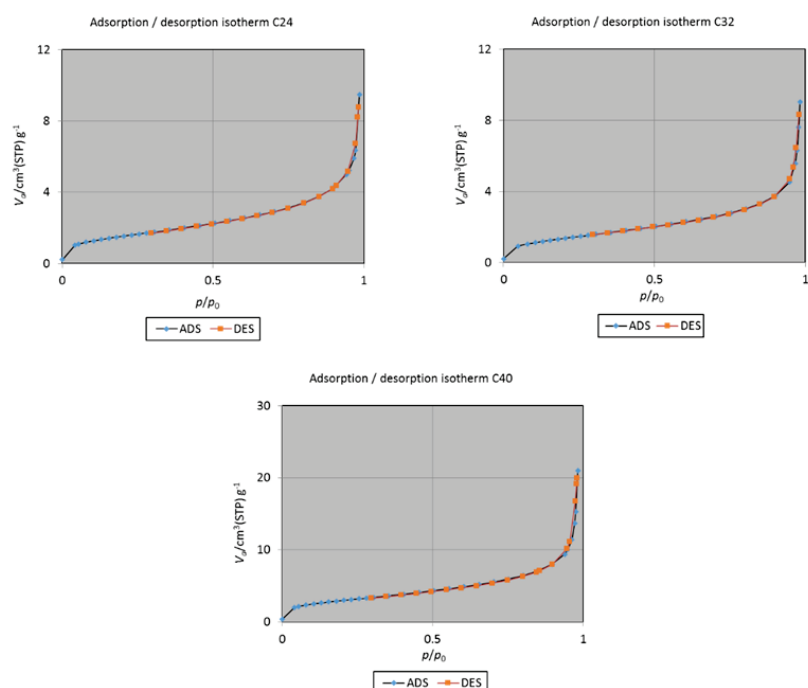
Figure 8. Adsorption and desorption isotherms of the tested glass samples

Table 3 summarises pore size, pore volume and surface area of the three materials. The relationship between Ca content and surface features is shown in fig. 9. No significant difference was found between the total pore volume of C24 and C32, however, in the C40 glass particles it was about 2.3 times larger than the other two glasses. The pore size slightly increases with increasing Ca content. The surface area is directly proportional to calcium: it increases by 1.9 times from C24 to C40, and 2.1 times from C32 to C40.

Table 3. Pore volume, pore size and surface are of the glasses after BET analysis

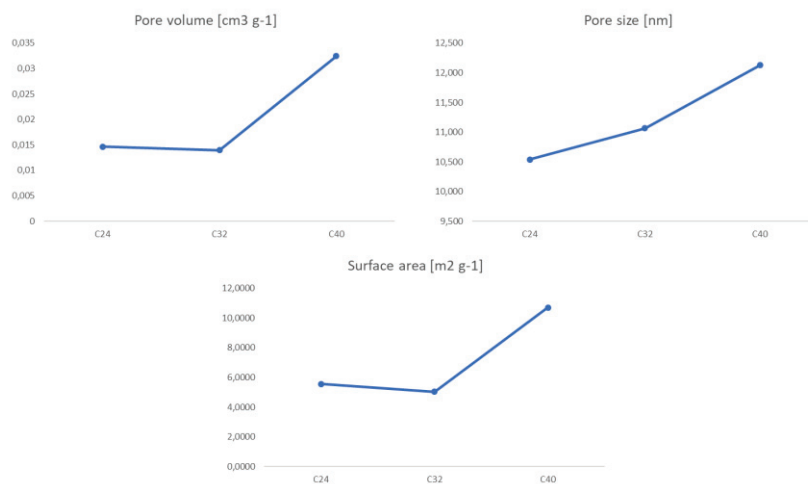| Glasses	Pore volume [$cm^3\ g^{-1}$]	Pore size [nm]	Surface area [$m^2\ g^{-1}$]
C24	0.014651	10.537	5.5619
C32	0.013949	11.065	5.0427
C40	0.032437	12.129	10.698

Figure 9. Variations of pore volume, pore size and surface area as function of Ca increment

4.3.1.1.6   Thermal analysis

Thermogravimetric analysis (TGA/DSC) was performed on the phosphate glass sample containing 32 mol% of Ca in its composition. The TGA curve (fig. 10) revealed that two mass loss events happened when the PBG was heated: the first one was characterized by a broad peak between 250 and 330 °C; the second one between 430 and 450 °C with a sharper peak. The total mass loss during the analysis was 6.7%, however, those two events alone were responsible of 5.9% of the mass loss.
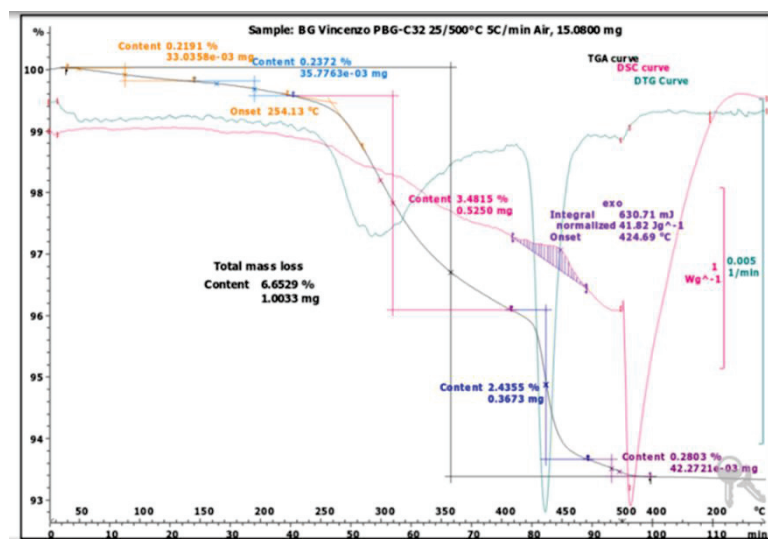
Figure 10. Thermal behaviour by thermogravimetric analysis of the glass C32

The DSC courve revealed the presence of an exothermic phenomenon between 400 and 460 °C. This phenomenon is often associated to the crystallization and, indeed, an XRD analysis performed on the powder after the thermal analysis (fig. 11) revealed the presence of two main phases, sodium calcium phosphate and calcium oxide phosphate, which were not present before (fig. 1B). Remarkably, no endothermic phenomenon associated to a melting event was detected within the range of temperature considered.
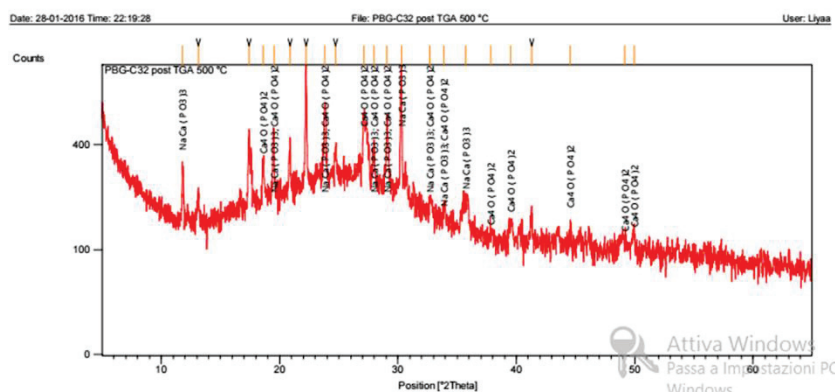

Figure 11. XRD analysis on the C32 glass powder after TGA

4.3.1.2 *Effect of phosphate precursors*

Objectives: The two most commonly used phosphate precursors in sol-gel phosphate glass chemistry are Et/P and Bt/P[45]. The effects produced on the glass system P_2O_5 53% - CaO 24% - Na_2O 23% (mol%) by using one precursor rather than the other were studied and reported.
Methods: For this study, the glasses were prepared as follows. Bt/P or Et/P was added dropwise to NaOMe and left mixing for 1h. Afterwards, Ca-methoxyethoxide was added. Composition, phase and surface structure were characterized by using XRF, XRD and BET/BJH.
Results and discussions: By using different phosphate sol-gel precursors it is possible to control the surface characteristics of the glass particles.

4.3.1.2.1 Composition and yield

The PBG produced using the Et/P precursor had composition closer to the expected one as compared with the Bt/P precursor. However, the yield seemed to not be significantly

improved by the change of the precursor: the yield of the glass produced with Et/P was 5% larger than the glass produced using Bt/P precursor (table 4).

Table 4. Composition (in mol%) obtained by XRF of the phosphate glasses produced by sol-gel using different phosphate precursors

Glasses	P_2O_5	CaO	Na_2O	Yield (%)
Bt/PBG	49	24	27	78
Et/PBG	56	24	20	83

4.3.1.2.2 Phase

The broad peak in the XRD patterns measured for the tested glasses (fig. 12) indicated that the materials had an amorphous glassy phase. It is noted that the type of precursors used did not affect the phase in the final material.
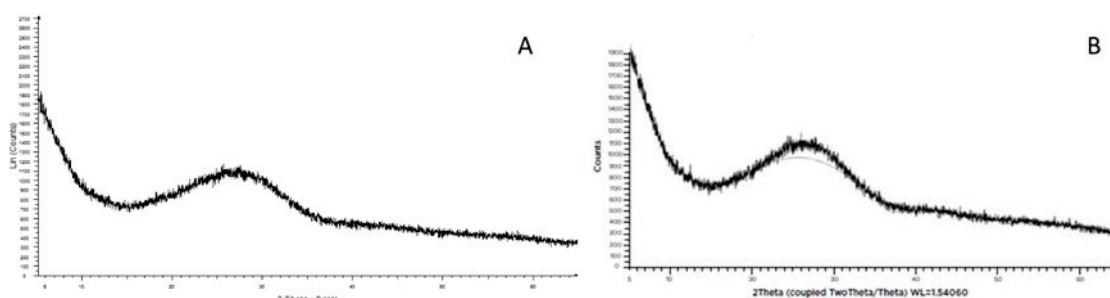

Figure 12. 1 XRD graphs of Bt/PBG (A) Et/PBG (B) glasses

4.3.1.2.3 Structure

More information on the structure and nature of the bonding can be gained from the infrared analysis. Fig. 13 reports the FTIR spectra of the glasses prepared by sol-gel. The assignments are listed in table 5 along with the related Q states.
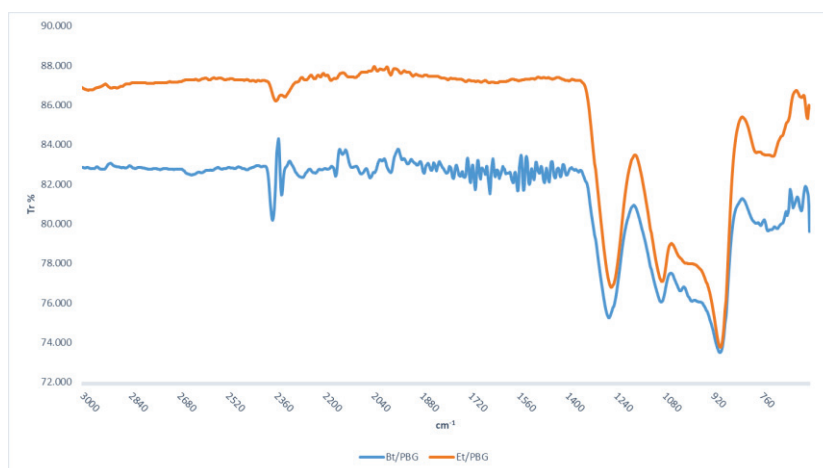
Figure 13. Infra-red spectra in the range 600-3000 cm^{-1}

The spectra of the sol-gel samples displayed the characteristic bands for P-O-P bonding: for the Bt/PBG glass the peaks were identified at 708 cm^{-1}, 762 cm^{-1} and 896 cm^{-1}; for the Et/PBG glass the P-O-P bonding peaks were recognized at 698 cm^{-1}, 722 cm^{-1} and 896 cm^{-1}. In both glasses the first peaks represent the P-O-P bond in symmetric configuration, whereas, the second and third peaks characterise the same bond in asymmetric mode. The pairs of the peaks at 1028 cm^{-1} and 1090 and 1034 cm^{-1} and 1088 cm^{-1} were recognised and assigned to the $(PO_3)^{2-}$ bond in the symmetric and asymmetric state respectively for the first and second member of each pair. Further peaks at 1264 cm^{-1} and 1254 cm^{-1} belonging respectively to Bt/PBG and Et/PBG glass can be detected and assigned to the asymmetric $(PO_2)^-$ bond.

Table 5. Infrared peak positions (cm^{-1}) and assignment of the observed bands for sol-gel glass samples

Samples	Peaks (cm^{-1})/Q states					
	$v_{as}(PO_2)^-$/Q2	$v_{as}(PO_3)^{2-}$/Q1	$v_s(PO_3)^{2-}$/Q1	$v_{as}(POP)$/Q2	$v_s(POP)$	$v_s(POP)$
Bt/PBG	1264	1090	1028	896	726	708
Et/PBG	1254	1088	1034	896	722	698

All the spectra contain Q1 and Q2 units: Specifically, Q1 for the symmetric and asymmetric $(PO_3)^{2-}$ and Q2 for the asymmetric P-O-P and $(PO_2)^-$ bond.

Based on the shape of the FTIR traces it is possible to conclude that the type of phosphate source used to produce the two glasses did not generate differences in the atomic

scale structure of the glasses and in the nature of the bonding. Moreover, it may be concluded that both glasses comprise chains dominated by Q2 units.

4.3.1.2.4   pH measurement in water

The aqueous pH dropped to 3.27and 3.20 considering Bt/PBG and Et/PBG glass respectively after 24 hours of incubation in water. It is concluded that the two different precursors lead to no significant difference in pH.

4.3.1.2.5   Surface features

For the tested glasses, the BET analyses gave a type II hysteresis (fig. 14) typical of nonporous adsorbents.
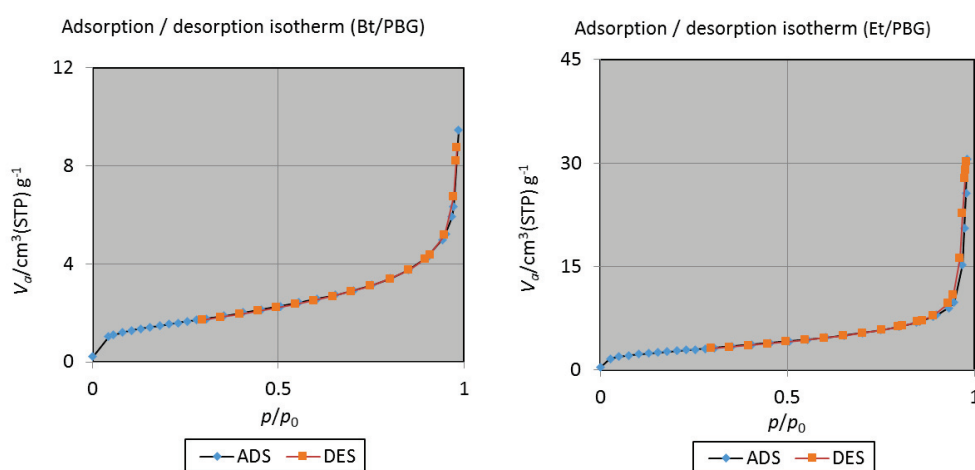

Figure 14. Adsorption and desorption isotherms of the Bt/PBG and Et/PBG glasses

Table 6 summarises pore size, pore volume and surface area of the two materials. The relationship between phosphate precursors and surface features is shown in fig. 15. A great difference was found between the pore volume of Bt/PBG and Et/PBG: the calculated pore vole of Et/PBG was 3.2 times bigger than Bt/PBG glass. The pore size increases by 1.8 times when ethyl-phosphate was used as precursor instead of butyl-phosphate. The surface area was 1.8 times bigger in Et/PBG glass particles.

Those results suggest that using different phosphate precursors could determine different surface properties.
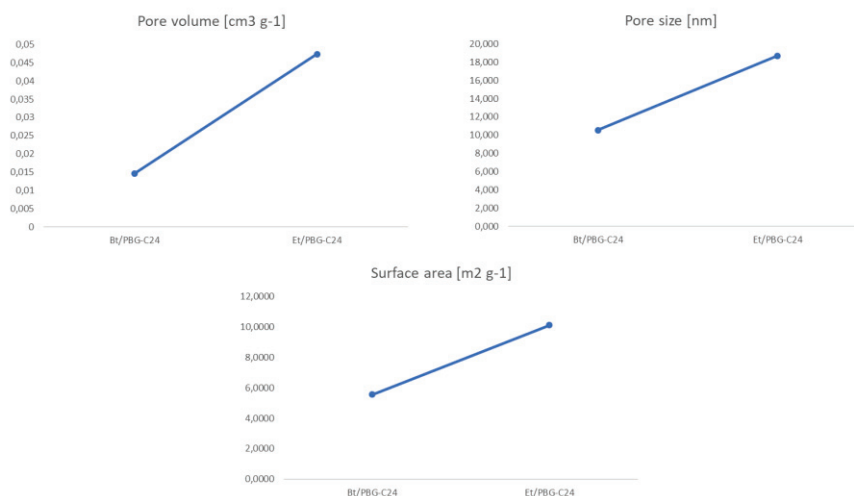

Figure 15. Variations in pore volume, pore size and surface area as function of phosphate precursors

Table 6. Pore volume, pore size and surface area of the glasses obtained by BET analysis

Glasses	Pore volume [cm^3 g^{-1}]	Pore size [nm]	Surface area [m^2 g^{-1}]
Bt/PBG	0.014651	10.537	5.5619
Et/PBG	0.047313	18.711	10.115

4.3.1.2.6   Other considerations

The change of phosphate precursor affected other aspects of the procedure. The dry-step time was significantly reduced when Et/P was used instead of the Bt/P and the delay in the gelation time ensured a more controllable reaction. In addition, a clear and transparent solution was obtained after adding all the precursors (NaOMe first and Ca- methoxyethoxide then) instead of a white milky solution when Et/P was used.

4.3.1.3   *The scale-up effect*

Objectives: When production progress from the lab to the industrial scale, retaining the homogeneity and so the target characteristics may be a challenge. In this section, the effects of scaling-up the sol-gel production of P_2O_5 53% - CaO 24% - Na_2O 23% (mol%) glass were studied at a 3-fold increased scale. The findings are reported below.

Methods: The sol-gel route was used to produce two different bulks of PBGs. Briefly, under constant stirring, Bt/P was added dropwise to NaOMe and left mixing for 1h. Afterwards, the Ca precursor was added. Composition, phase and surface features were characterized in agreement with the manual of the tools.

Results and discussion: The findings reported here suggested that when the production is scaled, differences between small and large scale could be detected. During the design of any experiment, this possibility should be considered to not waste time and precious resources.

4.3.1.3.1   Composition and yield

The up-scaling of the sol-gel production did not bring any variation to the final composition. The XRF analysis (table 7) proved that the actual compositions of both glasses were quite close to each other but equally far from the expected one.

After heat treatment the glass powders were weighed to quantify the yield: the scaled-up preparation gave 47% of the expected material, whereas the lower scale gave 76%.

Table 7. Composition obtained by XRF of the sol-gel glass preparations

Glasses	P_2O_5	CaO	Na_2O	Yield (%)
C24/30	49	24	27	77
C24/100	48	23	29	47

4.3.1.3.2   Phase

The XRF graphs (fig. 16) showed an amorphous phase is replicated in the scaled-up sol-gel glass. This indicates that the size of the production does not affect the phase of the material.
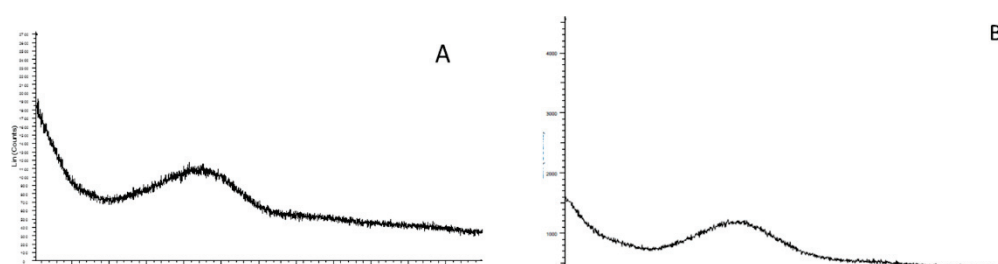

Figure 16. XRD graphs of C24/30 (A) and C24/100 (B) sol-gel glass samples

4.3.1.3.3 Structure

The infrared spectra (fig. 17) provided more information on the structure and on the nature of the bonding of the glasses prepared by sol-gel at a different scale. The peaks were assigned as described by Brow, R. at al 2000[8]. The assignments are listed in table 8 and the related Q states were given where it was possible.
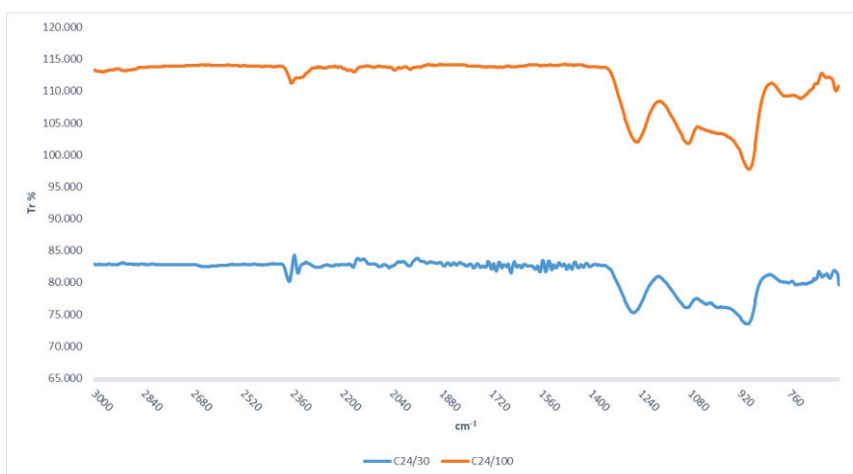

Figure 17. Infra-red spectra in the range 600-3000 cm^{-1}

Table 8. Infrared peak positions (cm^{-1}) and assignment of the observed bands of sol-gel glasses

Samples	Peaks (cm^{-1})/Q states					
	$v_a S(PO_2)^-$/Q2	$v_{as}(PO_3)^{2-}$/Q1	$v_s(PO_3)^{2-}$/Q1	$v_{as}(POP)$/Q2	$v_s(POP)$	$v_s(POP)$
PBG-C24/30	1264	1090	1028	896	726	708
PBG-C24/100	1252	1086	1019	890	758	701

The spectra of the sol-gel samples had the characteristic bands of the P-O-P bonding: for the PBG-C24/30 glass the peaks were identified at 708 cm^{-1}, 726 cm^{-1} and 896 cm^{-1}; for the PBG-C24/100 glass the P-O-P bonding peaks were recognized at 701 cm^{-1}, 758 cm^{-1} and 890 cm^{-1}. In both glasses the first two peaks represent the P-O-P bond in symmetric configuration, whereas, the third peaks characterise the same bond in asymmetric mode. The pairs of the peaks at 1028 cm^{-1} and 1090 and 1019 cm^{-1} and 1086 cm^{-1} were recognised and assigned to the $(PO_3)^{2-}$ bond in the symmetric and asymmetric state respectively for the first and second member of each pair. Further peaks at 1264 cm^{-1} and 1252 cm^{-1} belonging

respectively to PBG-C24/30 and PBG-C24/100 glass; these peaks were assigned to the asymmetric $(PO_2)^-$ bond.

All the spectra contain Q1 and Q2 units: specifically, Q1 for the symmetric and asymmetric $(PO_3)^{2-}$ and Q2 for the asymmetric POP and $(PO_2)^-$ bond.

Based on the shape of the FTIR traces, it is possible to conclude that the scale of production did not result in any modification to the atomic scale structure of the glasses or to the nature of the bonding. Moreover, it may be concluded that both glasses are made by long chains dominated by Q2 unit.

4.3.1.3.4   pH measurement

When soaked in UPW for 24h, the glass prepared at the larger scale showed an augmented stability of the network leading to a less dramatic pH decrease: 4.67 for the PBG-C24/100 compared to 3.27 for the PBG-C24/30.

4.3.1.3.5   Surface area

For the sol-gel glass samples, the BET analysis gave a type II hysteresis (fig. 18) typical of non-porous materials.
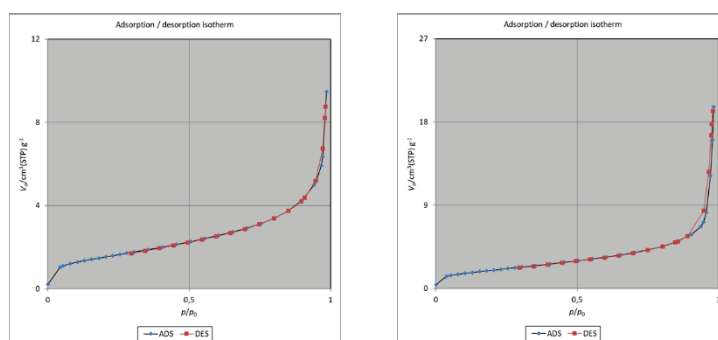

Figure 18. Adsorption and desorption isotherms of the C24/30 (left) and C24/100 (right) sol-gel glasses
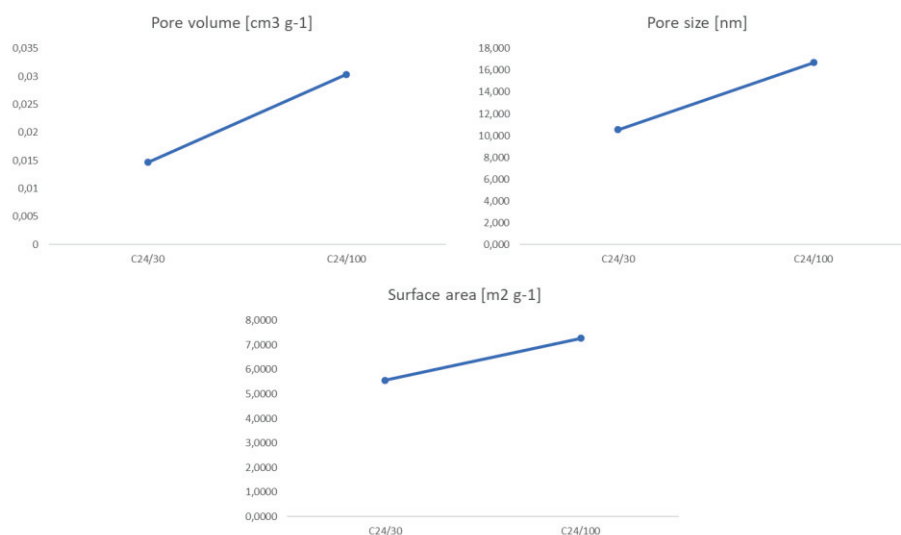
Figure 19. Relationship between surface features and production scale

Table 9 summarises pore size, pore volume and surface area data for the two glasses. The relationship between production scale and surface structure is shown in fig. 19. A difference was found between the pore volume of PBG-C24/30 and PBG-C24/100: the pore volume of the higher scale glass was 2.1 times bigger than for the lower scale glass. The pore size increased 1.6 times and the surface area was 1.3 times bigger for larger-scale production

Table 9. Pore volume, pore size and surface area of the glasses after BET analysis

Glasses	Pore volume [cm^3 g^{-1}]	Pore size [nm]	Surface area [m^2 g^{-1}]
C24/30	0.014651	10.537	5.5619
C24/100	0.030392	16.702	7.2788

All together these results prove that the scale-up of the production may affect some parameters of the material. Factorial Experimental Design (FED) work thus needs to be undertaken when progressing studies from the lab to the industrial scale in order that a robust Standard Operating Procedure (SOP) can be defined.

4.3.2 The FED experiments

Objectives: The initial aim was to produce PBGs by sol-gel route and then apply the glass products in the dental field. Since the materials were intended to be used in humans, issues

about the safety and eligibility of some precursors and solvents were raised. Thus, the need to replace them with non-toxic chemicals arose. Changing precursors and/or solvents might lead to changes in the sol-gel structure formation and so the FED was used to identify preferred processing ranges. By fixing some parameters (for instance the glass composition - P_2O_5 53% - CaO 24% - Na_2O 23% (mol%)) and varying others ((i) EtOH to EG ratio, (ii) time under reflux and (iii) temperature under reflux), the FED software was used to understand how those variables affected the sol-gel reaction to find the optimal conditions in terms of sample yield, phase and colour.

Methods: The yield was determined by directly weighting the sample mass after thermal treatment. The phase was evaluated by XRD (% amorphous phase) and the composition by XRF (deviation from target mol% values for each oxide). The colours underwent a visual examination (subjective scoring on a scale of 1 to 5). The impact that the varying parameters had on yield, phase, colour and composition of the sol-gel preparations was evaluated by using the FED software. Constrains (range of possibility) were imposed and experiments were performed accordingly to the FED software output generated. For each critical response on the final product (phase, yield and colour) a weighting was assigned based on their relative importance.

Results and discussions: The software identified the optimal performing-region/conditions at the edge of the explored area; moreover, inconsistency between repeated points was encountered. More experiments to explore wider range of possibilities was necessary but due to the lack of time, the trials were not taken forward.

4.3.2.1   _Phase_

The phase(s) associated with each of the 11 FED runs were analysed by XRD and data plotted as amorphous phase percentage (wt%). For all the runs, sodium salicylate was recognized as the main crystalline phase. In addition, in the crystalline phases of the runs #2, #5 and #8 the presence of both Na-succinate and Na-maleate was documented.

In depth analysis of the graphs (fig. 20) revealed that it is possible to group the experiments into two sets: runs #1, #11, #10, #9 and #8 and runs #6, #2, #3, #5 and #7. Run

#4 in the middle acts as a linking point. The first group belongs to all the runs characterized by a low EtOH/EG ratio; the second group belongs to all the runs characterized by a high EtOH/EG ratio.

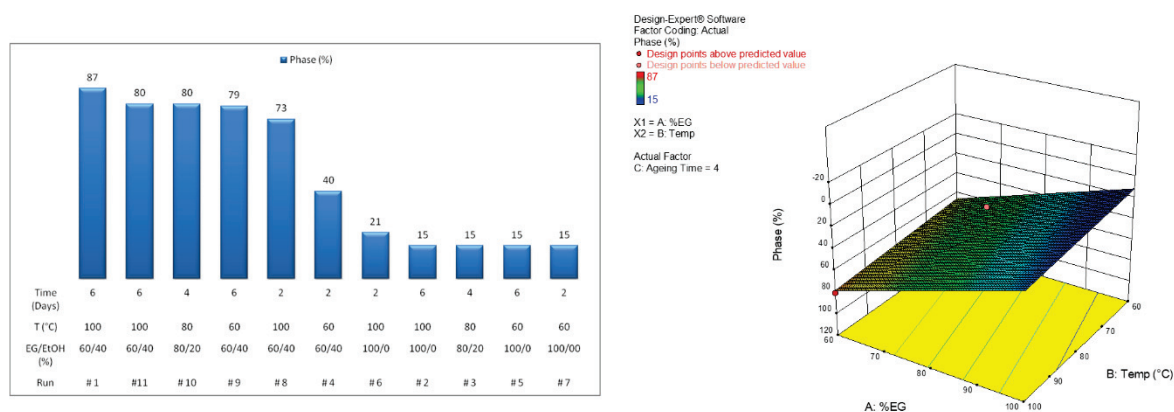Considered together, the results show that the EtOH/EG ratio was the main influencing factor.

Figure 20. Bi-dimensional (left) and tri-directional (right) representation of the trend of the phases in relationship with the variations of solvents ratio, time and temperature

4.3.2.2   Yield

After the heat treatment, the powders were weighed, and their final yield recorded and plotted (fig. 21) as a percentage of the expected product (20g).
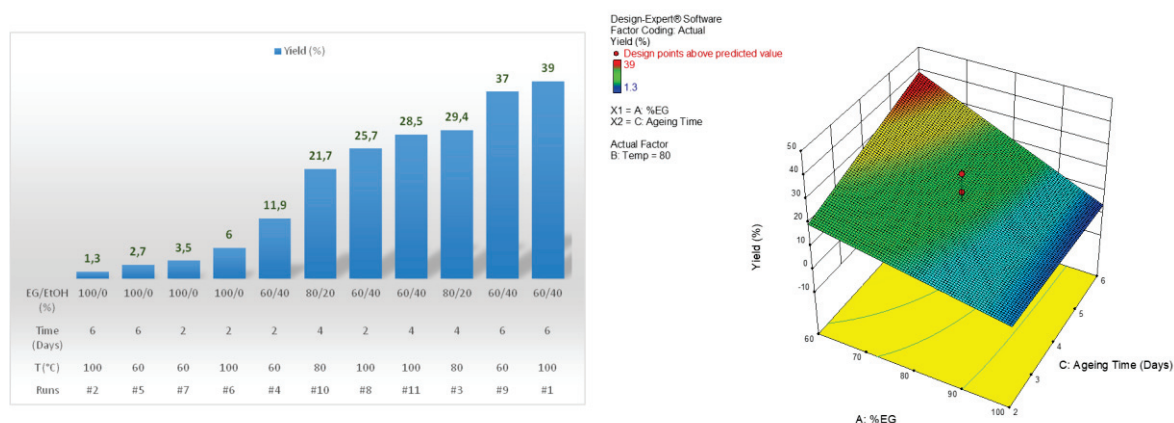

Figure 21. Bi-dimensional (left) and tri-directional (right) representation of the tendency of the yield in relationship with the variations of solvents ratio, time and temperature

It is possible again to cluster the experiments in two groups: group 1 containing the runs #1, #9, #3, #11, #8 and #10; group 2 holding the runs #2, #5, #6 and #7. The run #4 was in the middle as a connecting point. The first group contains all the runs characterized by a low EtOH/EG ratio, whereas, the second group belongs to all the runs characterized by a high EtOH/EG ratio. This trend is in good agreement with the trend described in the section 3.2.2.

Considering those findings, it is possible to conclude that EG/EtOH ratio was the variable that affected the most the yield.

4.3.2.3   Colour

The colour change of the runs after heat treatment (fig. 22) fitted well with the observed trends. All the powders belonging to the first group had a colour varying from brown to light yellow. The others included in the group 2, #4 included, had white colour.

All together those observations lead to the conclusion that colour and phase were linked: while increasing the content of the amorphous phase, the glass powders tended to the brown; the white colour was more typical for highly crystalline materials.
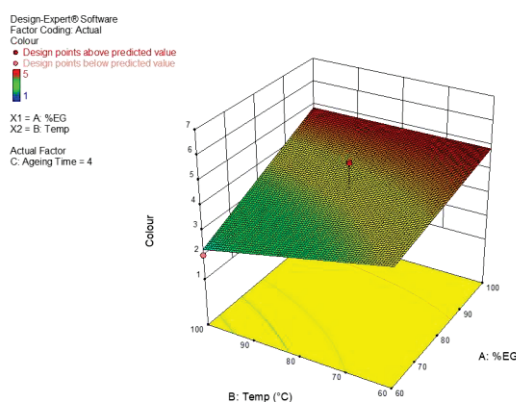

Figure 22. *Tri-directional representation of the colour range in relationship with the variations of solvents ratio, time and temperature*

4.3.2.4   Composition

The compositions of the most promising runs (#3, #9, #8 and #10) were determined by XRF (table 10). The runs #9 and #10 showed the closest composition to the target one.

Table 10. Compositions (in mol%) by XRF of the most promising FED-derived runs

Runs	P_2O_5 (53%)	CaO (32%)	Na_2O (15%)
#10	50%	38%	12%
#9	50%	38%	13%
#3	44%	52%	4%
#8	45%	46%	8%

4.3.3 Glasses by precipitation

Objective: Due to its relative ease of execution, room temperature reaction and non-toxic chemicals used, this methodology was considered as a promising new approach to produce phosphate glasses by a soft and wet chemistry route.

Method: A calcium chloride solution was added to a pyrophosphate solution using a peristaltic pump at a constant volumetric flowrate (7.5 mL min^{-1}). After the complete addition of the calcium reagent, the solutions were stirred for five minutes, and the final colloidal solutions centrifuged at 5000 rpm for 10 min. The resulting gel was washed two times with UPW and heated at 70 °C for 7 days.

Results and discussions: The methodology has some intrinsic limitations like the narrow range of compositions allowed and low yield that strongly limit the applicability of this method for producing desired phosphate glass compositions. As such, it was deemed unsuitable for the purpose of this thesis.

From the article[48] containing the procedure adopted in this work, it is evident that the Ca/P ratio represents an important factor in this methodology because by increasing this ratio the obtained material becomes more and more prone to unwanted crystallinity. In addition, the concentration of the precursors and so the volume of the solutions might have potential to affect the outcome.

In order to validate the procedure and verify the technical feasibility of this method to be adapted to our glass composition (P_2O_5(48%)-CaO(28%)-Na_2O(24%) - mol%) and scale, 6 sets of experiments were planned and organized as follows:

- RUN 1: the concentration of the precursors and the volume of the solutions were kept the same as described in the article. The expected yield was 3.45g

- RUN 2: A scale-up trial was performed increasing the yield up to 10g. In this case, the concentration of the sources was maintained as described. However, due to the increase in yield, the volumes of the solutions were bigger (from 200mL up to 578mL for the $Na_4P_2O_7$ and from 20mL of Ca up to 55mL)

- RUN 3: A trial corresponding to the PYG-00 composition described in the paper but using $Na_4P_2O_7$ (instead of $K_4P_2O_7$) - $\{[(Ca^{2+})_{1-x}(H^+/Na^+)_{2x}]_2[(P_2O_7^{\ 4-})_{1-y}(PO_4^{\ 3-})_{4y/3}]\}n(H_2O))$

- RUN 4: Matching the PYG-01 formulation described in the article but using $Na_4P_2O_7$ (instead of $K_4P_2O_7$) - $\{[(Ca^{2+})_{1-x}(H^+/Na^+)_{2x}]_2[(P_2O_7^{\ 4-})_{1-y}(PO_4^{\ 3-})_{4y/3}]\}n(H_2O))$

- RUN 5: The PYG-00 composition described in the paper using $K_4P_2O_7$ - $\{[(Ca^{2+})_{1-x}(H^+/K^+)_{2x}]_2[(P_2O_7^{\ 4-})_{1-y}(PO_4^{\ 3-})_{4y/3}]\}n(H_2O))$

- RUN 6: The PYG-01 formulation described in the article using $K_4P_2O_7$ - $\{[(Ca^{2+})_{1-x}(H^+/K^+)_{2x}]_2[(P_2O_7^{\ 4-})_{1-y}(PO_4^{\ 3-})_{4y/3}]\}n(H_2O))$

4.3.3.1 *pH measurement*

For runs 1 and 2 the pH of each step was measured as undertaken in the article. The values are reported in table 11. Those values were in good agreement with the expected ones.

Table 11. pH progress during the different steps of the protocol

		pH measurement			
Samples	$CaCl_2$ solution	$Na_4P_2O_7$ solution	After mixing (Ca + P solution)	After centrifuge	After water washing
RUN 1	8.26	10.48	10.05	10.04	9.21
RUN 2	8.30	10.52	10.53	10.04	9.41

After the drying step, all the materials appeared white, brittle and in a fine granular form. The yields of the RUNS were recorded by weighing the powders and are reported below in table 12. The yields of the RUNS 5 and 6 were 6% and 15% respectively and as expected they matched RUNS 3 and 4. The yield of the reactions was very low representing a problem in terms of economically viable production.

From the graph shown in fig. 23 it is evident that the yield was Ca-dependent.

Table 12. Yield of the four materials obtained by precipitation

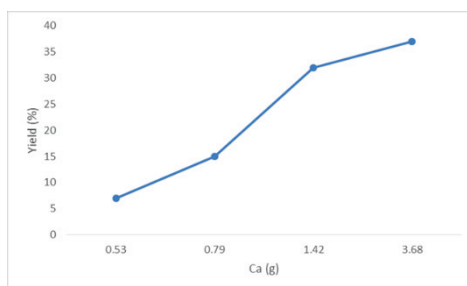| Samples	RUN 1	RUN 2	RUN 3	RUN 4	RUN 5	RUN 6
Yield (%)	37	32	7	15	6	15

Figure 23. Yield of the four materials as a function of the quantity of Ca

4.3.3.3   *Phase*

It seems that the phase of the materials obtained by this procedure is Ca-dependent. By increasing the Ca content (or increasing the Ca/P molar ratio) the material becomes more prone to crystallization. The Ca/P molar ratio of the composition under investigation here is 0.292 which falls within the crystallization range.

The XRD analysis of the RUNS 1 to 4 showed a crystallization phase corresponding to calcium di-sodium pyrophosphate tetra-hydrate ($CaNa_2(P_2O_7)\cdot 4H_2O$). In contrast, RUNS 5 and 6 were totally amorphous.

4.3.4 Coacervate-based phosphate glass

Objective: Investigate a novel approach to produce phosphate glasses with wet and soft chemistry at room temperature with non-toxic precursors and solvents.

Methods: The samples were prepared by slowly adding a 2 M solution of calcium chloride to an equal volume of a 4 M solution of sodium polyphosphate (Graham's salt) at a rate of 5 ml/min under constant stirring. Then, the coacervate layer was washed twice with UPW before leaving to stand overnight. After removal of the water layer, the coacervate layer was dried at room temperature in a vacuum desiccator.

Results and discussions: This methodology seemed to be promising, allowing to explore a wider range of compositions and incorporate further ions into the structure. Moreover, it ensured high yield.

To test this procedure, four different trials were performed:

1. Attempts were made to re-produce the $(Na_2O)0.15(CaO)0.35(P_2O_5)0.50 \cdot yH_2O$-mol% composition of glass described in a literature article[49]
2. Scale-up of the composition mentioned in 1. at a x5 scale
3. Sr-doping by fully and partially replacing Ca in trial 1.
4. Preparation of a different composition (P_2O_5(53%)-CaO(32%)-Na_2O(15%) - mol%)

4.3.4.1 _Repeating work described in the article_

The coacervate phosphate glass studied by D. M. Pickup, et al. 2013 was reproduced as described in the "Materials and methods" section. In agreement with the phase description in the article, fig. 24 shows that the material obtained was totally amorphous to indicate the possibility to obtain a fully amorphous glass material by using the coacervate process.
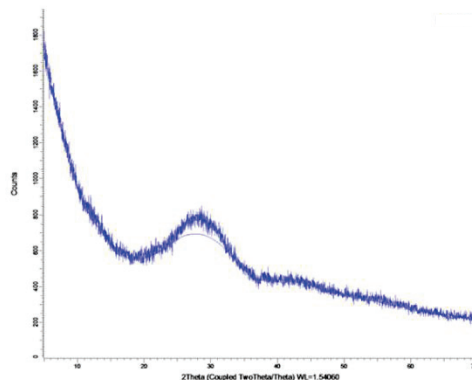
Figure 24. XRD trace of the coacervate phosphate glass reported in the article

4.3.4.2 *Scale-up*

The same composition was scaled up by 5 times. The material obtained was a bulk of 10.08 g (corresponding to about 80% of the expected yield) and containing 95 wt% of amorphous phase as detected by XRD (fig. 25). The crystal phase recorded was assigned to NaCl. This proved that the production can be scaled-up without significantly affecting either the yield or the phase (in term of quality) of the material.
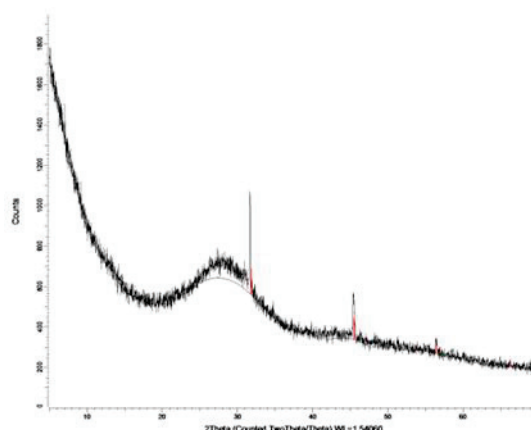

Figure 25. XRD graph of the up-scaled phosphate glass composition reported by the Pickup, et al. 2013

4.3.4.3 *Sr-doping*

Before doping the glass, to check the real possibility to incorporate Sr by using this procedure, Ca was fully replaced by Sr using $SrCl_2 \cdot 6H_2O$ (2M) as source.

After the reaction, the material obtained was a white flocculated mixture (a curd) of coacervate Sr-phosphate. The weight recovered was 1.24 g (corresponding to a 67% of the yield) and 99 wt% of amorphous phase (fig. 26).
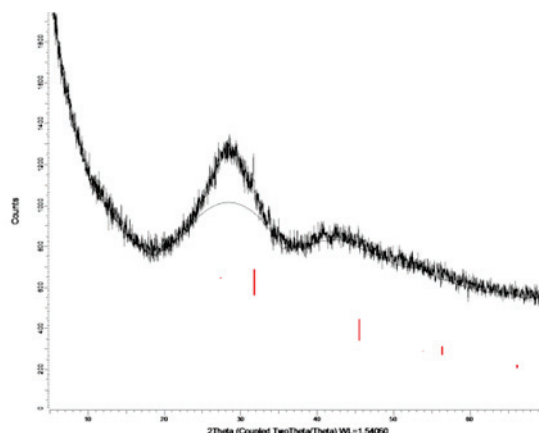

Figure 26. XRD of the full Sr phosphate glass obtained by coacervation process

In the second of the Sr formulations, Ca was partially replaced by Sr in the composition. The $SrCl_2 \cdot 6H_2O$ (1 M) is very soluble in water and when mixing with $CaCl_2$ (1M) and added to the $(NaO_3P)_n$ solution two different coacervate phases were recognized: one oily/gel-like and one flocculated. This was due to the different size and weight of the doping ions (Ca and Sr). The final material weighed 1.0g (corresponding to about 50% of the expected yield) with 100 wt% amorphous phase (fig. 27). Furthermore, XRF data (Appendix 2) confirmed the incorporation of the Sr (as SrO) in the glass network.

All together these results proved that it is possible to use the coacervation methodology to incorporate Sr into a phosphate glass composition without affecting the phase of the final materials.
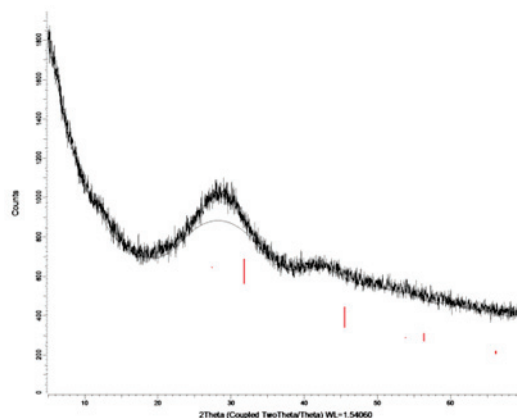
Figure 27. XRD graph of the coacervate-derived Sr-doped phosphate glass

4.3.4.4 Different composition

To check if the phase of the material obtained with this process is Ca dependent (or Ca/P dependent), another glass formulation was run. The XRD pattern (fig. 28) shows the amorphous halo typical of glass materials. It is therefore possible to conclude that the coacervate technique gives amorphous materials over a wide range of compositions. This means that the technique is adaptable and can be used to tailor the formulation of the material in agreement with our need to dope the glass with other ions.
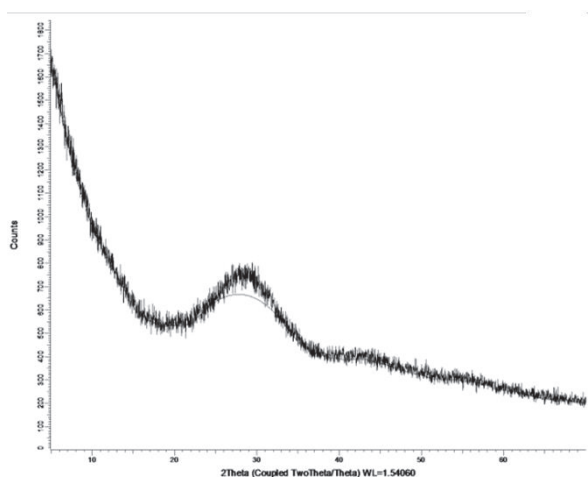

Figure 28. XRD pattern of different composition of phosphate glass by using coacervation process

4.3.4.5 *Surface features*

To further characterize and understand the properties of the material obtained by this method, the coacervate glass powder was submitted for BET/BJH and SEM analysis.

Fig. 29 (left) shows the adsorption/desorption curve for the tested material. According to the IUPAC rules, it is a type 2 physisorption isotherm common of non-porous adsorbents. This data is supported by fig. 25 B where no porosity is visible.
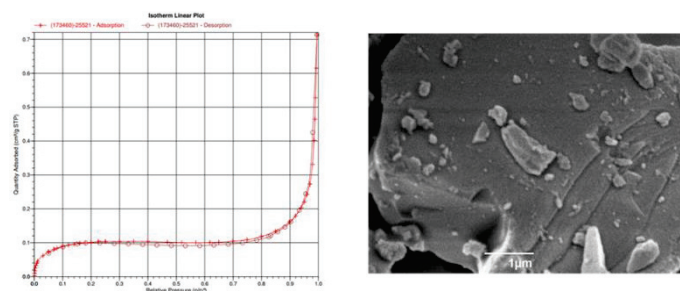

Figure 29. Isotherm linear plot (A) and SEM image (B) of coacervate derived phosphate glass particle

Visualized by microscopy (fig. 30), the material appeared made by particles of irregular shape and different size with sharp edges and well-defined sides. It is possible to notice that faces are smooth with some smaller particles standing above.
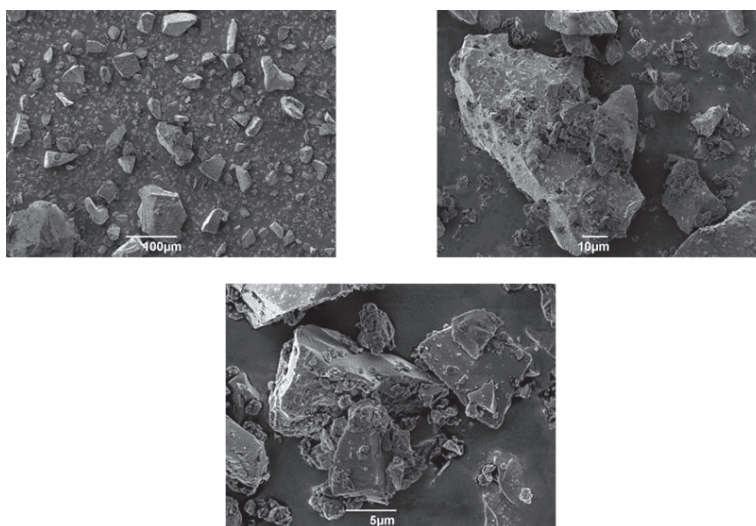

Figure 30. SEM imagines of coacervate phosphate glass particles

4.3.5 Collagen-based scaffolds containing Sr-doped melt-quenched phosphate glasses

4.3.5.1 *Compression test*

Collagen fibres are not soluble in water, indeed, when soaked they become rehydrated rather than solubilized. In an attempt to improve their solubilization, 0.02 N of glacial acetic acid (AcOH) was added to the collagen fibres suspension. In addition, to enhance the incorporation of glass particles within collagen fibres, the concentration of collagen crosslinker was increased by 10 times. Four groups of samples were then prepared as a 2 x 2 matrix experiment:

- Group 1 (G1): without AcOH and 1x of crosslinkers
- Group 2 (G2): with AcOH and 1x of crosslinkers
- Group 3 (G3): without AcOH and 10x of crosslinkers
- Group 4 (G4): with AcOH and 10x of crosslinkers

To verify the possibility that these treatments might have affected mechanical properties of the scaffolds, a compression test was carried out. The results plotted in fig. 31 reveal that neither the addition of AcOH, nor an increase in crosslinker concentration (or both) caused any statistically meaningful changes in the mechanical properties of the scaffolds. Based on those results the G1 materials were retained for subsequent experiments.
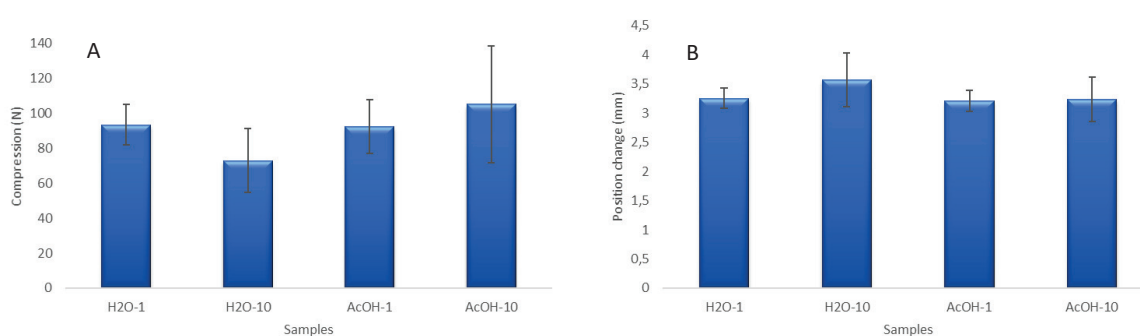

Figure 31. A, force (in Newton) necessary to compress the samples by 4mm. B, actual compression of the samples (in mm) recorded at the theoretical 4 mm

4.3.5.2 *Cytocompatibility assay*

Fig. 33 shows the vitality of hGFs seeded in contact with the scaffolds in comparison with the ctr for 7 days. The cells in contact with the tested materials displayed a vitality ranging between 20 and 30 % of the control; in addition, the incubation time seems to be not a determining factor.
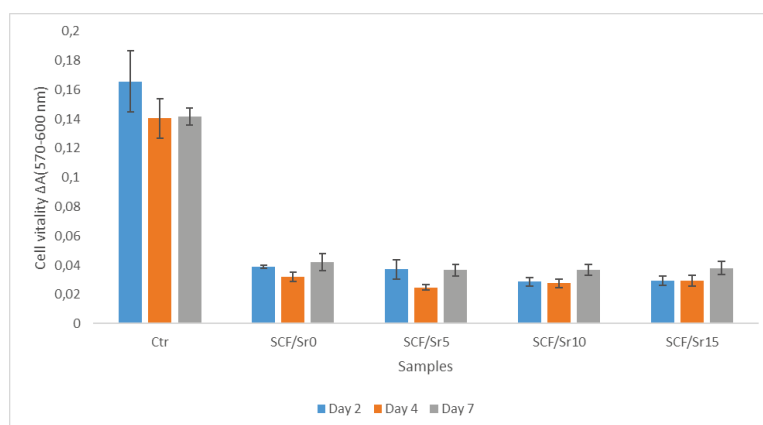

Figure 32. Vitality of hGFs seeded in contact with the scaffolds in comparison with the ctr

4.3.6 Melt-quench vs Sol-gel

Objective: In this section a comparison of the same glass composition ((P_2O_5(53%)-CaO(32%)-Na_2O(15%) - mol%) produced both by sol-gel and melt-quench is described.

Methods: The sol-gel glass was synthesized by adding, under constant stirring, Bt/P to NaOMe. After 1h, the Ca precursor (Ca-methoxyethoxide – CME) was added dropwise.

The melt-quenched glass was prepared by placing a homogeneous blend of raw materials in a quartz crucible and heating it at 1300°C for about four hours. After, the molten mixtures were quickly quenched by pouring onto a steel plate. After quenching, the obtained glass was milled to a particle size ranging between 20 and 200 μm using a TEMA Mill machinery model T 750 k.

Results and Discussions: The methodology used can impact the surface features of the same material. This might determine drastic changes in its behaviour (water solubility for example). This becomes particularly important when it comes to medical applications: different topology (rough surface rather than smooth, for instance) can trigger different cell response

or different degradation time and this can be used to tailor the material in agreement to the application or the host tissue.

4.3.6.1 *Composition and yield*

Table 13 shows the actual final composition of both SG and MQ glasses with respect to the target values. It is possible to notice that the MQ glass delivers a composition closer to that expected when compared to the SG glass. The MQ glass is deficient in P, suggesting losses from volatilization. Moreover, the table shows the relative yield of both preparations: the MQ technique provides for a higher yield than SG for the tested composition. The only losses in MQ arise from glass adhered to the refractory pot used for melting; for SG, there is potential for unreacted precursors to be lost during processing to isolate and purify the solid phases.

Table 13. *Composition in mol% of sol-gel and melt-quenched glasses*

Glass/mol%	P_2O_5 (53%)	CaO (32%)	Na_2O (15%)	Yield (%)
MQ/PBG-C32	51	34	15	81
SG/PBG-C32	49	30	21	50

4.3.6.2 *Phase*

The XRD patterns of both MQ (Fig. 33 B) and SG (Fig. 33 A) glasses show a broad peak indicating that the materials are totally amorphous. It demonstrates elegantly how both techniques equally give high quality materials.
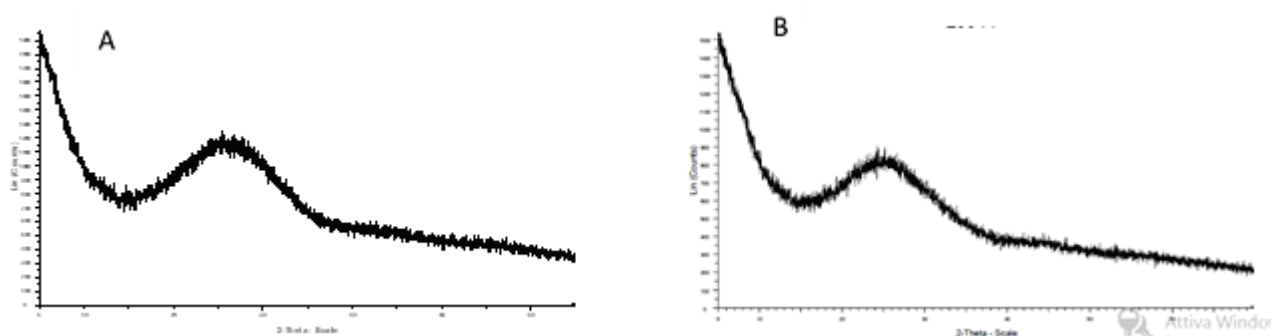

Figure 33. XRD graphs of sol-gel (A) and melt-quenched (B) glasses

142

4.3.6.3 *Structure*

The FTIR spectra of the glasses (fig. 34) prepared by sol-gel (blue line) and melt-quenching (red line) gave further information on the structure and on the bonding in both glass networks. The peaks were assigned and listed in table 14. The associated Q state was also given.

Table 14. *Infrared peak positions (cm-1) and assignment of the observed bands of sol-gel and melt-quenched glass samples*

Samples	Peaks (cm^{-1})/Q states					
	vas(PO_2)$^-$/Q2	vas(PO_3)$^{2-}$/Q1	vs(PO_3)$^{2-}$/Q1	vas(POP)/Q2	vs(POP)	vs(POP)
SG-PBG	1254	1088	1028	898	776	705
MQ-PBG	1266	1090	1031	890	768	624
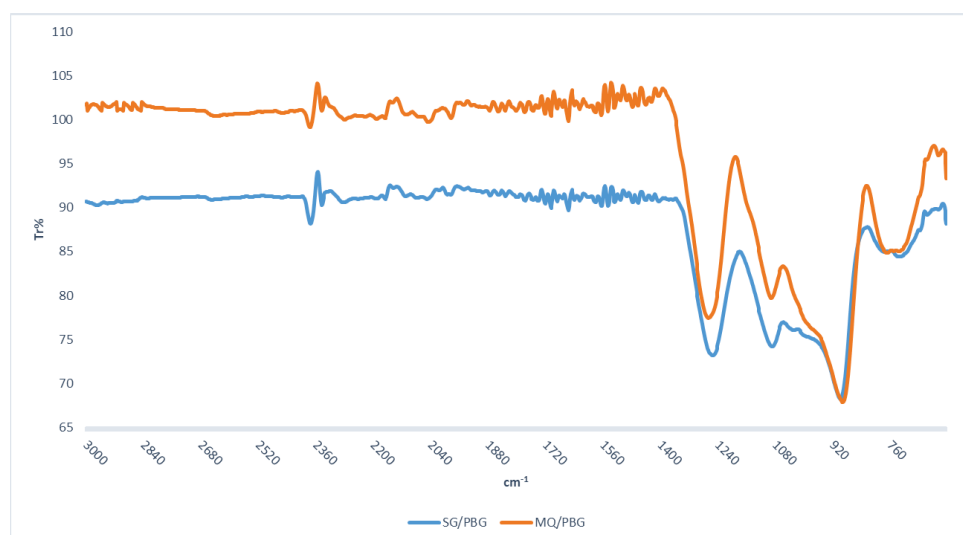
Figure 34. Infra-red spectra in the range 600-3000 cm^{-1}. SG glass (blue line), MQ glass (red line)

The spectrum for the sol-gel sample presents the characteristic band of the P-O-P bonding at 705, 776 and 898 cm^{-1}; in particular, the first two in symmetric configuration, the last in asymmetric mode. In addition, two further peaks at 1028 and 1088 cm^{-1} can be identified and assigned to the (PO_3)$_{2-}$ in symmetric and asymmetric stretch mode respectively. The peak at 1254 cm^{-1} was recognized as asymmetric (PO_2)$^-$. For the MQ glass sample, the P-O-P bond can be recognized both in symmetric and asymmetric configuration (624, 768 and

890 cm^{-1}); the asymmetric and symmetric (PO$_3$)$^{2-}$ at 1090 and 1031 cm^{-1} respectively. The (PO$_2$)$^-$ in asymmetric arrangement at 1266 cm^{-1} can be recognized.

All the spectra contain Q1 and Q2 units: especially, Q1 for the symmetric and asymmetric (PO$_3$)$^{2-}$ and Q2 for the asymmetric POP and (PO$_2$)$^-$.

4.3.6.4 *pH measurement in water*

Fig. 35 shows the pH variation over time. After 2 hours of incubation, the water pH dropped to 4.27±0.06 and 3.51±0.04 for SG-PBG and MQ-PBG respectively. After this time, the pH had stabilized for both glasses.
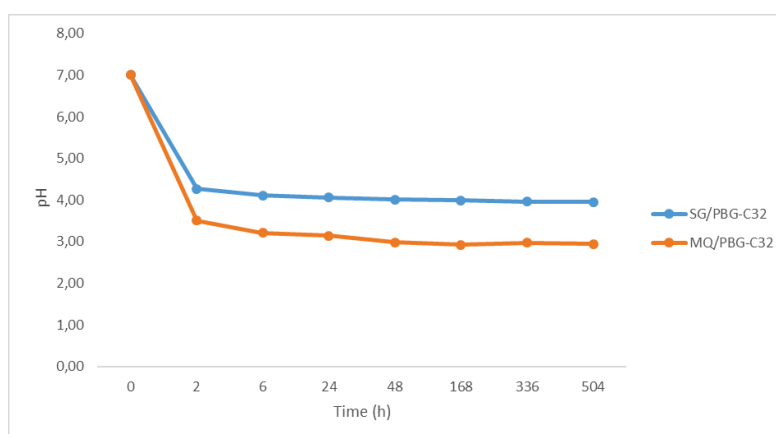

Figure 35. pH variation of the water after three weeks of incubation of MQ/PBG (orange) and SG/PBG (blue) glasses

4.3.6.5 *Dissolution in water*

Both glasses were found to degrade in water but with different kinetics (Fig. 36). The MQ glass showed a linear degradation during the first 24 hours for all the three ions; after this, a plateau phase was reached. The concentration of the ions in the water reflected their content in the glass formulation: the leached phosphate had the highest value because of its highest content in the glass, then the Ca and Na the lowest. In addition, the ion content influenced the release kinetics of the three ions during the linear phase: P had the highest rate followed by Ca and then Na. The SG glass, instead, presented a fast, burst release: the content of ions in the medium (water) reached the highest level already after two hours of

incubation. A deeper observation revealed a subsequent small decrease in ion concentration over time - more evident for P whilst barely visible for sodium and calcium. This may be due to salt precipitation. Also, in this case, the relative content of the ions in solution reflected their concentration in the glass formulation: it should be notice that Na and Ca had the same kinetics due to their almost equally content in the actual composition.
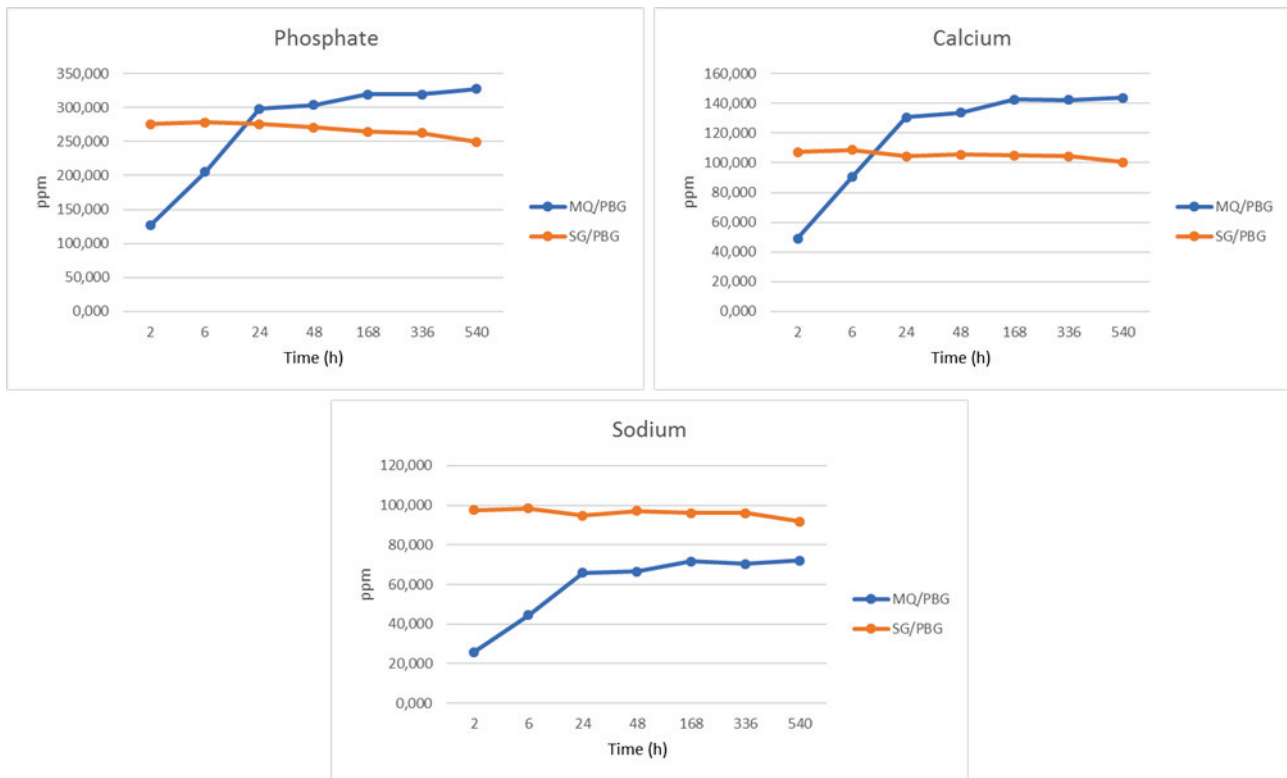
Figure 36. Cumulative release (ppm) of P (A), Ca (B) and Na (C) ions as a function of time (h) for MQ and SG glasses

4.3.6.6 *pH measurement in SBF*

Fig. 37 shows the variation of pH as a function of the MQ and SG incubation time. Surprisingly, the pH of the media became more basic, up to 8.04 and 8.13 for SG and MQ respectively after three weeks. One can notice that between the tested glasses, there is no significant difference in the pH trend development over time.

The green triangle and the violet "X" represent, respectively, the pH of the SBF for the MQ glass and SG glass recorded after 24h of incubation when 10 times the glass concentration is used in the dissolution test (that means 10mg/mL instead of 1mg/mL). Remarkably, despite

such a high glass powder concentration, the pH remained quite stable without reaching a critical value. In addition, a difference between the two glasses is detectable in this case: the MQ glass demonstrated a more stable and neutral pH than the SG glass.
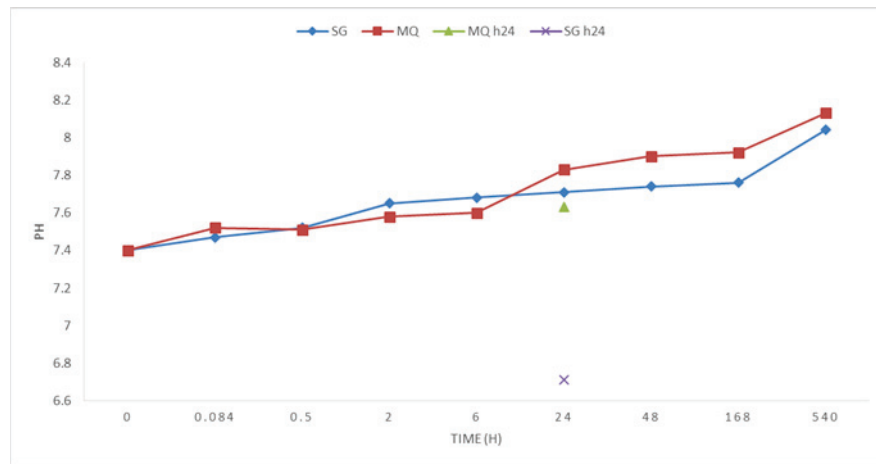
Figure 37. Variation of SBF pH as a function of the incubation time

4.3.6.7 *Comparison of pH variation between water and SBF*

Fig. 38 compares the pH variation of both SG and MQ glasses both in water and SBF during 3 weeks of incubation. It is possible to notice that for both glasses the water pH dropped quickly to 4.27 and 3.51 respectively after 2 hours and it stabilized during the time course. The same glasses in SBF acted differently: the pH remained quite stable during whole the experiment becoming even slightly more basic (8.04 and 8.13 for SG glass and MQ respectively after three weeks).
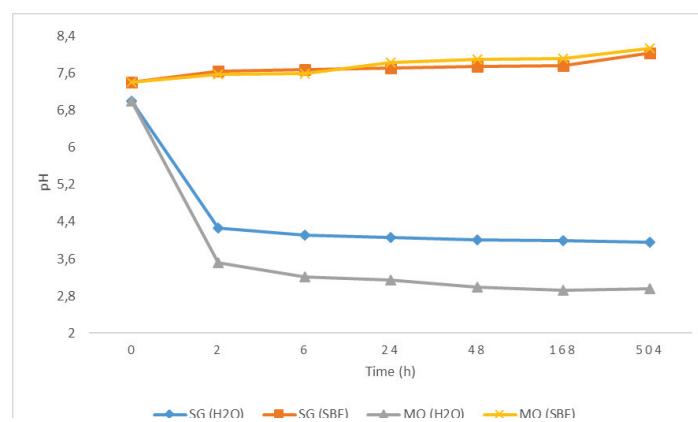
Figure 38. pH variations measurement of both water and SBF for three weeks due to MQ and SG glass soaking

146

From the SEM images (fig. 39) of the glass particles it is possible to notice that their surface topologies and shape were significantly different. The particles of the glass produced by sol-gel had a rough and jagged surface. Whereas, the surface of the particles of the melt-quenched glass were smooth. Also different was the overall shape of the particles: more rounded for the sol-gel glass particles but polygonal for the melt-quenched. In addition, on the surface of the sol-gel particles, needle-like structures were visible absent in the melt-quench preparation.

Figure 39. SEM images at different magnitudes of sol-gel and melt-quench phosphate glasses

5 Discussion

5.1 Sol-gel phosphate glasses

5.1.1 Effect of increasing Ca content on the microstructure

Table 1 summarizes the actual composition (with respect to the expected values reported in section 3.1.1) of three phosphate-based glasses produced by sol-gel where Ca content increases progressively at the expense of Na with the P concentration fixed.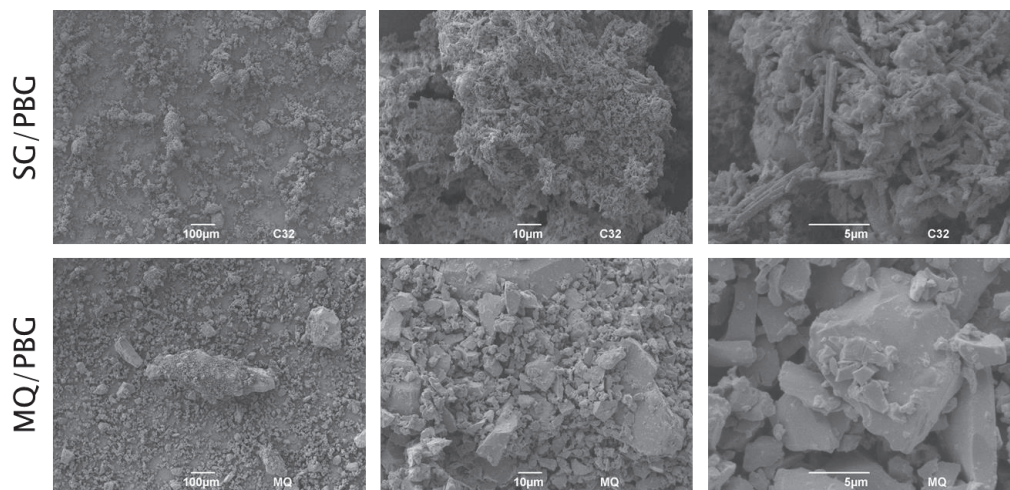 From the data obtained by XRF it is possible to notice that for all three glasses, P content was lower than expected. This difference may be explained by one or a combination of the following possibilities:

1. Under the conditions trialled the phosphoric esters have low reactivity so it may be reasonable to think that some of the butyl-P molecules did not take place in the network forming condensation reactions[45]

2. The semi-quantitative nature of the analysis itself

3. The greater volatilization of the phosphate in the SG glass system due to the low density of the SG powder[92,93]

4. A possible arrangement between phosphate and Ca may have subtracted those ions from the sol-gel polymerization

5. The subsequent washing step may have washed away soluble CaP species along with any unreacted precursor.

However, the aim to increase Ca content was reached. In addition, all three glasses gained Na in their composition. This might be explained considering the role that NaOMe plays in the reaction. NaOMe is a strong Lewis base and it has the task to react and activate P precursors. Its action is proved by the fact that when Na is added, the mixture heats up and the solution turns into a white, thick and milky blend. This fits well with the proposed mechanism and, due to this important role, it is the first precursor to be added. It is known that in sol-gel chemistry the order of addition matters in determining structure and composition.

The yield of phosphate sol-gel product reduces with increasing Ca; in other words, it reduces by reducing the relative amount of sodium precursor used in the reaction. Again, this

can be explained considering the previous discussion: a reduced amount of sodium precursor results in less P precursor being activated, and as such less reactive network former is generated and subsequently fewer condensation reactions take place resulting in a lower glass product yield.

Ca is present in the sol-gel mixture as free ions and it is eventually incorporated into the glass network by coordinating the NBOs of the P tetrahedra in the chains.

XRD analysis as shown in Fig. 1 revealed that all products were totally amorphous, despite the increased Ca/P ratio. (It may have been expected that an increased Ca/P ratio would result in the preferential formation of stable crystalline calcium phosphate phases). This can be explained considering the random distribution of the ions within the network.

The FTIR spectra (fig. 2) reveal no differences in the atomic bonding of the network components attributable to the fact that the P content (as the only network former present) is equal across the three tested glasses.

Fig. 3 shows that after 24 hrs of incubation, the pH of the water dropped in a Ca-dependent manner. Overall the drop of the pH is due to the presence of phosphate ions in the media as a result of the hydrolysis of the P-O-P phosphoester bonds in the glass network. Whereas, the changing composition-dependent trend could be explained by the fact that by increasing Ca content, the amount of sodium being leached from the glasses is also reduced. This has a consequent impact on the ability to buffer the phosphate-induced acidification of the media.

The hysteresis loops of the glasses are shown in fig. 4. They are typical of non-porous materials[94]. The relationship between Ca content and surface features is reported in the graphs in fig. 5. A clear correlation between Ca content and surface topography is evident. The increase in surface area could be due to both the significant increase in pore volume and comparable pore size. The direct correlation between Ca content and surface area could be explained considering that Ca ions have higher coordination number compared to Na and act as an inter-chains cross-likers, whereas Na is linked to just one chain[95,96]. This results in a greater disorder of the phosphate network for the sample containing the lower level of Ca. It means that the sol-gel system evolves from a 3D-network of phosphate chains linked by Ca

to a more disordered system of separated phosphate chains as Ca progressively reduces (or Na increases).

Due to its "average" Ca content, the sample C32 was chosen to be evaluated for its thermal properties (fig. 6). The shape and the temperature of the first broad peak (corresponding to the first mass loss event) was likely due to the volatilization of structural water, phosphates, by-products, maybe unreacted precursors and/or some residual solvent molecules. This is also supported by the fact that it represents the biggest mass loss event in agreement with the high molecular weight of some chemicals used for the reaction. The second mass loss event overlaps with the crystallization phenomenon observed. Due to this and its shape, the two phenomena were thought to be correlated. The cause could be due to the volatilization of some structural components of the glass network and/or further organics.

The following XRD analysis performed on the powder after TGA (fig. 7) shows that two main crystal phases appeared: sodium calcium phosphate and calcium oxide phosphate.

5.1.2   Phosphate precursor effect on the sol-gel chemistry and surface features

Table 4 shows that when butyl-phosphate (Bt/P) was replaced with ethyl-phosphate (Et/P), the actual composition of the glass was closer to that as expected. A deeper observation reveals that the content of P in the Et-PBG was bigger than in the Bu-PBG, whereas, the Na follows the opposite trend. In contrast to what was observed in the presence of the Bt/P (see section 4.1.1), when NaOMe was added to Et/P, the blend appeared clear and transparent, moreover, the gelling time was extended. These findings can be explained considering the different reactivity of the two phosphate precursors. It is possible to speculate that the relative lower reactivity of the ethyl precursor allows the Na precursor to activate and recruit more P precursors. This in turn ensures the target composition is achieved and with less material loss. Ca is present as free ions able to coordinate the chains. The yield seems to not be affected by the replacing of P precursor. From what said, it seems that the ethyl-P is a better precursor.

Fig. 8 shows that the final phase of the materials is independent of which phosphate precursor is used. This is important because it is possible to tailor the physical characteristic

of the sol-gel products based on the intended application by modifying the precursors used without altering the phase.

The FTIR spectra reported in fig. 9 show no significant differences between the glasses despite the different phosphate precursors used. A slightly bigger definition for the peaks at 896 and 722 cm^{-1} (v_{as}(POP) and v_s(POP) respectively) can be observed for the glass made by using the Et/P. This could be explained considering the higher P content in this glass compared to the Bt/PBG (table 4).

The drop of the water pH after 24 hrs of glass incubation did not show any difference despite the different P precursors used. This suggests that the dissolution properties of the material are independent of the phosphate precursor used.

A type 2 hysteresis (fig. 10) typical of non-porous materials was obtained for both glasses after BET analysis, independent of the phosphate precursor used to carry out the sol-gel reaction. The relationship between textural features and P precursor is shown in fig. 11. The difference in surface area could be due to the big increase in pore volume and pore size in Et/PBG glass. The influence of the phosphate precursors on the surface profile of glass particles may be explained by considering the alkoxide groups of the two precursors used for this study. The butyl group has four atoms of carbon in its structure, whereas, the ethyl group has two atoms of carbon. The steric influence of the two groups is different, being bigger for the butyl group as compared with the ethyl group. Therefore, the use of different phosphate sol-gel precursors reveals differences in the properties of the phosphate glass products and the kinetics of the sol-gel reactions taking place. A possible reaction mechanism could be suggested where the butyl is displaced and replaced faster than the ethyl. In addition, due to the smaller size, the ethyl remains trapped easily into the network during the formation, explaining the bigger values (pore size and pore volume and surface area) found.

5.1.3   The scale-up effect

The XRF-obtained composition of the materials produced at lower and higher reaction scales (table 7) did not show any significant difference. That means that the scale of the reaction process did not compromise the material in terms of composition. On the contrary,

the yield seems to be compromised: the higher scale gave the lowest yield. This could be a consequence of the volume of the reaction and the dilution effect: the volume of the higher scale reaction was 500 mL compare to the 200 mL of the lower scale. Since a temperature of 60 °C is necessary to obtain the complete gelation, a difference in temperature could have been created between the edge of the flask (closer to the heat source) and the core of the reaction (far from the heat source). This might have dispersed the reactant subtracting them from being activated and being incorporated in the sol-gel network. However, the phase of the glasses was preserved despite the scale (fig. 12).

From the spectra reported in fig. 13 it is possible to gather the production scale did not determine any change in the atomic structure of the PBGs.

The difference in the drop of the water pH after 24 hrs of incubation is interesting. It is known that Na prefers the surface of the glass rather than the bulk[97]. A bigger reaction volume could have allowed a better mixing and so ensure the ions occupy easily their favourite position. Ions on the surface are more prone to be released and exchanged with the media rather the ones in the bulk. Due to this scenario, the faster release of bigger quantities of Na of the higher scale glass compare to the smaller one could explain the pH values detected (3.27 and 4.67).

Fig. 14 shows a non-porous hysteresis loop for the two scale glasses under study. The relationship between scale production and surface features is reported in fig. 15. The higher surface parameters could be explained considering the reaction volume: the phosphate chains had more space to build the network and this entailed for bigger pores of the existed ones.

5.2   The FED experiments

Despite the sol-gel route gave good glass materials which were fully characterized, the need to use less hazardous precursors driven by the intended (biological and clinical) end-application stimulated the research of more suitable alternative precursors (Appendix 3). In this context the FED software was used in an attempt to optimize the experimental set-up of a new route of sol-gel reaction involving alternative and more safety chemicals.

Figs. 16 and 17 (left hand) show respectively the trend of phase and yield from the 11 FED runs. As described in the previous sections (3.2.1 and 3.2.2), it is possible to assemble the runs in two separate groups based on the EG/EtOH ratio. The highest yield and amorphous phase content (wt%) was given by the runs with high EtOH content. This can be explaining considering the viscosity of the solvents: 0.983 and 16.9 mPa.s for EtOH and EG respectively. It is well-known that the viscosity of the media affects the reaction by reducing the reaction rate. The increasing concentration of the EtOH had the effect of reducing the viscosity of the reaction media favouring the sol-gel reaction.

The temperature, rather than the time under reflux, seemed to play a synergic role: the increasing temperatures had the effect to further reduce the viscosity of the medium encouraging more efficient sol-gel reactions.

Another parameter to be affected by the temperature and the "mixing effect" (but not related with viscosity) is the density of the reaction medium. In this this case both increasing EtOH concentration and increasing temperature had the effect of reducing the density of the medium favouring the reactions. Considering this, it is possible to conclude that the viscosity rather than the density or a combination of both were responsible for the observed trends. Therefore, it is not surprising that the closest composition to the target belongs to the runs #10 and #9 (table 10).

In the light of what has been said, one can suppose that the optimal experimental condition could have been met by keeping the EG as low as possible and rising the temperature as high as possible. This thought was corroborated by the 3D-graphs (figs. 16 and 17 – right hand – fig. 18) that placed the optimal region at the very edge of the graph. However, this position is unfavourable and makes the prediction unreliable. In fact, the run #1 (the best obtained) was repeated twice with different results. This lack of reproducibility was supported also by the run #3 which is present twice (run #10) in the experiments as a check point. Due to those difficulties, the sol-gel route was put aside to explore other methods more reliable and safety.

5.3   Glasses by precipitation

The precipitation method[48] was explored as a novel technique to obtain glassy materials by soft and wet chemistry. However, this methodology revealed some intrinsic limitations that make it not so suitable for our scopes. One of those was the extreme low yield. Two aspects of such a limitation were the high amount of waste material generated and the impossibility to run a complete set of experiments on the same preparation. In addition, the yield was strictly Ca dependent (table 12 and fig. 19): this was quite logic since the phosphate was constant and the Ca increased progressively. This revealed another limitation of within the procedure: the Ca/P ratio. It was shown that by increasing the Ca/P ratio (in other words increasing the Ca content) the tendency to produce crystalline products is increased. This imposes a limit to the range of compositions for which it is possible to make an amorphous product with this method. For instance, the Ca/P molar ratio of the targeted composition is 0.292 and when synthesis of this material by this new precipitation route was attempted the product was found to be highly crystalline. Comparing with the sol-gel preparation, the yield seems to follow the opposite trend: it reduces by increasing Ca. This may be due to the low Na precursors that recruit less phosphate precursors to make the glass. In addition, the sol-gel route seems to overcome the Ca/P issue.

A further limitation is given by the additional ions to Ca and P it is possible to incorporate in the composition. Keeping the Ca/P in the range of amorphous phase, by replacing K (as describe in the original method) with Na a crystal phase appeared. This might be due to the different size and ionic strength of the two ionic species. This limits further the application of this methodology to produce the compositions of interest for this study.

5.4   Coacervate phosphate glasses

To overcome the limitation described before (section 4.3) this new approach[49] was taken into consideration. In order to verify that the Ca/P ratio was not a restriction for this process, besides the composition described in the article, our own formulation was made. Both resulted in amorphous products and gave high yields (fig. 20 and fig. 24). The

composition studied in the article was scaled up by five times to check whether this would affect the phase purity of the product. The obtained yield was very high (80%) and XRD showed that the product glass was amorphous (fig. 21). The observed sodium chloride residue could have been due to an excess of ions coming from the augmented number of precursors and maybe, with the scale-up, a more extensive washing protocol is required.

The next step was to further verify the flexibility of the composition by fully replacing Ca with Sr or at least adding it at the expense of Ca. On replacement of Ca with Sr in the process, it was observed that the coacervate product went from being oily and gel-like to becoming flocculated and particle-like. This change in product consistency is likely to be due to the differing ionic radii of the calcium and strontium species involved in the reaction.[98]. Nevertheless, the material obtained was still totally amorphous (fig. 22). The joint presence of Ca and Sr did not affect the phase of the material, XRD again showed that this material was totally amorphous (fig. 23). During the reaction the two stages were recognised due to the co-existent in the solution of both Sr and Ca. In both cases, XRF data confirmed that the Sr was incorporated in the composition as oxide.

Fig. 25 reports a non-porous material type 2 isotherm for the coacervate phosphate glass. This may be explained considering that in the silica sol-gel the porosity comes from the removal of water resulting in the formation of pores and inter-particle voids. Since coacervation is an aggregation process due to the immiscibility of two phases that silica sol-gel mechanism does not happen, and pores are not formed. However, this result contrasts with W. Kopp, 2012[99]: for the same material he published a type 4 hysteresis typical of mesoporous materials. This difference may be explained by considering some differences in the methodology. First, in this work the drying step was performed under vacuum and at room temperature instead of 60 °C for 24 hours. In addition, in Kopp's paper, this step was followed by a thermal treatment at 500 °C for 24 hours which is missing in my case. Maybe the thermal treatment is the cause and explanation for the (meso)porosity (by removing water as for silica)?.

Altogether, these results confirm that the coacervate technique gives a non-porous glassy material formed by smooth polygonal particles (fig. 30).

5.5 Collagen-based bioscaffold containing melt-quenched derived Sr-doped phosphate glass particles

The initial scope of the project leading to this thesis was to produce porous phosphate glasses by sol-gel technique for dental applications. After some failed attempts, the successful protocol described in the section 2.2.1.1 was established. However, despite the initial expectations, the obtained glasses were non-porous.

The ultimate goal was to incorporate these materials in biocompatible scaffolds for human use, therefore, the presence of hazardous solvents (MtOH and 2-methoxyethanol) and precursors (Ca-2-methoxyethoxide) made this route infeasible and alternative precursors/solvents were explored. Table 1 in the Appendix 3 shows all the attempts made to find valid substitutes (like water or EtOH as solvents and acetate-based precursors) to obtain the PBGs via sol-gel process. After all, nothing really promising came, so the sol-gel route was put aside, and other room temperature methodologies were considered.

The first method explored was the precipitation method, however due to the aforementioned limitations, it proved to be unsuitable for our scope.

The coacervate process was highly promising but also in this case the materials obtained were non-porous.

Due to tight deadlines and still having obtained non-porous materials, the wet chemistry route to produce PBGs was laid aside in favour of the melt-quench technique which is more reliable in terms of composition and phase and gives easily high yield.

Considering all those facts together, in the end, phosphate glasses produced by melt-quench technique were chosen to be combined with collagen fibres to make porous scaffolds.

The Col1 fibres are not soluble in water undergoing a rehydration process rather than a proper solubilization. This might introduce limitations for the crosslinkers to react with collagen functional groups and interact with the particles. A weaker interaction between the fibres and the glass particles might affect some important mechanical properties.

To verify if an augmented solubility of the collagen fibres and/or a tighter link between the fibres and the glass particles could have improved some mechanical properties of the

scaffolds, a compression test was carried out on the four experimental groups described in the section 3.6.1. From the graph illustrated in fig. 31 it is possible to recognize some trends: 1. the presence of the AcOH (G1 vs G2) did not affect the properties of the scaffolds; 2. the increased concentration of cross-linkers seems to improve the resistance to compression only when the AcOH is present in the collagen suspension (G3 vs G4); more crosslinker seems, on the other hand, to reduce the mechanical properties of the scaffolds when only water is present (G1 vs G3 vs G4). From this, it is possible to conclude that the conditions in G4 gave the best scaffold performer. This could be explained considering that the AcOH could have made available more functional groups on fibres to react with the crosslinkers. However, the big standard deviation between the groups made those differences non-statistically significant (P=0.76, n=5). The presence of such big errors was to be attributed to the sponge-like nature of the materials and maybe its non-homogeneity due to the methodology used: within the same bulk there might have been microdomains where the concentration of glass particles or the aggregation/configuration of the fibres is bigger/different than other parts. For those reasons the ctrl group (G1) was chosen for the next experiments.

To check the biocompatibility of the scaffolds, hGFs were seeded in direct contact with the materials for 7 days. Fig. 32 shows that, for the whole experiment, the vitality of cells was low compare with the ctr (understood as cells seeded in an empty well): those data suggest that cells were in a state of suffering. The reason beyond this unwelcome condition is to be found within the scaffolds. As described in materials and methods section, the Col to PBG particles ratio was 1:1, that means that 50% of the bulk of each scaffold was made up of phosphate glasses. It is known that those glasses dissolve very quickly in water environments releasing great amount of phosphate ions which entails the acidification of the medium the glasses are soaked in. Thus, it is possible to conclude that the acidification of the cell medium below the physiological pH due to the release of phosphate ions following the hydrolysis of the glass network was the cause of such low values. This was confirmed by the phenol red (normally presents in the cell media as pH indicator): as soon as the medium was in contact with the scaffolds, it exhibited a transition to yellow indicating pH way below 6.0.

5.6   Melt-quench *vs* Sol-gel

Table 13 compares the actual composition the MQ glass and SG glass with respect to the expected composition. The difference between the actual and the expected composition for the SG preparation may be explained by one or a combination of the following possibilities, as described earlier in section 4.1.1: 1. The phosphoric esters are poorly reactive so it may be reasonable to think that some of the butyl-P molecules did not react[45]; 2. the semi-quantitative nature of the analysis itself; 3. the greater volatilization of the phosphate in the SG glass system due to the lower density of the SG powder compared with MQ powder[92]; 4. a possible arrangement between phosphate and Ca may have subtracted those ions from the sol-gel polymerization; 5. the subsequent washing step may have washed away soluble CaP species along with any unreacted precursor. These considerations (along with the bigger number of steps that the SG material went through) may also explain the difference in yield between SG and MG.

The relative phases are shown in fig. 33: both methodologies gave totally amorphous materials due the random and non-ordered arrangement of the atoms in the networks.

By comparing the FTIR spectra of the two glasses (fig. 34), it is interesting to note that the intensity of the bands at 1200 and 1100 cm^{-1} is greater for MQ glass. The same can be said for the bands at 770 and 725 cm^{-1}. Those differences suggest a more connected network for the MQ glass and a more open structure for the SG glass (also maybe to the fact that there is a higher amount of P_2O_5 in the MQ glass sample). However, based on the shape of the FTIR peaks and in agreement with the previous studies[92], it is possible to conclude that at the atomic scale, the structure of the two glass samples is similar.

Independently of the preparation method, fig. 35 shows that both glasses reduce the aqueous pH due to the presence of phosphate ions as results of the dissolution of the POP bond in the glass network.

The drastic difference of the release kinetics between MQ and SG glasses (fig. 36) may be explained considering both the relative density of the two networks and the dissolution mechanism. As reported[92,93], despite the similar atomic scale structure of the glasses coming from sol-gel and melt-quenching, the latter presents a higher density: tighter cross-linking

results in a further difficulty for the water to penetrate the glass network and hydrolyse the POP bonds. In addition, sol-gel glasses contain a significant amount of OH groups, compared with MQ glasses, which act as chain terminating groups[87] and strongly reduce the connectivity of the network. Moreover, it has been reported that the presence of OH groups reduces the chain length[100]: the bridging action of the modifiers is weaker resulting in less connectivity between the chains. The combination of these factors determines a faster protonation of the most external NBOs that causes the instant hydrolysis of the network and the burst release of the modifier ions.

The pH trend (fig. 37) of the SBF towards basic values after the glasses were soaked for three weeks could be explained by considering that the SBF, due to the presence of the tris-HCl, is a buffered system: it is able to subtract protons from the media stabilizing the pH. Due to this, the Na (and the Ca) coming from the glasses overtakes the "acidification power" associated with the phosphates leached from the dissolving networks leading to a more basic value. This is supported by the 24 hours single points measured where despite the concentration of the powder is 10 times higher, the pH did not reach critical values. The difference between MQ and SG could be explained taking into consideration the concepts expressed immediately above.

By comparing the development of the water and SBF pH (fig. 38) one can observe that the same glass material can act differently in different solutions based on the properties of the solution itself. This can be explained considering what just said: buffer system, composition, ionic strength and so on.

The SEM images at different magnitudes of both MQ and SG/PBGs (fig. 39) show the different texture of the particles. The different surface feature can be explained considering the different approaches. In the sol-gel method (bottom-up approach) nanoparticles are built by progressive aggregation[101], whereas, in the melt-quench technique (top-down) particles are fused together generating more compact units. This provides the explanation of the different surface topologies observed between the two tested glasses coming from the two different methods and adds further support to what was observed for the dissolution behaviour.

Considering the previous discussion, it is possible to draw the conclusion that the surface features of the same material compositionally can be modified by changing the production route. This might determine drastic changes in the behaviour of the materials (water solubility for example). This becomes particularly important when it comes to medical applications: different topology (rough surface rather than smooth, for instance) can trigger different cell response or different degradation timing and this can be used to tailor the material in agreement to the application or the host tissue.

5.7   Melt-quench *vs* Sol-gel *vs* coacervation

Based on the samples with the same composition (P_2O_5(53%)-CaO(32%)-Na_2O(15%) - mol%) it possible to compare the data coming from the figures 5B and 28; 4B and 29A; 30 and 39 in order to underline differences and similarities between three different glass processing approaches: melt-quench, sol-gel and coacervation process. The first group of figures refers to the phase of the obtained materials: all the three methods were equally able to give totally amorphous glassy materials. The second group of figures analyses some surface parameters of the particles: the BET performed on the glass particles produced by sol-gel and coacervation gave a type 2 isotherm typical of non-porous materials. For the melt-quench derived glass particles the BET was not performed because it is known that such a technique generates non-porous materials. The biggest difference was revealed by SEM: whereas coacervation and melt-quench generate glass particles with the same topography (smooth surface and polygonal shape), the sol-gel route generates less well-shaped and defined particles with irregular edges and rough surfaces. Thus, it is possible to argue that the three materials might behave differently under the same condition. This further supports and is supported by what has been discussed in the previous paragraph (4.7). In terms of yield, the sol-gel route proved to be inferior.

It is possible to conclude that the choice of a particular processing method should be done considering the safety of the process, how the production route may affect the properties of the materials and considering the future applications.

6 Conclusion and future perspectives

In the presented thesis, different methods to produce bioactive glasses have been reported. The synthesised glasses were characterised in terms of structural properties including XRD, BET, SEM and FTIR spectroscopy that indicated the successful production of phosphate-based glasses. The composition was confirmed by XRF and dissolution behaviour by ICP.

Initially, the effects of increasing Ca at the expense of Na on sol-gel phosphate glasses were studied. However, there were some limitations: such phosphorus loss (4 mol%), lack of porosity and mainly toxicity of some solvents/precursors. To overcome the phosphorus loss, butyl phosphate was replaced with ethyl phosphate for sol-gel synthesise the ternary P_2O_5-CaO-Na_2O glass systems. Thus, the effects of replacing the precursors were analysed. The XRF revealed an increased phosphorus content.

In an attempt to find a safer sol-gel route, FED software was used to plan experiments with alternative precursors. The lack of reproducibility required the evaluation of alternative glass synthesis methods. The precipitation method was the first to be explored but the high limitation imposed by Ca/P ratio to obtain amorphous materials, ability to use alternative ions and very low yield obliged the exploration of alternative approaches.

The coacervation process was revealed to be promising and without limits. The feasibility of the method was validated by synthesizing different compositions, scales and introducing different ions. However, due to the lack of porosity and apparent lower reliability in reaching a target composition, in the end, the melt-quench technique was chosen to prepare glasses with the general formula of $(P_2O_5)53–(CaO)32-X–(Na_2O)15-X–(SrO)X$, where X = 0, 5, 10 or 15 mol% for dental application. The degradation studies revealed that the dissolution rate of these glasses reduced as Sr was substituted in place of Ca because of the enhanced cross-linking effect of strontium and gave an indication of how the solubility of the glasses can be controlled for various biomedical applications.

Subsequently, the MQ glasses were incorporated in collagen-based scaffolds for dental pulp regeneration application and cell-mediated remineralization. The effect of collagen crosslinking and improved collagen solubility was studied: the compression test revealed no significant improvement for the tested conditions. Scaffolds were presented as highly porous materials with interconnected channels to potentially favour nutrient and

163

oxygen flow to the regenerating host tissue. In water they were found to degrade indicating the possibility to be replaced by natural tissue (a property called bioresorbability). The collagen fibres were proved to interact with the glass by-products altering the dissolution rate of the glasses. This is an interesting property because this ion retention could facilitate crystal growth on the surface. In fact, one of the tested scaffolds was able to grow an HA-like layer after immersion in SBF for one week.

A comparison between the different methods described and used in this thesis has been made. The methodology used determined changes in some key features of the materials like particle shape, dissolution behaviour and surface topography which may generate different cell response. The application should be the driving force for choosing the most suitable method.

From this thesis it is evident that health, safe, repeatability and yield were the driving forces for determining the most suitable process. Considering the characterizations made on the materials coming from the explored methods, it is clear that the coacervation process seems to be the most promising route. The use of non-toxic precursors, the relatively fast execution, the high yield and the repeatability of the methodology, besides its flexibility in terms of compositional range make it a worthy route for future experimentations. This direction of research should focus on optimised thermal treatments to achieve porous materials and further doping with Ag for possible antibacterial effect and other ions for bioactivity, cytocompatibility and so on. Since, from the knowledge of the author, no commercial products for medical and in particular for dental application are on the market, possible incorporation of the materials coming from this route in a marketable product might be considered.

Another key point is the composition which determines all the final properties of the material. Considering the findings discussed in the present thesis and the literature review exposed in the introduction, a phosphate glass with high concentration of Ca, between 40 and 50 mol%, and a P content ranging around 40-45 mol% should guarantee a glass network stable enough to support cell attachment and proliferation, thus allowing them to create a natural extracellular matrix that would replace the glass during longer-term dissolution.

From the cytocompatibility test performed arises that, when it comes to composites, the ratio between the different constituents is an important feature of their formulation. In the case examined in this thesis, it is evident that the 1:1 ratio between col and PBG particles is too high leading to an unfavourable environment for cells. In the future, composite scaffolds where the glass particles content is way lower than collagen fibres content could be explored. Alternately, methods that increase the stability of the glasses (e.g. annealing) might be taken into consideration.

7 Appendix

7.1 APPENDIX 1

This section reports a comparison study on the dissolution behaviour of a single phosphate glass composition (P_2O_5 (53%) – CaO (32%) – Na_2O (15%) – mol%) produced by sol-gel versus melt-quench routes. In both trials the test involved three weeks of incubation in SBF at 37 ℃.
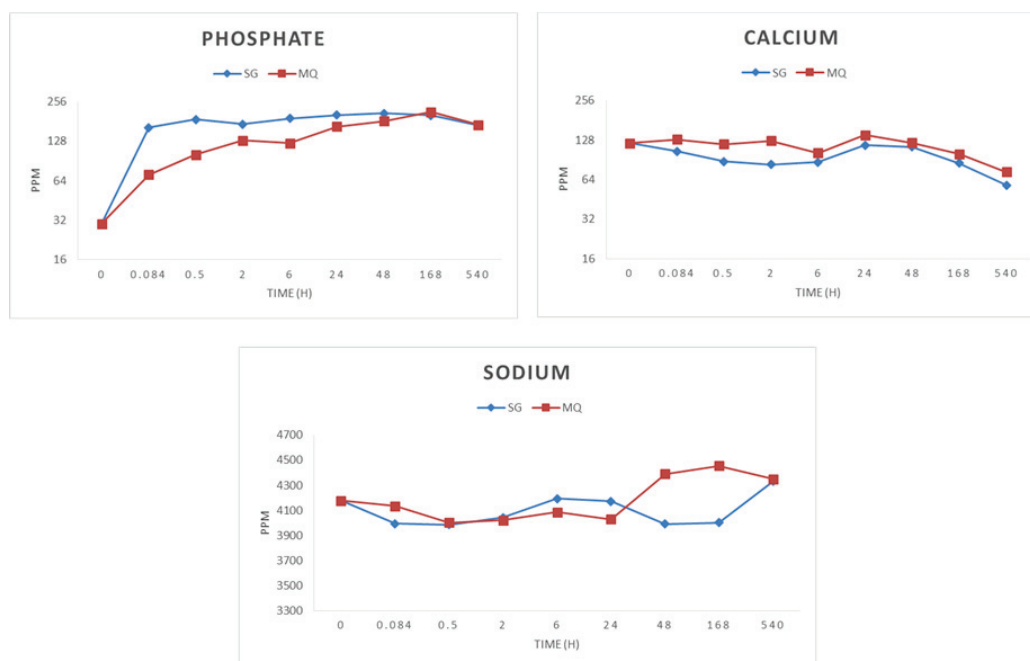

Figure 40. Dissolution kinetics of Ca, Na and P for MQ and SG glasses during 3 weeks of incubation in SBF

From fig. 39, it is possible to notice that the three ions dissolve into the SBF with different kinetics. In the MQ system, the phosphate was found to dissolve almost linearly for the first two hours to reach a plateau; whereas, in the SG system we have a burst release during the first 5 min of incubation immediately followed by a plateau. As explained in the section 4.7, it might be due to

1. lower density of the network
2. higher quantity of OH groups
3. reduced chain length
4. weaker network connectivity

Calcium release suggested similar kinetics between the two glass systems. It seems that there was almost no dissolution at all during the first 6 hours of incubation with the ~120

167

ppm measured coming exclusively from the SBF. A peak followed after 1 day to progressively reduce during the next 3 weeks. The Sodium presented even more different kinetics. Very little Na appears to dissolve / diffuse from the powder during the initial 24 hours of experiments. This holds for both in SG and MQ glasses. However, after 24 hours there is a divergence. For the MQ glass, its concentration rose for 2 days and 1 week to drop at week 3; in contrast a completely opposite kinetic trend was exhibited for the SG glass (a drop concentration between 2 days and 1 week of experiment and a rise at the third week to reach the same Na concentration of the MQ Na).

During the experiment, a visual change in the powder was recognised after 1 and 3 weeks for both the MQ and SG glasses. The powders resembled flakes rather than a scattered powder. The materials were collected and submitted for the XRD to check if any change in the phase had occurred. After 1 and 3 weeks of incubation, the only phase detectable in all cases was NaCl, the amount found being both glass and time dependent. For SG glass the amount of NaCl accumulated on the surface was 1.1 wt% and 13.0 wt% 1 and 3 weeks of incubation respectively. Whereas, for MQ glass 2.4 wt% and 5.8wt% of NaCl formed on the surface after 1 and 3 weeks of incubation respectively. This may explain the trend for Na seen in figure 1, namely that lower concentrations of Na in solution correlate to increased NaCl crystal formation

N.B. The data above must be taken into consideration carefully because: 1) the dilution of the conditioned SBF media for ICP analysis was performed using only ultrapure water without nitric acid (0.6% was usually used) which is needed to dissolve eventual precipitated salts; 2) the blank (the SBF alone without powder) was considered as a sample so was not subtracted out to level the background noise (which explains why, for example, we have more than 4000 ppm of Na and about 120 ppm of Ca associated exclusively with the media); 3) the concentration used (1mg/mL) might be too low to be actually measured.

7.2   APPENDIX 2

Below (fig. 40 and 41), the XFR data of the Sr-doped phosphate coacervate glasses is shown to indicate the successful incorporation of the Sr in the glass networks.

Result(s)		Units	
Sample Basis			Dried 110 deg C
Aluminium Oxide	Al_2O_3	%	0.02
Calcium Oxide	CaO	%	0.5
Potassium Oxide	K_2O	%	0.02
Sodium Oxide	Na_2O	%	8.2
Phosphorus Pentoxide	P_2O_5	%	63
Strontium (II) Oxide	SrO	%	29

Figure 41. XRF (wt%) of the full Sr phosphate glass obtained by coacervation process

Result(s)		Units	
Sample Basis			Dried 110 deg C
Calcium Oxide	CaO	%	12
Potassium Oxide	K_2O	%	0.03
Sodium Oxide	Na_2O	%	3.9
Phosphorus Pentoxide	P_2O_5	%	56
Strontium (II) Oxide	SrO	%	28

Figure 42. Composition (wt%) obtained by XRF of the coacervate-derived Sr-doped phosphate glass
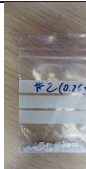
7.3 APPENDIX 3
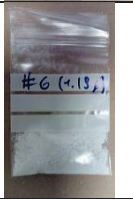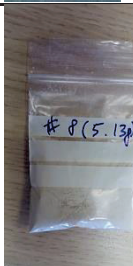
Here below is a complete table (table 15) summarizing all the attempts made to define an optimised sol-gel protocol. Optimisation was based on the use of alternative precursors (safer and less toxic compare to the established ones as well as offering high % yield in the final product) to produce phosphate glasses. The problems encountered, and the reason of the failures are documented. Where available, pictures of the obtained produced are shown.

Table 15 Procedures tested to define an optimized sol-gel protocol
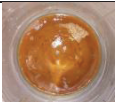
Sol-gel PBG-C32: P_2O_5 (53%) – CaO (32%) – Na_2O (15%) – mol%								
NON-aqueous system								
Precursors	**Solvent(s)**	**Catalyst**	**Heating (°C)**	**Reflux**	**Drying**	**Problems**	**Yield (g)**	**Pictures**
Ethyl-P CaOEt NaOEt (21%in EtOH)	EtOH	No	250	Yes	yes (120℃/1week)	Ca poorly soluble	Not recorded	
Ethyl-P CaOEt NaOEt (21%in EtOH)	EtOH	AcOH	No	yes	yes (120℃/1week)	Ca poorly soluble	Not recorded	
Ethyl-P CaOEt NaOEt (21%in EtOH)	EtOH	AcOH	No	No	No	Ca poorly soluble	Not recorded	
Butyl-P CaOEt NaOEt (21%in EtOH)	EtOH	No	No	No	No	Fust reaction between butyl-P and NaOEt so absolutely no solubility of CaOEt	Not recorded	
Butyl-P CaOEt	EtOH	AcOH	No	No	No	Fust reaction between butyl-P	Not recorded	

Precursors	Solvent(s)	Catalyst	Heating (°C)	Reflux	Drying	Problems	Yield (g)	Pictures
NaOEt (21%in EtOH)						and NaOEt so absolutely no solubility of CaOEt		
Ethyl-P CaOEt NaOEt (21%in EtOH)	EtOH	H_3PO_4	No	No	No	milky precipitation	Not recorded	
Ethyl-P Ca(NO$_3$)$_2$*4H$_2$O NaNO$_3$	EtOH (60mL) EG (90mL)	No	No	No	No	No reaction	Not recorded	
Ethyl-P Ca(NO$_3$)$_2$*4H$_2$O NaNO$_3$	DMFA (60mL) EG (90mL)	No	No	No	No	No reaction	Not recorded	
Butyl-P CaOEt NaOEt (21%inEtOH)	EtOH 60mL + EG 90 mL	NH4OH	No	No	1. 60°C for 8 hours 2. 150 °C for 48 hours	Measuring the pH	Not recorded	

AQUEOUS SYSTEM								
Precursors	**Solvent(s)**	**Catalyst**	**Heating (°C)**	**Reflux**	**Drying**	**Problems**	**Yield (g)**	**Pictures**
Ethyl-P CaAc NaAc	EtOH H$_2$O	AcOH	No	No	No	Ca and Na precursors not soluble in EtOH	Not recorded	
Ethyl-P CaAc NaOEt	EtOH H$_2$O	AcOH	No	No	No	No reaction	Not recorded	
Butyl-P CaAc NaOEt	EtOH H$_2$O	AcOH	No	No	No	No reaction	Not recorded	
Ethyl-P CaCl$_2$ NaCl	H$_2$O	NH4OH	No	No	No	No reaction	Not recorded	
Ethyl-P CaCl$_2$ NaCl	H$_2$O	HCl	No	No	No	Salts precipitation after solvent	Not recorded	

Precursors	Solvent(s)	Catalyst	Heating (°C)	Reflux	Drying	Problems	Yield (g)	Pictures
						evaporation		
Ethyl-P CaAc NaAc	H_2O	No	No	No	No	No reaction	Not recorded	
Ethyl-P CaAc NaAc	H_2O	AcOH	No	No	No	Salts precipitation	Not recorded	
Ethyl-P CaAc NaAc	H_2O	NH_4OH	No	No	No	No reaction	Not recorded	
Ethyl-P CaAc NaAc	H_2O	AcOH	250	Yes	yes (100℃/1week)	Salts precipitation	Not recorded	
Ethyl-P CaAc NaAc	H_2O	NH_4OH	250	Yes	yes (100℃/1week)	Salts precipitation	Not recorded	

Factorial Experimental Design (FED)

Precursors	Solvent(s)	Catalyst	Heating (°C)	Reflux	Drying	Problems	Yield (g)	Pictures
Ethyl-P CaAc NaAc	EtOH/EG (60/40)	No	250	Yes (100℃/6 days)	No		7.79g	
Ethyl-P CaAc NaAc	EtOH/EG (60/40)	No	250	Yes (100℃/6 days)	No	The repetition of the run below: CaAc not well dissolved	0.44	
Ethyl-P CaAc NaAc	EtOH/EG (100/0)	No	250	Yes (100℃/6 days)	No		0.26	
Ethyl-P CaAc NaAc	EtOH/EG (80/20)	No	250	Yes (80℃/4 days)	No		5.07	

Ethyl-P CaAc NaAc	EtOH/EG (60/40)	No	250	Yes (60℃/2 days)	No		2.28	
Ethyl-P CaAc NaAc	EtOH/EG (100/0)	No	250	Yes (60℃/6 days)	No		0.53	
Ethyl-P CaAc NaAc	EtOH/EG (100/0)	No	250	Yes (100℃/2 days)	No		1.19	
Ethyl-P CaAc NaAc	EtOH/EG (100/0)	No	250	Yes (60℃/2 days)	No		0.70	
Ethyl-P CaAc NaAc	EtOH/EG (60/40)	No	250	Yes (100℃/2 days)	No		5.13	
Ethyl-P CaAc NaAc	EtOH/EG (60/40)	No	250	Yes (60℃/6 days)	No		7.40	
Ethyl-P CaAc NaAc	EtOH/EG (80/20)	No	250	Yes (80℃/4 days)	No		4.3	
Ethyl-P CaAc NaAc	EtOH/EG (60/40)	No	250	Yes (100℃/4 days)	No		5.7	
Post-FED								

Precursors	Solvent(s)	Catalyst	Heating (°C)	Reflux	Drying	Problems	Yield (g)	Pictures
Ethyl-P CaAc NaAc	EtOH/EG (60/40)	No	250	Yes (100℃/6 days)	Yes Yes (100℃/7 days)		Not recorded	
Ethyl-P CaAc NaG	EtOH/EG (60/40)	No	250	Yes (100℃/6 days)	Yes Yes (100℃/7 days)		Not recorded	
Ethyl-P CaAc NaAc	EtOH/DMFA (60/40)	No	250	Yes (100℃/6 days)	Yes Yes (100℃/7 days)		Not recorded	
Ethyl-P CaAc NaG	EtOH/DMFA (60/40)	No	250	Yes (100℃/6 days)	Yes Yes (100℃/7 days)		Not recorded	
Ethyl-P CaAc NaAc (Inverted order: CaAc first)	EtOH/EG (60/40)	No	250	Yes (100℃/6 days)	Yes Yes (100℃/7 days)		Not recorded	
Ethyl-P CaAc NaAc (15g final yield instead of 20)	EtOH/EG (60/40)	No	250	Yes (100℃/6 days)	Yes Yes (100℃/7 days)		Not recorded	
Ethyl-P CaAc NaAc (Keeping the EG/EtOH *ratio* (60%:40%), increase the volume)	EtOH/EG (60/40)	No	250	Yes (100℃/6 days)	Yes (100℃/7 days)		Not recorded	

Precursors	Solvent(s)	Catalyst	Heating (°C)	Reflux	Drying	Problems	Yield (g)	Pictures
Butyl-P CaAc NaAc	EtOH/EG (60/40)	No	250	Yes (100℃/6 days	Yes (100℃/7 days)	Milky solution CaAc not completely dissolved	Not recorded	
Butyl-P CaAc NaG	EtOH/EG (60/40)	No	No	Yes (100℃/6 days	Yes (100℃/7 days)	Milky solution CaAc not completely dissolved	Not recorded	
Butyl-P CaAc NaAc	EtOH/DMFA (60/40)	No	No	Yes (100℃/6 days	Yes (100℃/7 days)	CaAc not completely dissolved	Not recorded	
Butyl-P CaAc NaG	EtOH/DMFA (60/40)	No	No	Yes (100℃/6 days	Yes (100℃/7 days)	CaAc not completely dissolved	Not recorded	
Ethyl-P CaAc NaAc	EtOH/EG (60/40)	No	250	Yes (100℃/6 days	Yes (100℃/7 days)		Not recorded	
Ethyl-P CaAc NaAc	EtOH/EG (60/40)	No	250	Yes (100℃/6 days	NO		Not recorded	
Ethyl-P CaAc NaAc	EtOH/EG (60/40)	No	300	Yes (100℃/6 days	NO		Not recorded	
Ethyl-P CaAc NaAc	EtOH/EG (60/40)	No	350	Yes (100℃/6 days	NO		Not recorded	
Sr-doping	**PBG-S10: P_2O_5 (53%) – CaO (22%) – Na_2O (15%) – SrO (10%) PERFORMED 4 TIMES**							
Precursors	**Solvent(s)**	**Catalyst**	**Heating (°C)**	**Reflux**	**Drying**	**Problems**	**Yield (g)**	**Pictures**

| Ethyl-P CaAc NaAc SrAc | EtOH/EG (60/40) | No | 250 | Yes (100℃ /6 days | No | Turbid solution after 24h | Not record ed | |

8 Bibliography

1. *The Williams Dictionary of Biomaterials*. (Liverpool University Press, 1999).

2. Williams, D. F. On the mechanisms of biocompatibility. *Biomaterials* **29,** 2941–2953 (2008).

3. Chai, F., Raoul, G., Wiss, A., Ferri, J. & Hildebrand, H. F. [Bone substitutes: Classification and concerns]. *Rev. Stomatol. Chir. Maxillofac.* **112,** 212–221 (2011).

4. L Hench, L. The Story of Bioglass®. *J. Mater. Sci. Mater. Med.* **17,** 967–78 (2006).

5. Hench, L. L. & Thompson, I. Twenty-first century challenges for biomaterials. *J. R. Soc. Interface* **7,** S379–S391 (2010).

6. Mitchell, K. A. R. Use of outer d orbitals in bonding. *Chem. Rev.* **69,** 157–178 (1969).

7. Cruickshank, D. W. J. 1077. The rôle of 3d-orbitals in π-bonds between (a) silicon, phosphorus, sulphur, or chlorine and (b) oxygen or nitrogen. *J. Chem. Soc. Resumed* **0,** 5486–5504 (1961).

8. Brow, R. K. Review: the structure of simple phosphate glasses. *J. Non-Cryst. Solids* **263–264,** 1–28 (2000).

9. Knowles, J. C. Phosphate based glasses for biomedical applications. *J. Mater. Chem.* **13,** 2395–2401 (2003).

10. Tommaso, D. D., Ainsworth, R. I., Tang, E. & Leeuw, N. H. de. Modelling the structural evolution of ternary phosphate glasses from melts to solid amorphous materials. *J. Mater. Chem. B* **1,** 5054–5066 (2013).

11. Al Hasni, B. *et al.* Molecular dynamics modelling of sodium and calcium metaphosphate glasses for biomaterial applications. *Phys. Chem. Glas. - Eur. J. Glass Sci. AndTechnology Part B* **57,** 245–253 (2016).

12. Ruiz Hernandez, S. E., Ainsworth, R. I. & de Leeuw, N. H. Molecular dynamics simulations of bio-active phosphate-based glass surfaces. *J. Non-Cryst. Solids* **451,** 131–137 (2016).

13. Saidak, Z. & Marie, P. J. Strontium signaling: molecular mechanisms and therapeutic implications in osteoporosis. *Pharmacol. Ther.* **136,** 216–226 (2012).

14. Pors Nielsen, S. The biological role of strontium. *Bone* **35,** 583–588 (2004).

15. Neel, E. A. A. *et al.* Structure and properties of strontium-doped phosphate-based glasses. *J. R. Soc. Interface* (2009). doi:10.1098/rsif.2008.0348

16. Sistla, R. K. & Seshasayee, M. Structural study of lithium phosphate glasses by X-ray RDF and computer simulations. *J. Non-Cryst. Solids* **349,** 22–29 (2004).

17. Ahmina, W., Moudane, M. E., Zriouil, M. & Taibi, M. 'hamed. Glass-forming region, structure and some properties of potassium manganese phosphate glasses. *Phase Transit.* **89,** 1051–1061 (2016).

18. Suzuya, K., L Price, D., Loong, C.-K. & Kohara, S. Structure of magnesium phosphate glasses. *J. Phys. Chem. Solids - J PHYS CHEM SOLIDS* **60,** 1457–1460 (1999).

19. Stoch, P. *et al.* Structural properties of iron-phosphate glasses: spectroscopic studies and ab initio simulations. *Phys. Chem. Chem. Phys. PCCP* **16,** 19917–19927 (2014).

20. Mogus-Milankovic, A., Gajovic, A., Santic, A. & Day, D. E. Structure of sodium phosphate glasses containing Al_2O_3 and/or Fe_2O_3. Part I. *J. Non-Cryst. Solids* **289,** 204–213 (2001).

21. Mogus-Milankovic, A., Gajovic, A., Santic, A. & Day, D. E. Structure of sodium phosphate glasses containing Al_2O_3 and/or Fe_2O_3. Part I. *J. Non-Cryst. Solids* **289,** 204–213 (2001).

22. Silva, A. M. B., Correia, R. N., Oliveira, J. M. M. & Fernandes, M. H. V. Structural characterization of TiO2–P2O5–CaO glasses by spectroscopy. *J. Eur. Ceram. Soc.* **30,** 1253–1258 (2010).

23. Sastry, S. S. & Rao, B. R. V. Spectroscopic characterization of manganese-doped alkaline earth lead zinc phosphate glasses. *Bull. Mater. Sci.* **38,** 475–482 (2015).

24. Sastry, S. S. & Rao, B. R. V. Structural and optical properties of vanadium doped akaline earth lead zinc phosphate glasses. *IJPAP Vol5207 July 2014* (2014).

25. Smith, C. The structure and properties of ternary zinc phosphate glasses for optical applications. *Dr. Diss.* (2014).

26. Ahsan, M. R., Uddin, M. A. & Mortuza, M. G. Infrared study of the effect of P 2 O 5 in the structure of lead silicate glasses. (2005).

27. Dayanand, C., Bhikshamaiah, G., Tyagaraju, V. J., Salagram, M. & Murthy, A. S. R. K. Structural investigations of phosphate glasses: a detailed infrared study of the x(PbO)-(1–x) P2O5 vitreous system. *J. Mater. Sci.* **31,** 1945–1967 (1996).

28. Bae, B.-S. Behavior, properties and structure of copper phosphate glasses. (1993).

29. Harada, T., In, H., Takebe, H. & Morinaga, K. Effect of B2O3 Addition on the Thermal Stability of Barium Phosphate Glasses for Optical Fiber Devices. *J. Am. Ceram. Soc.* **87,** 408–411 (2004).

30. Brow, R. K., Kirkpatrick, R. J. & Turner, G. L. The short range structure of sodium phosphate glasses I. MAS NMR studies. *J. Non-Cryst. Solids* **116,** 39–45 (1990).

31. Franks, K., Abrahams, I. & Knowles, J. C. Development of soluble glasses for biomedical use Part I: In vitro solubility measurement. *J. Mater. Sci. Mater. Med.* **11,** 609–614 (2000).

32. Ruiz Hernandez, S. E., Ainsworth, R. I. & de Leeuw, N. H. Molecular dynamics simulations of bio-active phosphate-based glass surfaces. *J. Non-Cryst. Solids* **451,** 131–137 (2016).

33. Bunker, B. C., Arnold, G. W. & Wilder, J. A. Phosphate glass dissolution in aqueous solutions. *J. Non-Cryst. Solids* **64,** 291–316 (1984).

34. Knowles, J. C., Franks, K. & Abrahams, I. Investigation of the solubility and ion release in the glass system K2O-Na2O-CaO-P2O5. *Biomaterials* **22,** 3091–3096 (2001).

35. Franks, K., Salih, V., Knowles, J. C. & Olsen, I. The effect of MgO on the solubility behavior and cell proliferation in a quaternary soluble phosphate based glass system. *J. Mater. Sci. Mater. Med.* **13,** 549–556 (2002).

36. Fredholm, Y. C. *et al.* Influence of strontium for calcium substitution in bioactive glasses on degradation, ion release and apatite formation. *J. R. Soc. Interface* **9,** 880–889 (2012).

37. Yu, X., Day, D. E., Long, G. J. & Brow, R. K. Properties and structure of sodium-iron phosphate glasses. *J. Non-Cryst. Solids* **215,** 21–31 (1997).

38. Brauer, D. S., Karpukhina, N., Law, R. V. & Hill, R. G. Effect of TiO2 addition on structure, solubility and crystallisation of phosphate invert glasses for biomedical applications. *J. Non-Cryst. Solids* **356,** 2626–2633 (2010).

39. Gao, H., Tan, T. & Wang, D. Effect of composition on the release kinetics of phosphate controlled release glasses in aqueous medium. *J. Control. Release Off. J. Control. Release Soc.* **96,** 21–28 (2004).

40. Shaharyar, Y. *et al.* Structure-solubility relationships in fluoride-containing phosphate based bioactive glasses. *J. Mater. Chem. B* **3,** 9360–9373 (2015).

41. Döhler, F., Mandlule, A., van Wüllen, L., Friedrich, M. & Brauer, D. S. 31 P NMR characterisation of phosphate fragments during dissolution of calcium sodium phosphate glasses. *J. Mater. Chem. B* **3,** 1125–1134 (2015).

42. Pickup, D. *et al. New sol–gel synthesis of a (CaO)0.3(Na2O)0.2(P2O5)0.5 bioresorbable glass and its structural characterisation*. **17,** (2007).

43. Brinker, C. J. & Scherer, G. W. *Sol-gel Science: The Physics and Chemistry of Sol-gel Processing*. (Gulf Professional Publishing, 1990).

44. Averbuch-Pouchot & Durif, A. *Topics in Phosphate Chemistry.* (World Scientific Publishing Company, 1996).

45. Livage, J., Barboux, P., Vandenborre, M. T., Schmutz, C. & Taulelle, F. Sol-gel synthesis of phosphates. *J. Non-Cryst. Solids* **147–148,** 18–23 (1992).

46. Carta, D. *et al.* Structural studies of bioactive sol-gel phosphate based glasses. *Phys. Chem. Glas.* **46,** 365–371 (2005).

47. Lee, B. I., Samuels, W. D., Wang, L.-Q. & Exarhos, G. J. Sol-gel synthesis of phosphate ceramic composites I. *J. Mater. Res.* **11,** 134–143 (1996).

48. Soulié, J. *et al.* Development of a new family of monolithic calcium (pyro)phosphate glasses by soft chemistry. *Acta Biomater.* **41,** 320–327 (2016).

49. Pickup, D. M. *et al.* Characterisation of phosphate coacervates for potential biomedical applications. *J. Biomater. Appl.* **28,** 1226–1234 (2014).

50. Van Wazer, J. R. *Phosphorus and its compounds*. (New York, 1958).

51. Kopp, W. *et al.* Calcium polyphosphate coacervates: effects of thermal treatment. *J. Sol-Gel Sci. Technol.* **63,** 219–223 (2012).

52. Yu, W. *et al.* Strontium-Doped Amorphous Calcium Phosphate Porous Microspheres Synthesized through a Microwave-Hydrothermal Method Using Fructose 1,6-Bisphosphate as an Organic Phosphorus Source: Application in Drug Delivery and Enhanced Bone Regeneration. *ACS Appl. Mater. Interfaces* **9,** 3306–3317 (2017).

53. Gao, H., Tan, T. & Wang, D. Dissolution mechanism and release kinetics of phosphate controlled release glasses in aqueous medium. *J. Controlled Release* **96,** 29–36 (2004).

54. Delahaye, F., Montagne, L., Palavit, G., Claude Touray, J. & Baillif, P. Acid dissolution of sodium–calcium metaphosphate glasses. *J. Non-Cryst. Solids* **242,** 25–32 (1998).

55. Cerruti, M., Greenspan, D. & Powers, K. Effect of pH and ionic strength on the reactivity of Bioglass 45S5. *Biomaterials* **26,** 1665–1674 (2005).

56. Icenhower, J. P. & Dove, P. M. The dissolution kinetics of amorphous silica into sodium chloride solutions: effects of temperature and ionic strength. *Geochim. Cosmochim. Acta* **64,** 4193–4203 (2000).

57. Sharmin, N., Gu, F., Ahmed, I. & Parsons, A. J. Compositional dependency on dissolution rate and cytocompatibility of phosphate-based glasses: Effect of B2O3 and Fe2O3 addition. *J. Tissue Eng.* **8,** (2017).

58. Sharmin, N. & Rudd, C. D. Structure, thermal properties, dissolution behaviour and biomedical applications of phosphate glasses and fibres: a review. *J. Mater. Sci.* **52,** 8733–8760 (2017).

59. Ahmed, I., Lewis, M. P., Nazhat, S. N. & Knowles, J. C. Quantification of Anion and Cation Release from a Range of Ternary Phosphate-based Glasses with Fixed 45 mol% P2O5. *J. Biomater. Appl.* **20,** 65–80 (2005).

60. Ahmed, I., Lewis, M. P. & Knowles, J. C. Quantification of anions and cations from ternary phosphate based glasses with fixed 50 and 55 mol% P2O5 using ion chromatography. *Phys. Chem. Glas.* **46,** 547–552 (2005).

61. Kesisoglou, A., Knowles, J. C. & Olsen, I. Effects of phosphate-based glasses on T lymphocytes in vitro. *J. Mater. Sci. Mater. Med.* **13,** 1189–1192 (2002).

62. Gough, J. E., Christian, P., Scotchford, C. A., Rudd, C. D. & Jones, I. A. Synthesis, degradation, and in vitro cell responses of sodium phosphate glasses for craniofacial bone repair. *J. Biomed. Mater. Res.* **59,** 481–489 (2002).

63. Gough, J. E., Christian, P., Scotchford, C. A. & Jones, I. A. Long-term craniofacial osteoblast culture on a sodium phosphate and a calcium/sodium phosphate glass. *J. Biomed. Mater. Res. A* **66A,** 233–240 (2003).

64. Salih, V. *et al.* Development of soluble glasses for biomedical use Part II: the biological response of human osteoblast cell lines to phosphate-based soluble glasses. *J. Mater. Sci. Mater. Med.* **11,** 615–620 (2000).

65. Uo, M., Mizuno, M., Kuboki, Y., Makishima, A. & Watari, F. Properties and cytotoxicity of water soluble Na2O-CaO-P2O5 glasses. *Biomaterials* **19,** 2277–2284 (1998).

66. Fujita, T. *et al.* Phosphate provides an extracellular signal that drives nuclear export of Runx2/Cbfa1 in bone cells. *Biochem. Biophys. Res. Commun.* **280,** 348–352 (2001).

67. Massera, J., Kokkari, A., Närhi, T. & Hupa, L. The influence of SrO and CaO in silicate and phosphate bioactive glasses on human gingival fibroblasts. *J. Mater. Sci. Mater. Med.* **26,** 196 (2015).

68. Salih, V., Patel, A. & Knowles, J. C. Zinc-containing phosphate-based glasses for tissue engineering. *Biomed. Mater. Bristol Engl.* **2,** 11–20 (2007).

69. Abou Neel, E. A. *et al.* In vitro bioactivity and gene expression by cells cultured on titanium dioxide doped phosphate-based glasses. *Biomaterials* **28,** 2967–2977 (2007).

70. Ahmed, I., Collins, C. A., Lewis, M. P., Olsen, I. & Knowles, J. C. Processing, characterisation and biocompatibility of iron-phosphate glass fibres for tissue engineering. *Biomaterials* **25,** 3223–3232 (2004).

71. Ahmed, I. *et al.* Cytocompatibility and effect of increasing MgO content in a range of quaternary invert phosphate-based glasses. *J. Biomater. Appl.* **24,** 555–575 (2010).

72. Navarro, M., Ginebra, M.-P. & Planell, J. A. Cellular response to calcium phosphate glasses with controlled solubility. *J. Biomed. Mater. Res. A* **67,** 1009–1015 (2003).

73. Qaysi, M. A., Petrie, A., Shah, R. & Knowles, J. C. Degradation of zinc containing phosphate-based glass as a material for orthopedic tissue engineering. *J. Mater. Sci. Mater. Med.* **27,** (2016).

74. Pessan, J. P., Al-Ibrahim, N. S., Buzalaf, M. A. R. & Toumba, K. J. Slow-release fluoride devices: a literature review. *J. Appl. Oral Sci.* **16,** 238–244 (2008).

75. Shelton, R. M., Rasmussen, A. C. & Davies, J. E. Protein adsorption at the interface between charged polymer substrata and migrating osteoblasts. *Biomaterials* **9,** 24–29 (1988).

76. Gristina, A. G. Biomaterial-centered infection: microbial adhesion versus tissue integration. *Science* **237,** 1588–1595 (1987).

77. Ahmed, I., Ready, D., Wilson, M. & Knowles, J. C. Antimicrobial effect of silver-doped phosphate-based glasses. *J. Biomed. Mater. Res. A* **79,** 618–626 (2006).

78. Mulligan, A. M., Wilson, M. & Knowles, J. C. The effect of increasing copper content in phosphate-based glasses on biofilms of Streptococcus sanguis. *Biomaterials* **24,** 1797–1807 (2003).

79. Valappil, S. P. *et al.* Controlled delivery of antimicrobial gallium ions from phosphate-based glasses. *Acta Biomater.* **5,** 1198–1210 (2009).

80. Zhang, L. & Eckert, H. *Sol–Gel Synthesis of Al2O3–P2O5 Glasses: Mechanistic Studies by Solution and Solid State NMR*. **14,** (2004).

81. Pickup, D. M. *et al.* Preparation, structural characterisation and antibacterial properties of Ga-doped sol–gel phosphate-based glass. *J. Mater. Sci.* **44,** 1858–1867 (2009).

82. Knowles, J. C., Hastings, G. W., Ohta, H., Niwa, S. & Boeree, N. Development of a degradable composite for orthopaedic use: in vivo biomechanical and histological evaluation of two bioactive degradable composites based on the polyhydroxybutyrate polymer. *Biomaterials* **13,** 491–496 (1992).

83. Knowles, J. C. Development of a natural degradable polymer for orthopaedic use. *J. Med. Eng. Technol.* **17,** 129–137 (1993).

84. Shah, R., Ready, D., Knowles, J. C., Hunt, N. P. & Lewis, M. P. Sequential identification of a degradable phosphate glass scaffold for skeletal muscle regeneration. *J. Tissue Eng. Regen. Med.* **8,** 801–810 (2014).

85. Kim, Y.-P. *et al.* Phosphate glass fibres promote neurite outgrowth and early regeneration in a peripheral nerve injury model. *J. Tissue Eng. Regen. Med.* **9,** 236–246 (2015).

86. Ferreira, A. M., Gentile, P., Chiono, V. & Ciardelli, G. Collagen for bone tissue regeneration. *Acta Biomater.* **8,** 3191–3200 (2012).

87. Pickup, D. M. *et al.* New sol–gel synthesis of a (CaO) 0.3 (Na 2 O) 0.2 (P 2 O 5) 0.5 bioresorbable glass and its structural characterisation. *J. Mater. Chem.* **17,** 4777–4784 (2007).

88. Pickup, D. M. *et al.* Characterisation of phosphate coacervates for potential biomedical applications. *J. Biomater. Appl.* **28,** 1226–1234 (2014).

89. Kokubo, T. & Takadama, H. How useful is SBF in predicting in vivo bone bioactivity? *Biomaterials* **27,** 2907–2915 (2006).

90. Cai, S. *et al.* Microstructural characteristics and crystallization of CaO–P 2 O 5–Na 2 O–ZnO glass ceramics prepared by sol–gel method. *J. Non-Cryst. Solids* **355,** 273–279 (2009).

91. Thommes, M. *et al.* Physisorption of gases, with special reference to the evaluation of surface area and pore size distribution (IUPAC Technical Report). *Pure Appl. Chem.* **87,** (2015).

92. Carta, D. *et al.* A structural study of sol–gel and melt-quenched phosphate-based glasses. *J. Non-Cryst. Solids* **353,** 1759–1765 (2007).

93. Carta, D. *et al.* Structural studies of bioactive sol-gel phosphate based glasses. *Phys. Chem. Glas.* **46,** 365–371 (2005).

94. Thommes, M. *et al.* Physisorption of gases, with special reference to the evaluation of surface area and pore size distribution (IUPAC Technical Report). *Pure Appl. Chem.* **87,** 1051–1069 (2015).

95. Ruiz Hernandez, S. E., Ainsworth, R. I. & de Leeuw, N. H. Molecular dynamics simulations of bio-active phosphate-based glass surfaces. *J. Non-Cryst. Solids* **451,** 131–137 (2016).

96. Christie, J. K., Ainsworth, R. I., Hernandez, S. E. R. & Leeuw, N. H. de. Structures and properties of phosphate-based bioactive glasses from computer simulation: a review. *J. Mater. Chem. B* **5,** 5297–5306 (2017).

97. Ruiz Hernandez, S. E., Ainsworth, R. I. & de Leeuw, N. H. Molecular dynamics simulations of bio-active phosphate-based glass surfaces. *J. Non-Cryst. Solids* **451,** 131–137 (2016).

98. Van Wazer, J. R. *Phosphorus and its compounds*. (New York, 1958).

99. Kopp, W. *et al.* Calcium polyphosphate coacervates: effects of thermal treatment. *J. Sol-Gel Sci. Technol.* 219–223 (2012). doi:10.1007/s10971-012-2749-z

100. Averbuch-Pouchot, M. T. & Durif, A. *Topics in Phosphate Chemistry*. (World Scientific Pub Co Inc, 1996).

101. Lin, S., Ionescu, C., Pike, K. J., Smith, M. E. & Jones, J. R. Nanostructure evolution and calcium distribution in sol–gel derived bioactive glass. *J. Mater. Chem.* **19,** 1276–1282 (2009).